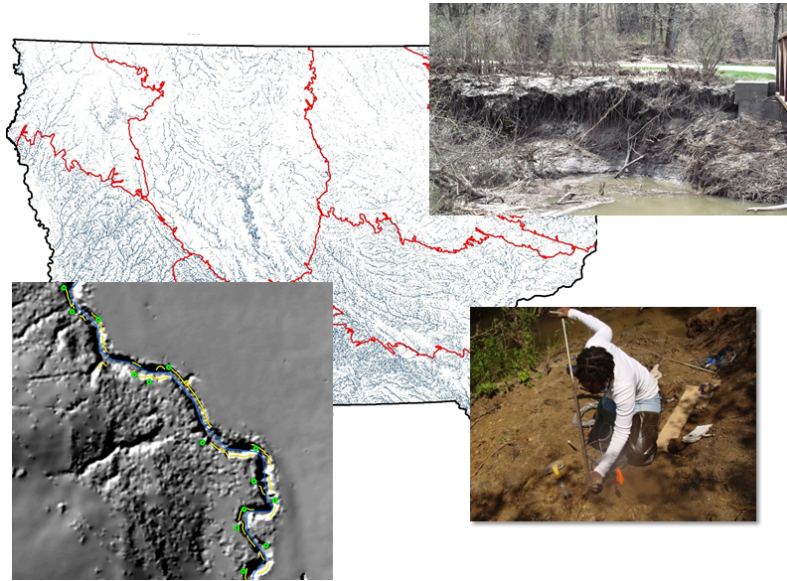


Bank Stability Assessment Tool for Bridge and Abutment Infrastructure in Iowa

FINAL REPORT



Submitted to:
David Claman
Iowa Department of Transportation
800 Lincoln Way
Ames, IA 50010

Submitted by:
Calvin Wolter, Primary Investigator
Iowa Department of Natural Resources
502 East 9th Street
Wallace State Office Building, 4th Floor
Des Moines, IA 50319-0034

January 2021



Iowa Department
of Transportation

IOWA



DISCLAIMER

The opinions, findings, and conclusions expressed in this publication are those of the authors and not necessarily those of the Iowa Department of Transportation or the United States Department of Transportation, Federal Highway Administration. The views and conclusions contained in this document should not be interpreted as necessarily representing the official policies, either expressed or implied, of the sponsors.

The sponsors assume no liability for the contents or use of the information contained in this document. This report does not constitute a standard, specification, or regulation. Additionally, the sponsors do not endorse products or manufacturers mentioned in this report. Trademarks or manufacturers' names appear in this report only because they are considered essential to the objective of the document.

NON-DISCRIMINATION STATEMENT

The University of Tennessee does not discriminate on the basis of race, color, age, religion, national origin, sex, sexual orientation, gender identity, marital status, disability, or status as a U.S. veteran. Inquiries can be directed to the Office of Equity and Diversity at the University of Tennessee, (865) 974-2498.

The University of Iowa prohibits discrimination in employment, educational programs, and activities on the basis of race, creed, color, religion, national origin, age, sex, pregnancy, disability, genetic information, status as a U.S. veteran, service in the U.S. military, sexual orientation, gender identity, associational preferences, or any other classification that deprives the person of consideration as an individual. For additional information on non-discrimination policies, contact the Director, Office of Equal Opportunity and Diversity, the University of Iowa, 202 Jessup Hall, Iowa City, IA 52242-1316, 319-335-0705 (voice), 319-335-0697 (TDD), diversity@uiowa.edu.

The Iowa Department of Natural Resources abides under Title VI of the 1964 Civil Rights Act, Section 504 of the Rehabilitation Act of 1973, the Age Discrimination Act of 1975 and Title IX of the Education Amendments of 1972, federal regulations prohibit discrimination on the basis of race, color, national origin, or handicap. If you believe that you have been discriminated against in any program, activity, or facility as described above, or if you desire further information, please write to, Director, Iowa Department of Natural Resources, Wallace State Office Building, 502 E. 9th St., Des Moines, IA 50319-0034

Technical Report Documentation Page

1. REPORT NO. 2020-01		2. GOVERNMENT ACCESSION NO.		3. RECIPIENT CATALOG NO.	
4. TITLE AND SUBTITLE Bank Stability Assessment Tool for Bridge and Abutment Infrastructure in Iowa				5. REPORT DATE January 31, 2021	
				6. PERFORMING ORGANIZATION CODE	
7. AUTHOR(S) Calvin Wolter, Keith Schilling, and Christopher G. Wilson				8. PERFORMING ORGANIZATION REPORT NO.	
9. PERFORMING ORGANIZATION NAME AND ADDRESS Iowa Department of Natural Resources 502 East 9th Street Wallace State Office Building, 4th Floor Des Moines, IA 50319		Department of Civil & Environmental Engineering University of Tennessee Knoxville, TN 37996		10. WORK UNIT NO.	
				11. CONTRACT OR GRANT NO. RB10-014	
12. SPONSORING AGENCY NAME AND ADDRESS Iowa Department of Transportation 800 Lincoln Way Ames, IA 50010				13. TYPE OF REPORT AND PERIOD COVERED Final Report 09/02/2014 – 05/31/2020	
14. ABSTRACT <p>In Iowa, bank erosion is a persistent and severe problem. Yet, the lack of field data and remote sensing imagery inhibits characterization of the spatial and temporal variability of soil strength and erodibility, which influences bank erosion mechanisms. There is a critical need for a geomorphic-geotechnical-hydraulic approach that utilizes currently available tools (e.g., LiDAR; GIS; PEEPs; recirculating flumes; numerical models) to quantify the extent of bank erosion near bridges at a suitable spatial scale and over time.</p> <p>The Iowa Department of Natural Resources, Iowa Geological Survey, and the University of Tennessee-Knoxville provide a multi-dimensional approach to identify and map currently eroding banks in 3rd - 6th order streams that intersect with bridge structures in Iowa. This approach includes geotechnical and hydraulic data that capture the spatial and temporal variability of the bank soil strength under changing climate, moisture and land-use conditions to provide the likelihood and severity of bank erosion.</p> <p>This study substantiates spatial patterns and temporal cycles of bank erosion in the Major Land Resource Areas (MLRAs) of the state. MLRAs 107A, 107B, 108C, and 108D exhibit similar patterns due to the loess soils covering western and southern Iowa. These soils have higher average critical shear stresses than the coarser, till-derived soils in MLRAs 103 and 104 of north central and northeast Iowa. However, MLRAs 107A and 107B have Factors of Safety less than one for at least 95% of their observed flows suggesting that fluvial erosion is highly likely and thus, they have the highest density of eroding banks.</p> <p>Regression models using existing databases and new GIS coverages developed during this project were established using eleven parameters including bank height, stream sinuosity, stream slope, available water capacity, clay content, and bulk density, among other parameters. Stream length to bridge length ratios were used to identify the potential threat for bridges in the near future. In addition, streambank polygons were developed and intersected with right-of-way features to identify roads that may be impacted by lateral channel migration. Bridges with a high ratio and a stream having a high potential for migration were flagged.</p> <p>The greatest number of bridges threatened by stream migration were found in MLRAs 107B and 108D, followed closely by MLRAs 103 and 107A. The greatest risk to roadways were in MLRAs 107B and 103. The project identified 1,515 bridges and 281 road right-of-ways in Iowa that were considered to be at high or moderate risk of future erosion by channel migration. The study provides a means to prioritize those bridge structures across the state that need further protection from pending bank failures.</p>					
15. KEY WORDS Bank Erosion, MLRA, Iowa, Bridge Safety			16. DISTRIBUTION STATEMENT No restrictions		
17. SECURITY CLASSIFICATION (of this report) None		18. SECURITY CLASSIFICATION (of this page)		19. NO. OF PAGES 100	20. PRICE NA

Bank Stability Assessment Tool for Bridge and Abutment Infrastructure in Iowa

FINAL REPORT
January 2021

Sponsored by
Iowa Department of Transportation
For the period September 2, 2014 to May 31, 2020

Report authored by
Calvin Wolter, Primary Investigator
Iowa Department of Natural Resources
502 East 9th Street
Wallace State Office Building, 4th Floor
Des Moines, IA 50319-0034
Email: calvin.wolter@dnr.iowa.gov

Keith Schilling, Co-Investigator
Iowa Geological Survey
University of Iowa
300 Trowbridge Hall
Iowa City, IA 52242-1585
Email: keith-schilling@uiowa.edu

Christopher Wilson, Co-Investigator
Department of Civil & Environmental Engineering
University of Tennessee
851 Neyland Drive
Knoxville, TN 37996-2313
Email: cgw24@utk.edu

ACKNOWLEDGEMENTS

This research was sponsored by the Iowa Department of Transportation and the Federal Highway Administration. The authors are indebted to David Claman for serving as the Technical Advisor and providing productive input to improve this project and the applicability of the Bank Erosion Assessment Tool. The authors would also like to thank Dr. Thanos Papanicolaou for his help with this project, as well as the following students and post-docs from the University of Iowa and the University of Tennessee: Ben Abban, Fabienne Bertrand, John Boys, Matthew Davis, Mohammad Ghaneizad, Brandy Hawkins, Bradley Kruceman, Theodoros Kyriakopoulos, Adam Maxwell, Kaity Patterson, Tommy Sutarto, Achilles Tsakiris, and Micah Wyssmann.

Des Moines, IA
January, 2021

Calvin Wolter
Keith Schilling
Christopher Wilson

TABLE OF CONTENTS

Section	Title	Page
	Disclaimer	ii
	Non-Discrimination Statement	ii
	Technical Report Documentation Page	iii
	Title Page	iv
	Acknowledgements	v
	Table of Contents	vi
	List of Figures	vii
	List of Tables	ix
	Executive Summary	xi
1.	Introduction & Background	1
1.1	Problem Statement	1
1.2	Bank Erosion Mechanisms	2
1.2.1	Subaerial Processes	3
1.2.2	Surface Fluvial Erosion	3
1.2.3	Mass Fluvial Erosion	4
1.2.4	Mass Failure	6
1.2.5	Meandering	7
1.3	Available Methods for Estimating Bank Stability Parameters	7
1.3.1	Surface Fluvial Erosion Methods	7
1.3.2	Mass Fluvial Erosion Methods	8
1.3.3	Mass Failure Methods	9
1.3.4	LiDAR and Aerial Mapping	9
1.4	Interaction among Bank Erosion Mechanisms	10
2.	Project Goals & Products	12
2.1	Overview of Project Goals	12
2.2	Organization of this Report & Products	12
3.	An Assessment of Streambank Recession Rates in Iowa	14
3.1	Goal Statement	14
3.2	Methodology	14
3.2.1	Methodological Overview	14
3.2.2	Regional Setting	14
3.2.3	Erosion Pins	15
3.2.4	Aerial Imagery Analysis of Stream Migration	16
3.3	Results and Discussion	17
3.3.1	Erosion Pin Recession Rates	17
3.3.2	Recession Rates from Aerial Imagery	19
3.3.3	Estimating Bank Recession Rates in Iowa	20
3.4	Conclusions	21
3.5	Products	21
4.	Quantifying the Extent of Eroding Streambanks in Iowa	23
4.1	Goal Statement	23
4.2	Methodology	23
4.2.1	Methodological Overview	23
4.2.2	Rathbun Lake Watershed Streambank Erosion Mapping	23
4.2.3	Delineating Eroding Streambank Extent in Rathbun Lake Watershed	24

4.2.4	Estimating Eroding Streambanks in Iowa	25
4.2.5	Ancillary Data	26
4.3	Results	27
4.3.1	Model Validation	27
4.3.2	Eroding Streambanks	29
4.3.3	Eroding Lengths by Stream Order	29
4.4	Discussion	30
4.4.1	Regional Patterns	31
4.4.2	Relation to Explanatory Factors	34
4.4.3	Limitations	35
4.4.4	Implications	36
4.5	Conclusions	36
4.6	Products	37
5.	In-situ and Laboratory Measurements of Parameters Influential to Bank Erosion	38
5.1	Goal Statement	38
5.2	Methodology	38
5.2.1	Methodological Overview	38
5.2.2	Identify Representative Stream Reaches for Field Monitoring	39
5.2.3	In-situ Measurements and Ancillary Data for Mechanical Soil Strength Estimates	39
5.2.3.1	In-situ Methods	39
5.2.3.2	Changes in Moisture	40
5.2.3.3	Stream Flashiness	41
5.2.4	Laboratory Measurements of Streambank Soil Samples from the Representative Reaches	41
5.2.4.1	Sample Collection	41
5.2.4.2	Geotechnical Measurements	42
5.2.4.3	Conduit Flume Runs to Quantify Critical Shear Strength and Erodibility	43
5.2.5	Photo-Electric Erosion Pin Measurements	45
5.3	Results & Discussions	45
5.3.1	Representative Stream Reaches	45
5.3.2	In-situ Measurements of Soil Strength and Ancillary Hydraulic Data	45
5.3.2.1	Torvane and Penetrometer Measurements	45
5.3.2.2	Soil Moisture Changes	47
5.3.2.3	Stream Flashiness	48
5.3.3	Measurements of Critical Shear Strength against Surface Fluvial Erosion and Erodibility	49
5.3.3.1	Geotechnical Measurements	49
5.3.3.2	Conduit Flume Analysis	49
5.3.4	PEEP Measurements and Mass Fluvial Erosion	51
5.3.4.1	Magnitude and Frequency of Mass Fluvial Erosion	51
5.3.4.2	Erodibility	52
5.4	Summary & Conclusions	53
5.5	Products	54
6.	Bank Erosion Modeling at Select Sites	56
6.1	Goal Statement	56
6.2	Methodology	56
6.2.1	Methodological Overview	56
6.2.2	Empirical Estimates	56
6.2.3	Flow Characteristics and Frequency Analysis	58
6.2.4	Quantifying Bank Retreat Rates under Different Condition Using BSTEM	58

6.3	Results	60
6.3.1	Analytical Estimates of Strength and Erodibility Parameters	60
6.3.2	Spatial Variability of $\tau_{c,f}$ and M_f	61
6.3.3	Temporal Variability of Strength and Erodibility Parameters	63
6.3.4	Flow Frequency Analyses	65
6.3.5	Fluvial Erosion Estimates Using BSTEM	66
6.4	Summary & Conclusions	68
6.4.1	Assessing Variability of Streambank Soil Strength and Erodibility Parameters in Iowa	68
6.4.2	Compilation of Geomorphic, Geotechnical, and Hydraulic Assessments	69
6.5	Products	71
7.	Risk Assessment of Bridge and Road Infrastructure to Streambank Erosion	72
7.1	Goal Statement	72
7.2	Regression Modeling of Stream Migration	72
7.2.1	Methodology	72
7.2.2	Regression Modeling Results	72
7.2.3	Application of the Regression Model at the State Level	76
7.3	Risk to Bridges and Roads from Bank Erosion due to Stream Migration	76
7.3.1	Methodology	76
7.3.2	Risk Assessment	79
7.3.3	Risk Assessment Summary	80
7.4	Conclusions	83
7.5	Products	83
8.	Overall Project Summary	84
8.1	Existing Knowledge Gap	84
8.2	Project Benefits and Key Findings	85
8.3	Product Summary and Future Work	87
9.	References	88

LIST OF FIGURES

Number	Title	Page
1.1	Examples of bank erosion in Iowa.	1
1.2	Conceptual model of bank erosion mechanisms along a stream corridor.	2
1.3	Fluvial erosion mechanisms.	4
1.4	An example of mass failure near a bridge abutment in Clear Creek, IA.	6
1.5	Bank erosion measurement equipment.	8
3.1	Location of MLRA regions in Iowa.	15
3.2	Stream migration measured in a third-order watershed.	17
3.3	Stream migration measured in a sixth-order watershed.	18
3.4	Annual streambank recession rates measured in Walnut Creek, IA.	19
3.5	Comparison of annual pin-measured streambank recession rates in 3 rd order channels to mean channel migration rates for 3 rd to 6 th -order.	21
4.1	Location of measured eroding lengths in Rathbun Lake watershed in southern Iowa.	24
4.2	Conceptual schematic of modeling approach to estimate severely eroding streambanks.	25
4.3	Relation of streambank heights to bank angle of adjacent 1-m LiDAR elevation cells in the Lake Rathbun watershed.	26

4.4	Spatial correlation of the location of the beginning of a severe bank erosion segment mapped in Walnut Creek watershed.	28
4.5	Location of severely eroding streambank lengths in 3 rd - 6 th order streams of Iowa.	29
4.6	Density of eroding lengths in HUC-8 watersheds in Iowa.	30
4.7	Relation of the fraction of streambank in 3 rd - 6 th order streams in Iowa MLRAs to the average bank heights.	32
5.1	Map of representative sites.	39
5.2	Torvane and penetrometer measurements.	40
5.3	A soil block excavated from a streambank for that determining critical soil strength and erodibility.	42
5.4	Sieving and hydrometer particle size analysis.	43
5.5	The conduit flume to measure critical soil strength and erodibility for surface fluvial erosion.	44
5.6	The photo-electric erosion pin.	45
5.7	Corresponding measurements from a cone penetrometer and Torvane shear stress tester.	46
5.8	Average annual soil moisture measurements.	47
5.9	The Richards-Baker Stream Flashiness Index per drainage area.	49
5.10	Example graphs of the erosion rate vs. the applied shear stress from the conduit flume runs for different soils.	50
5.11	Flume run for freeze-thaw soils.	51
5.12	Time series of (a) water stage, applied shear stresses and the smoothed exposure lengths for the PEEPs at the (b) crest, (c) upper midbank, (d) lower midbank, and (d) toe.	53
6.1	Empirical relationships between critical shear strength and inherent soil properties.	61
6.2	Cumulative density functions for strength and erodibility parameters.	62
6.3	A plot of critical shear stress vs. erodibility.	63
6.4	Changes in critical shear stress and erodibility over the year due to the combined effects of moisture and freeze-thaw cycles.	65
6.5	A plot of critical shear stress vs. erodibility considering subaerial processes.	66
6.6	An example of the flow duration curves.	66
6.7	The relationship between channel slope and fluvial erosion rate determined with BSTEM.	69
7.1	Relation of mean stream migration rates measured in stream segments to all river segments in Iowa.	76
7.2	1980 (a) and 2016 (b) photographs of Highway 38 bridge over the Wapsipinicon River showing encroaching river migration into the bridge infrastructure.	77
7.3	1980 (a) and 2016 (b) photographs of Highway 48 bridge over the East Nishnabotna River showing encroaching river migration into the bridge infrastructure.	78
7.4	1980 (a) and 2016 (b) photographs of Highway 175 bridge near the Maple River showing encroaching river migration into the roads.	78
7.5	1980 (a) and 2016 (b) photographs of Highway 183 bridge near the Soldier River showing encroaching river migration into the roads.	79
7.6	1980 (a) and 2016 (b) photographs of Highway 183 bridge near the Soldier River showing encroaching river migration into the roads.	80

LIST OF TABLES

Number	Title	Page
3.1	Summary of annual streambank recession rates measured with erosion pins.	16
3.2	Summary of annual streambank recession by stream order and MLRA estimated using changes in channel morphology over 25 years.	22
4.1	Summary of eroding streambank lengths and watershed density by MLRA.	31

4.2	Summary of streambank erosion by MLRA, stream order and relation to landscape properties.	33
5.1	Representative sites.	46
5.2	Freeze-thaw cycles.	48
5.3	USGS sites near the sampling locations.	48
5.4	Soil characteristics of surface samples collected at each representative site.	49
5.5	Comparison of observed bank retreat lengths and rates for the PEEPs and pins.	52
5.6	Erodibility parameters for mass fluvial erosion.	54
6.1	Empirical relations for stress and erodibility values.	57
6.2	Strength & erodibility parameters.	61
6.3	Average monthly moisture content per MLRA.	64
6.4	Partition of freeze-thaw cycles.	64
6.5	Flow exceedance values.	67
6.6	The effect of seasonally variable critical shear strength on bank erosion.	67
6.7	Factors of Safety for fluvial erosion.	68
7.1	Variables considered in regression models to describe stream migration.	73
7.2	Final regression models that describe stream mitigation in 3 rd order streams.	74
7.3	Final regression models that describe stream mitigation in 4 th order streams.	74
7.4	Final regression models that describe stream mitigation in 5 th order streams.	75
7.5	Final regression models that describe stream mitigation in 6 th order streams.	75
7.6	Summary of risk assessment evaluation for bridges and road right-of-way by MLRA for 3 rd order streams.	81
7.7	Summary of risk assessment evaluation for bridges and road right-of-way by MLRA for 4 th order streams.	81
7.8	Summary of risk assessment evaluation for bridges and road right-of-way by MLRA for 5 th order streams.	82
7.9	Summary of risk assessment evaluation for bridges and road right-of-way by MLRA for 6 th order streams.	82
7.10	Summary of risk assessment evaluation for bridges and road right-of-way by MLRA for all streams and rivers.	82
7.11	Summary of risk assessment evaluation for bridges and road right-of-way by MLRA for all streams and rivers.	83

EXECUTIVE SUMMARY

In Iowa, bank erosion is a persistent and severe problem that constantly threatens the state's highways and bridge crossings. However, the lack of field data and remote sensing imagery inhibits characterization of the spatial and temporal variability of the soil strength and erodibility parameters causing bank erosion. There is a critical need for a coupled geomorphic-geotechnical-hydraulic approach that utilizes currently available tools (e.g., LiDAR; GIS; PEEPs; recirculating flumes; numerical models) to provide a quantitative, science-based, assessment of bank erosion severity near bridges at a suitable spatial scale and over time.

The Iowa Geological Survey, Iowa Department of Natural Resources, and Hydraulics & Sedimentation Lab at the University of Tennessee-Knoxville provide here an innovative, multi-dimensional approach that utilizes aerial LiDAR surveys to map currently eroding banks in 3rd - 6th order streams that intersect with bridges in Iowa. This approach includes geotechnical and hydraulic data that consider the spatial and temporal variability of bank soil strength under changing climate, moisture, and land-use conditions to provide projected Factors of Safety, as well as the likelihood and severity of bank erosion across Iowa.

Herein, we characterized the range of bank erosion rates in Iowa by examining existing studies. Annual recession rates ranged from -1.2 cm/yr (deposition) in central Iowa to 34.2 cm/yr in southern Iowa. The average recession rate in 3rd order streams was 12.4 ± 10.3 cm/yr. The mean recession rates increased systematically for stream orders 4 through 6 to 18.1, 31.9 and 53.8 cm/yr, respectively. These past studies, though, were limited to the reach scale. Thus, we developed a new approach for identifying severely eroding streambanks that uses the slopes between adjacent cells in a high-resolution LiDAR coverage map to characterize the relationship between streambank angles and streambank heights. The method was applied to the 3rd - 6th order streams across the state for a first-order approximation of eroding streambank lengths in Iowa. Approximately 35,200 km of the banks along 3rd to 6th order rivers in Iowa are severely eroding, which is 41% of the total streambank length in the state. This is double that of a "natural" stream, which suggests streambank erosion has been enhanced by external forcings.

With this degree of variability in soil properties, topography, weather, land-uses and hence erosion rates in Iowa, it would seem inappropriate to develop a single predictive relationship for all of the state's stream miles. We did observe some regional generalities, though, that would help minimize the number of needed relationships. This study substantiated spatial patterns and temporal cycles of bank erosion in the Major Land Resource Areas (MLRAs) of the state. MLRAs 107A, 107B, 108C, and 108D have similarities most likely due to the loess soils in western and southern Iowa. These soils have higher average critical shear stresses than the coarser till-derived soils in MLRAs 103 and 104 of north central and northeast Iowa. However, MLRAs 107A and 107B have Factors of Safety less than one for ~95% of their observed flows suggesting that fluvial erosion is likely. Thus, they have high densities of eroding banks per area.

Along with this spatial variability in soil strength and erodibility, there is temporal variability related to soil moisture and freeze-thaw cycles which weaken the soil's strength. The critical shear strength reaches minimum values during March and April when soil moisture is high and there are several freeze-thaw events. The strength peaks in August when the effects of freeze-thaw are non-existent and soil moisture is at a moderate level. Over the winter, MLRAs 103 and 107A have high critical shear stress values during the winter due primarily to low

moisture content, while MLRAs 104 and 108D have high moisture content over the winter and thus lower critical shear stress values.

Regression models using existing databases and new GIS coverages developed during this project were established using eleven parameters including bank height, stream sinuosity, stream slope, available water capacity, clay content, and bulk density, among other parameters. Stream length to bridge length ratios were used to identify the potential impact for bridges in the near future. For the roadways, stream migration polygons were buffered 20 feet and intersected with right-of-way features to identify roads that may be impacted by lateral movement from streams. Bridge crossings with a high ratio and a stream having a high potential for migration were flagged.

Overall, the greatest number of bridges threatened by stream migration were found in MLRA 107B and 108D, followed closely by MLRAs 103 and 107A. The greatest risk to road ROWs were also assessed in MLRA 107B and 103. All-together, the project identified 1,515 bridges and 281 road right-of-ways in Iowa that were considered to be at high or moderate risk to future erosion and channel migration.

This study produced four published peer-reviewed manuscripts (and 1 manuscript in preparation), which included an estimation of bank erosion in the state, as well as an assessment of the degree of spatial and temporal heterogeneity of bank soil strength, erodibility, and Factors of Safety for a range of flows conditions. This study also provided a LiDAR-based algorithm to identify eroding streambanks at a regional scale and regression models at the regional scale using common geomorphic and geotechnical parameters to quantify bank retreat. Geodatabases and coverage maps of severely eroding stream banks that intersects with bridge and roadway infrastructure were provided to the Iowa Department of Transportation as a means to prioritize those bridge structures across the state that need further protection from pending bank failures.

SECTION 1: INTRODUCTION & BACKGROUND

1.1 Problem Statement

The link between streambank stability with the safety of bridge and roadway infrastructure has been well established through several hydraulic studies (e.g., Odgaard & Lee, 1984; Lagasse et al., 2001; Ettema et al., 2006; Johnson, 2006a; Barkdoll et al., 2007). In Iowa, with bank erosion being a persistent and severe problem (Simon & Klimetz, 2008; Wilson et al., 2008; Schilling et al., 2011), the state's bridge crossings are constantly at risk (Figure 1.1).

The exacerbated stream bank erosion observed in Iowa results from channel instability triggered by extensive land-use change and channelization that occurred throughout the early 20th century (Rhoads, 2020). Since that time, the accumulated damage to bridges, roadways, pipelines, fiber-optic cables, and adjacent farmland totals in the billions of dollars (e.g., Hadish et al., 1994; Schmidt, 2017).

State and county entities, including the Iowa Department of Transportation, have examined multitudes of installed barbs, vanes, weirs, riprap, and other stabilization structures to determine their effectiveness at preventing further damage to the downstream infrastructure (Behm et al., 1998; Wipf et al., 2003; Papanicolaou & Elhakeem, 2006; Bressan et al., 2014; Elhakeem et al., 2017). Despite this attention, little ground has been gained to minimize the persistent bank erosion threat. Because further action is still required but financial resources are dwindling, it is becoming increasingly difficult to monitor and address existing problem sites, let alone to identify and plan for upcoming problems. As it stands, the funding shortfall in Iowa over the next few decades to address existing problems exceeds \$1.6 billion per year (Iowa Department of Transportation, 2011).

Major obstacles against addressing the excessive bank erosion rates are the highly variable geomorphic, geotechnical, and hydraulic factors affecting bank erosion which occur across multiple spatial and temporal scales (e.g., Palmer et al., 2014). Mechanisms driving streambank erosion (i.e., subaerial processes; fluvial and mass erosion; mass wasting) not only differ among watersheds, but even within the same watershed (Fox et al., 2016). Annual streambank contributions to the sediment load of a single river can range from <10% during dry

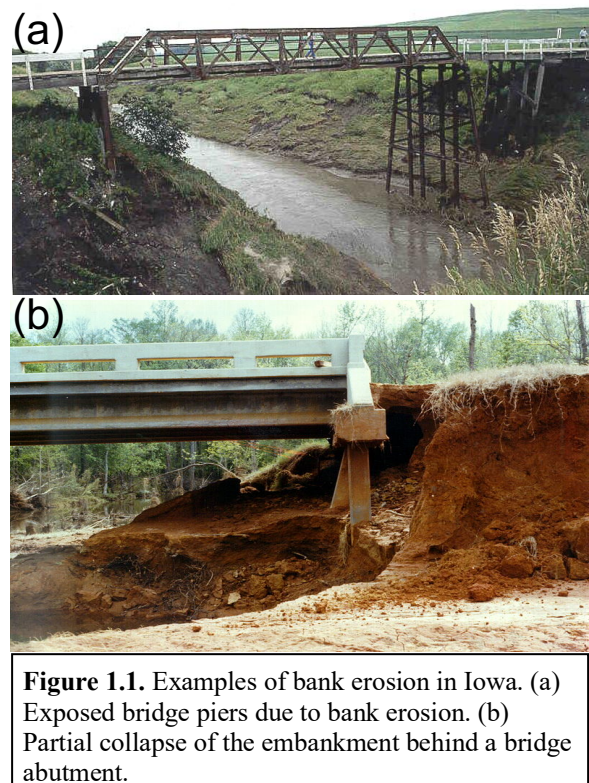


Figure 1.1. Examples of bank erosion in Iowa. (a) Exposed bridge piers due to bank erosion. (b) Partial collapse of the embankment behind a bridge abutment.

years to almost 96% during wet years (e.g., Wilkin et al., 1982; Hamlett et al., 1983; Thoma et al., 2005; Belmont et al., 2011; Willett et al., 2012; Wilson et al., 2014). This inherent variability is intensified by ever-changing land-use and a transitional climate with rising temperatures, as well as more frequent freeze-thaw and wet-dry cycles that weaken bank soil strength (Peizhen et al., 2001; Ferrick & Gatto, 2006; Wynn et al., 2008).

Mechanistic understanding of bank erosion processes has been obtained at individual sites (e.g., Lawler, 1992a; Simon & Collison, 2002; Fox et al., 2007; Fox & Wilson, 2010; Daly et al., 2015), but there is a lack of field-oriented and remotely sensed data to characterize the spatial and temporal variability of the processes at larger scales. Current bank stability assessment techniques include standardized checklists that characterize “healthy” versus “threatened” streambanks based on single site visits (Doheny, 1996; Newton et al., 1998; Rosgen, 2001; Johnson, 2005; Keil, 2006). Most of these assessments have been reasonably effective at identifying existing problems but they are unable to project upcoming problems as they do not evaluate channel degradation holistically by considering the geomorphic, geotechnical, and hydraulic properties, as well as the multiple mechanisms of bank erosion over a wide range of stream orders, climate conditions, and discharges (Bryan, 2000).

Thus, a critical need exists to develop a *data-driven* protocol that identifies and quantifies the severity of bank erosion near bridge sites *at a suitable spatial scale and over time*. The protocol can facilitate a decision-making process that selects near-optimal stabilization methods for a site considering the complex interactions between local soil types, vegetation, intense agricultural activity, increasing urbanization, and climate non-stationarity.

1.2 Bank Erosion Mechanisms

Bank retreat is the integrated outcome of subaerial processes, surface & mass fluvial erosion, mass failure, and meandering (Rinaldi & Darby, 2008). Figure 1.2 conceptualizes where each mechanism occurs within a watershed and is most prevalent. It is apparent from the figure that the mechanisms, for the most part, occur throughout the entire watershed but to different degrees.

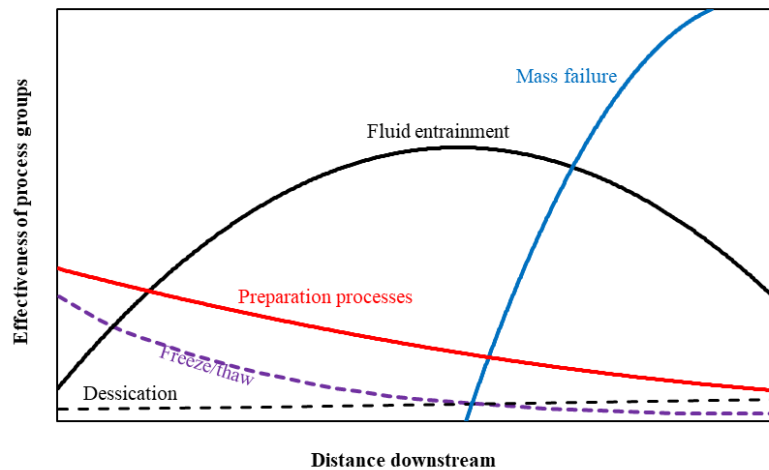


Figure 1.2. Conceptual model of bank erosion mechanisms along a stream corridor (after Lawler, 1992a).

Thus, the subaerial, hydraulic, geomorphic, and geotechnical driving factors must all be considered when quantifying bank erosion risk (Lawler, 1992a).

1.2.1 Subaerial Processes

Subaerial processes are characterized as “preparatory” processes (Couper & Maddock, 2001) since they lead to an overall weakening of the bank soil, thus increasing its erodibility (Thorne, 1982). The different processes result from changing weather and include the prewetting, desiccation, and freezing-thawing of the surface soil (Lawler et al., 1997). Pre-wetting mechanisms increase the streambank soil moisture content. They can include high flows during storm events, water table rises, and rainfall infiltration. The increasing water content under wetting lowers the cohesion between clay particles within aggregates fairly quickly (Bryan, 2000). Desiccation mechanisms dry the soil and cause it to crack and exfoliate, while freezing-thawing disintegrates soil structure and reduces aggregation. The degree of disintegration has been reported to be directly related to the soil water content at freezing and the freezing rate. (Mostaghimi et al., 1988).

Subaerial processes are most prevalent in the upper reaches of river systems (Figure 1.2). As they occur, they both increase erodibility and can release soil directly to the stream channel (Lawler et al., 1997). Significant increases in erosion have been observed following subaerial events (Prosser et al., 2000; Couper & Maddock, 2001).

1.2.2 Surface Fluvial Erosion

Fluvial erosion is the entrainment of bank soils into the flow resulting from an applied fluid shear stress, τ_w (Millar & Quick, 1998; Huang et al., 2006). Surface fluvial erosion is a low-magnitude mechanism with a characteristic retreat scale during an event on the order of singular soil grains or flocs, i.e., millimeters (Figure 1.3a). In addition, surface fluvial erosion is a high frequency, quasi-continuous process occurring in all storm runoff events and potentially along several segments of the channel reach (Rinaldi & Darby, 2008).

Grain entrainment begins when fluid shear forces acting over the bank face supersede the resistance offered by the effective cohesion between the soil grains (Righetti & Lucarelli, 2007; Partheniades, 2009) from the combination of electrostatic, Coulomb, van der Waals, hydration, and biological forces (e.g., Ferrick & Gatto, 2005). For cohesive and semi-cohesive soils, the resistance is modulated by biogeochemical properties including pore water chemistry, clay mineralogy, and soil composition (Arulanandan, 1975; van Klaveren & McCool, 1998) that influence the inter-particle attraction forces. A surrogate measure of this resistance is the *critical*

fluvial erosional stress, $\tau_{c,f}$ (Pa), which is a microscale quantity (e.g., Partheniades, 1965). The rate of surface fluvial erosion, E_f (m/s), can be determined using an excess shear stress equation (Kandiah, 1974):

$$E_f = M_f (\tau_w - \tau_{c,f}) \quad (1.1)$$

where M_f ($\text{m}^3/\text{N}\cdot\text{s}$) is the erodibility coefficient. The stability of a streambank against surface fluvial erosion is quantified as the ratio of resisting forces to the applied shear stress (e.g., Millar & Quick, 1998):

$$FS_f = \frac{\tau_{c,f}}{\tau_w} \quad (1.2)$$

where FS_f is the Factor of Safety that defines the ratio. The bank face will likely experience surface fluvial erosion when $FS_f < 1$. In contrast, bank soils will be resistant to fluvial shear if $FS_f > 1$.

1.2.3 Mass Fluvial Erosion

With fluvial entrainment certain researchers have noticed a shift in the erosion behavior above a shear stress that is greater than $\tau_{c,f}$ (Papanicolaou et al., 2017). This shift has been observed both with coastal sediments (e.g., Chapuis, 1986; Mostafa et al., 2008; Winterwerp et al., 2012), as well as with upland and streambank soils (e.g., Kamphuis et al., 1990; Wilson, 1993a,b; Gaskin et al., 2003; Kothyari & Jain, 2008; Al-Madhhachi et al., 2014). With the recognition of this shift, the resulting different regimes of

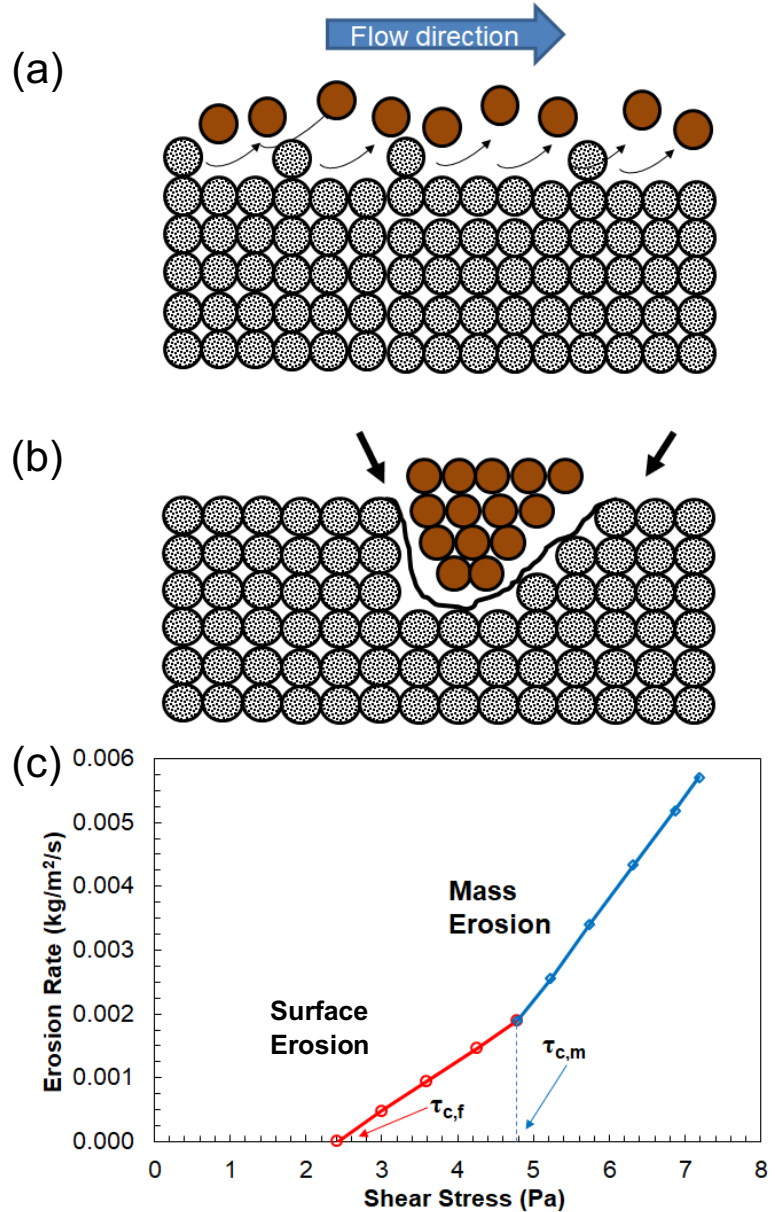


Figure 1.3. Fluvial erosion mechanisms. (a) Schematic of surface fluvial erosion with entrainment of individual grains; (b) Schematic of mass fluvial erosion with detachment of soil clods. (c) Ideal illustration of threshold between fluvial surface erosion (red line) and mass erosion (blue line). Both a and b are from Winterwerp & Van Kesteren (2004); c is from Papanicolaou et al. (2017).

fluvial erosion have been partitioned into the *surface fluvial erosion* regime (Figure 1.3a) and the *mass fluvial erosion* regime (Figure 1.3b).

Under surface fluvial erosion, the available stock of easily erodible, fine soil particles on the bank face can deplete to exhaustion. The inability of low-shear-stress flows to dislodge coarser, sand-sized particles which remain on the bank surface may be a triggering mechanism for the shift to mass fluvial erosion. The larger sediment particles armor the bank face and anchor incoming finer size particles (Reed et al., 1999; Le Hir et al., 2011; Motta et al., 2012).

Clay minerals and calcium carbonates, which can be found in loess-derived soils, also adhere to the coarser sand particles. With favorable proportions of sand and clay, this adherence can lead to cementation (e.g., Krintzsky & Turnbull, 1967) as the attached particles form a thin coat or layer (e.g., Trhlikova, 2013). As these layers consolidate, added resistance to the flow develops, producing the need for higher applied shear stresses to overcome the armoring and cementation so that erosion can continue (e.g., van Kessel & Blom, 1998; Winterwerp et al., 2012).

The transition from surface to mass fluvial erosion occurs when τ_w surpasses a second threshold value, called the critical shear stress for mass fluvial erosion, $\tau_{c,m}$ (e.g., Huang et al., 2006). This shift can be visualized as a change in the gradient for a plot of erosion rate versus τ_w . Figure 1.3c is a conceptual schematic of the gradient change and the shift from surface fluvial erosion (red circle-marked line) to mass fluvial erosion (blue square-marked line) once the shear stress surpasses $\tau_{c,m}$. The slope of the segment corresponding to mass fluvial erosion is also higher than the one for surface fluvial erosion, indicating higher erosion rates. When this second threshold is reached, the thin layers of adhering particles are plucked from the soil surface (Figure 1.3b).

Mass fluvial erosion is also a quasi-continuous process (Vermeyen, 1995) but it results in a larger retreat compared to surface fluvial erosion with event-scale retreat lengths in centimeters (e.g., Gaskin et al., 2003). Similar to surface fluvial erosion, the mass erosion rate, E_m , can be determined using a similar excess shear stress formula as Equation 1.1. The stability of a streambank against mass erosion can also be expressed with a Factor of Safety, FS_m , similar to Equation 1.2.

Understanding the transition from surface to mass fluvial erosion and quantifying mass fluvial erosion rates are crucial for constructing the spectrum of hydraulic conditions over which bank erosion occurs. Few studies, thus far, consider the spectrum of hydraulic conditions across the two fluvial regimes. This knowledge is also important for developing watershed-scale sediment budgets that account for eroded bank material contributions (e.g., Wilson et al., 2012).

1.2.4 Mass Failure

Mass failure is a high-magnitude erosion process with a characteristic length scale usually in meters (Figure 1.4). It is also a low-frequency process occurring discretely in time and it is more localized in space than fluvial surface and mass erosion, occurring at “isolated” locations along the stream corridor where critical bank heights have been exceeded (Rinaldi & Darby, 2008).



Figure 1.4. An example of mass failure near a bridge abutment in Clear Creek, IA.

Mass failure usually occurs as the slumping of soil blocks along an embedded plane due to interrelated mechanical and hydrologic mechanisms, such as the development of positive pore water pressure within the bank profile (e.g., Pizzuto, 1984; Millar & Quick, 1998; Simon & Rinaldi, 2000), the rapid drawdown of the water stage (e.g., Langendoen, 2010), and the occurrence of high seepage gradient forces (e.g., Chu-Agor et al., 2009; Midgley et al., 2012). In addition to slumping, mass failure can occur from rotational failure, piping, and groundwater sapping (e.g. Thorne, 1982; Langendoen, 2000).

The collapse of a soil block is determined with the relationship between its bulk weight and the different resisting forces from root vegetation, the temporary confining pressure of the stream water during high stages (e.g., Pollen & Simon, 2005; Pizzuto, 2009), and its soil shear strength, S_r (Pa), integrated over the slip plane area. According to the Mohr-Coulomb theory, S_r is dependent on the internal friction angle, θ' (degrees), and the soil mechanical strength, c' (Pa), which is a macroscale parameter (Millar and Quick, 1998). The soil shear strength is defined as follows (Fredlund & Rahardjo, 1993):

$$S_r = c' + \sigma \tan\theta' - u \tan\theta^b \quad (1.3)$$

where σ (Pa) is the normal stress produced by the weight of the soil block; u (Pa) is the soil pore water pressure; and θ^b (degrees) is the angle expressing the rate of increase in shear strength relative to the matric suction. When the bank is saturated, matric suction diminishes and $\tan \theta' = \theta^b$. For quantifying the mass failure Factor of Safety, FS_{MF} , of a soil block, the block is subdivided into multiple vertical slices to ensure adequate representation of all soil layering found in the block. The driving and resisting forces are then calculated for each slice and

integrated over the whole block. The FS_{MF} can then be estimated as follows (Langendoen et al., 2009):

$$FS_{MF} = \frac{\sec \alpha \sum_{j=1}^K L_j S_{rj}}{\tan \alpha \sum_{j=1}^K W_j - F_w} \quad (1.4)$$

where α (degrees) is the angle of the planar failure surface; K is the total number of block slices; j denotes the slice number; L (m) is the length of the slice plane base; W (N) is the slice weight; and F_w (N) is the hydrostatic confining force exerted on the bank profile. The bank is considered stable if $FS_{MF} > 1$, whereas the bank is unstable if $FS_{MF} < 1$.

1.2.5 Meandering

Channel migration in a drainage basin is often evident across several spatial scales (Lagasse et al., 2004). Through a gradual shift of the bankline over time, the associated bank erosion undermines bridge abutments and scours the foundations of adjacent roadways (Briaud et al., 2007). Bank erosion rates can vary widely along a meandering reach, as they are influenced by complex interactions between flow, channel morphology (i.e., curvature), the density of vegetation on the floodplain, and the bank soil properties (Hooke, 1980). Several efforts have qualitatively described the impact of these local influences on meandering with more quantitative efforts lagging behind (Eke et al., 2014). The threat of meandering to bridge infrastructure is hard to predict due to the lack of quantitative methods.

1.3 Available Methods for Estimating Bank Stability Parameters

There have been substantial developments in bank erosion research recently (Papanicolaou et al., 2006; Grabowski et al., 2011). This new research has illuminated the importance of riparian vegetation (e.g., Wynn & Mostaghimi, 2006; Pollen, 2007), bank soil hydrology including porewater pressure and seepage flows (Rinaldi et al., 2004; Wilson et al., 2007; Fox & Wilson, 2010), form roughness (Darby et al., 2010), and secondary flows (Papanicolaou et al., 2007; Stoesser et al., 2010). Few studies, though, have applied this knowledge to quantify bank recession rates at suitable spatial and temporal management scales (Sutarto et al., 2014; Palmer et al., 2014). More studies using these techniques are needed to predict better bank erosion likelihood under changing climate and land-use conditions (e.g., Papanicolaou et al., 2017).

1.3.1 Surface Fluvial Erosion Methods

The various methods to identify the onset of surface fluvial erosion and quantify the corresponding strength and erodibility parameters, namely $\tau_{c,f}$ and M_f , can be divided into in-situ and laboratory techniques. In-situ techniques consist of submerged jet devices (Figure 1.5a;

Hanson & Cook, 2004; Al-Madhhachi et al., 2013; Mahalder et al., 2018) and mini-flumes (Figure 1.5b; Aberle et al., 2003; Roberts et al., 2003; Debnath et al., 2007). Both types have advantages and limitations associated to their portability, practicality, and ability to capture the processes occurring in nature. Jet devices apply an impinging flow to the soil surface, which deviates from the accepted assumption of shear being the primary driver of bank fluvial erosion (Sutarto et al., 2014). Moreover, the confinement of the impinging jet has been found to increase the derived critical shear stress and decrease the erodibility coefficient by a factor of ~ 2.4 relative to unconfined flow (Karamigolbaghi et al., 2017). Conversely, mini-flumes exert a shear force over the sample, but it is only low flows with low shear stress values due to their short lengths. Thus, the mini-flume is applicable only for estuarine bed sediments, which are mostly comprised of soft flocculent deposits that can be eroded at low shear stresses (e.g., Roberts & Jepsen, 2001).

Laboratory flumes can produce higher applied stresses, but bringing an intact sample into the lab is difficult. There are several types of laboratory flumes, namely annular (Parchure & Mehta, 1985; Gharabaghi et al., 2007; Figure 1.5c), straight open channel (e.g., Papanicolaou et al., 2007; 2020; Figure 1.5d), and closed conduit flumes (e.g., Roberts et al., 2003; Sutarto et al., 2014; Figure 1.5e). The rotating annular flume has an infinite flow length for establishing fully developed flow, but it generates significant secondary currents that produce non-uniform shear stress distributions in the lateral direction (Parchure & Mehta, 1985). Open channel flumes generate only low flows which are not suited for analyzing well compacted, cohesive, bank soils (e.g., Papanicolaou et al., 2007). To address these limitations, a conduit flume can be used (Sutarto et al., 2014).

1.3.2 Mass Fluvial Erosion Methods

Flumes and jet devices can measure surface fluvial erosion parameters, but they cannot reliably provide repeated measurements due to sediment exhaustion (e.g., Roberts & Jepsen, 2001; Al-Madhhachi et al., 2013; Sutarto et al., 2014). In-field measuring devices that measure bank retreat quasi-continuously to capture both the initiation and magnitude of these mass erosion events are needed (Papanicolaou et al., 2017). Traditional, field-based, measurement methods such as channel cross-section surveys, terrestrial photogrammetry, and conventional erosion pins cannot capture the quasi-continuous nature of mass fluvial erosion for relating retreat lengths with specific hydrologic events and corresponding stress levels, since they are conducted at discrete time instances (e.g., Myers et al., 2019). Remote sensing techniques, such as bathymetric Light Detection and Ranging (LiDAR) technology, cannot capture the localized response of a bank to a hydrologic event due to their limited accuracy for quantifying event-based, bank retreats at length scales (e.g., Pizzuto et al., 2010; Plenner et al., 2016).

Photo Electronic Erosion Pins (PEEPs; Figure 1.5f) have been used successfully for measuring quasi-continuous retreat lengths in response to different hydrologic events (e.g., Lawler, 1991; 1992b; Bertrand, 2010; Zaines & Schultz, 2015; Papanicolaou et al., 2017). A PEEP is a simple, optoelectronic device containing a series of either photo-resistant or photo-voltaic cells (i.e., diodes) enclosed within a waterproofed, transparent, acrylic tube (Lawler, 1991). The diodes are spaced at the centimeter scale making PEEP's ideal for acquiring retreat lengths corresponding to mass fluvial erosion of soil clods (Papanicolaou et al., 2017).

1.3.3 Mass Failure Methods

Current visual assessments of bank erosion, whether they are from the ground or the air, are helpful in determining the stage of evolution for the channel by looking at the shape of the cross-section and stream banks (e.g., Simon & Hupp, 1986; Rosgen, 1994; Simon & Klimetz, 2008). However, these assessments are qualitative in nature and can be highly subjective (Lawler, 2008). Moreover, the mapping of mass failure locations in a watershed using field reconnaissance is exhaustive and time-consuming, which probably explains why it is rarely done.

Additionally, assessments that utilize field measurements to quantify bank retreat involving conventional monitoring methods (e.g., erosion pins and channel surveys) provide only net bank retreat since the previous sampling making it difficult to capture the effects of the driving processes and the relationship between the triggering event and the response of the bank soils. Schilling and Wolter (2000) used global positioning system (GPS) technology alongside field measurements to map channel features, including severe streambank erosion, in a 12-km reach of an Iowa 4th-order stream. Other researchers have used similar field methodology to map eroding streambank lengths in Iowa (Tufekcioglu et al., 2012; Palmer et al., 2014; Beck et al., 2018). Studies that couple visual and monitoring methods provide valuable spatially diverse measurements, but they cannot capture the preparatory or triggering events that cause the erosion and that are needed for improving predictive ability.

1.3.4 LiDAR and Aerial Mapping

Because LiDAR data are readily available, especially in Iowa, they can be useful for quantifying stream channel planform geometry for entire drainage basins (e.g., Kessler et al., 2012). With a single LiDAR flight, thousands of points on the landscape surface can be scanned and when coupled with a GPS and inertial measurement unit record the aircraft's position and altitude (roll, pitch, and yaw), one can obtain a high-resolution (<1-m horizontal < 20-cm vertical) digital elevation map (Gilvear et al., 2004). Airborne LiDAR data of a river valley taken at two

different times provide an estimate of the change in the volume of the valley as a result of bank erosion, sloughing, and accretion (Michelli & Kirchner, 2002).

Additionally, the use of a geographic information system (GIS) and aerial imagery is an established way for measuring stream channel changes over time. Successive images can detect rates of meander migration and having it in a GIS format allows resource managers to use the results as a baseline for future studies (Gilvear et al., 2004). The GIS framework also allows for a comprehensive database to be developed linking the elevation statistics of bank height and angle with the images of bankline change. Moreover, the combination of these methods allows for developing regional trends and characteristics of net bank erosion.

1.4 Interaction among Bank Erosion Mechanisms

Figure 1.2 provides a good representation of the relationship between the different bank erosion processes along a river continuum. In the headwaters (i.e., 1st and 2nd order streams), subaerial processes are most apparent, along with surface fluvial erosion. For the middle reaches of a watershed (i.e., 3rd and 4th order streams) where the stream power, and therefore, the shearing action of flow is highest, fluvial and mass erosion will dominate. Generally, mass failure is most prominent in the lower reaches of a watershed (i.e., 5th and 6th order streams) where the critical bank height is more often exceeded.

The bank erosion mechanisms are likely to act in conjunction along a stream reach (Langendoen, 2000). Particularly in 3rd to 6th order drainage basins, bank retreat is likely to be driven by a combination of subaerial, fluvial and geotechnical driving forces. For example, fluvial erosion, which most often occurs at the bank toe, can cause bank steepening and toe undercutting, leading to mass failure. Because of the presence of all these mechanisms and higher erosion rates, this study will focus in these upper stream orders.

From a modeling perspective, the integration of the bank erosion mechanisms in a single framework is very important in order to estimate correctly the timing, frequency, and magnitude of erosion events (Langendoen & Alonso, 2008; Rinaldi & Darby, 2008). To capture fully the complex interactions between the bank erosion mechanisms, it is necessary to investigate bank changes at the intra-event scale. Logistical and safety concerns usually limit surveys and monitoring of bank erosion to singular, isolated visual assessments.

A coupled geomorphic-geotechnical-hydraulic approach that utilizes currently available tools (e.g., LiDAR; GIS; PEEPs; recirculating flumes; numerical models) can provide a more quantitative, process-based, assessment approach than field reconnaissance (e.g., RASCAL assessments; Keil, 2006).

Large-scale assessments using remote sensing techniques can capture the spatial variability of bank erosion at the watershed scale. The geomorphic information offers a snapshot of banks undergoing erosion and can be used to narrow down quickly the number of threatened reaches. The method can cover the whole state in less time than on-site assessments and provides the range of spatial variability (e.g., Schilling & Wolter, 2000; Johnson, 2006b; Palmer et al., 2014; Daly et al., 2015).

Localized measurements of geotechnical parameters in representative reaches coupled with PEEP measurements can capture the spatial and temporal variability of strength/erodibility parameters under a range of flow, weather, moisture, and land-use conditions. By quantifying changes in critical bank soil stresses over time in comparison with historical stream flow records, and other hydraulic information, it can be determined how often the stream reach experiences flows that exceed the critical shear stress and we get a likelihood of bank erosion. From a practical sense, the erosion likelihood values offer a means for prioritizing sites in need of some further monitoring or remedial work.

It also offers the ability to see what the bank would look like under that degree of erosion, as well as how far to extend a bank erosion countermeasure. Moreover, by looking at the bank profiles and the range of expected flows, a better idea of what type of countermeasure can be used (e.g., riprap vs. some form of bio-stabilization).

SECTION 2: PROJECT GOALS & PRODUCTS

2.1 Overview of Project Goals

Bank erosion is a persistent threat to highway and county road infrastructure in Iowa. In order to diminish this threat, the full extent of the problem must first be known. A broad-scale, multi-mechanistic assessment approach that is data-driven, supported by field studies and remote sensing surveys at representative sites to provide the range of variability in a region is needed so that the Iowa Department of Transportation, as well as other state, county, and municipal agencies can prioritize sites for rehabilitation.

The Iowa Geological Survey at the University of Iowa and the Iowa Department of Natural Resources, in collaboration with researchers from the Hydraulics & Sedimentation Lab at the University of Tennessee-Knoxville, provide herein an innovative, multi-dimensional approach that utilizes aerial LiDAR surveys to develop a map for currently eroding banks in 3rd - 6th order streams intersected with bridge structures in Iowa. This is combined with geotechnical and hydraulic data that consider both the spatial and temporal variability of the bank soil strength under changing climate, moisture, and land-use conditions to provide Factors of Safety, as well as the likelihood and severity of bank erosion across Iowa at selected sites. In sum, this coupled approach provides the Iowa Department of Transportation a means to prioritize those bridge structures across the state that need further protection from pending bank failures.

2.2 Organization of this Report & Products

The remaining sections of this report are structured as follows:

Section 3 details an evaluation of streambank recession rates in Iowa compiled from a multitude of erosion pin studies and coupled with aerial imagery to provide both local and watershed-scale estimates of annual streambank contributions. The study uses a top-down approach to look for similarities or patterns across stream orders that could be generalized and scaled up for regional assessments. This section provides a spatial context for evaluating streambank recession in Iowa that translates to a preliminary coverage map of severely eroding stream banks. It also offers a good overview of the state of bank erosion in Iowa.

Section 4 builds on these results to offer a new approach for assessing the extent of eroding streambanks in 3rd - 6th order streams using high resolution LiDAR elevation data. The approach is calibrated and validated using field mapping campaigns in two Iowa watersheds. When this approach is applied at the state level, it shows that the extent of streambank erosion is not uniform across the state, but it is regionally based.

Section 5 takes a more detailed approach looking within the various regions of the state at representative reaches to understand the spatial and temporal variability of bank soil strength and erodibility parameters for the different bank erosion mechanisms. The section discusses the collection of soils for geotechnical analyses, which includes measurements of surface fluvial erosion strength and erodibility. Additionally, the use of PEEPs to provide the strength and erodibility parameters for mass fluvial erosion is described.

Section 6 discusses the modeling of selected sites to quantify Factors of Safety that provide the likelihood and severity of bank erosion across Iowa. The field and lab measurements from the previous section were used as input parameters for the Bank Stability and Toe Erosion Model (BSTEM) to estimate the degree of erosion and Factors of Safety for a wide range of flow values.

Section 7 discusses the regression modeling that links channel planform migration to geomorphic and geotechnical characteristics including sinuosity, stream bed slope, bank height organic matter content, clay content, bulk density, and land-use. The regression models were used to assign relative risks to right-of-way coverages and identify those structures likely to be impacted by stream channel meandering.

Section 8 offers a summary of the conclusions drawn from the above studies, as well as recommendations to the Department of Transportation. The key products that are provided by this study are the following:

- A state-wide estimation of bank erosion in Iowa.
- An algorithm to identify eroding streambanks at a regional scale using high resolution LiDAR elevation data.
- Assessment of the degree of spatial and temporal heterogeneity of bank soil strength and erodibility parameters at bridge sites using in-situ bank strength measurements and critical shear strength from bank soil samples with a conduit flume.
- Quantification of Factors of Safety for a range of flows at selected bridge crossings using models and likelihood of erosion over time.
- A regression model at the regional scale using common geomorphic and geotechnical parameters to quantify bank retreat.
- Geodatabases and coverage map of severely eroding stream banks that intersects with Iowa DOT infrastructure data to determine potentially threatened structures.

SECTION 3: AN ASSESSMENT OF STREAMBANK RECESSION RATES IN IOWA

3.1 Goal Statement

In support of the overarching goal for this study to develop a broad-scale, multi-mechanistic assessment approach for identifying bridge and roadway infrastructure sites under the threat of severe bank erosion and quantifying the degree of the threat, this section looks for similarities or emergent patterns of streambank recession rates in Iowa that could be generalized across scales. This section examines erosion pin studies coupled with aerial imagery to quantify annual bank erosion rates and assess the variability across stream order and geographically similar areas.

3.2 Methodology

3.2.1 Methodological Overview

Various methods have been used to evaluate streambank erosion in Iowa, including cross-sectional surveys, photogrammetric methods, and sequential aerial photographs (Fox et al., 2016; Tomer & Van Horn, 2018). In low-order streams, erosion pins have been used to measure recession rates in targeted reaches with eroding bank segments (e.g., Zaimes et al., 2004; Tufekcioglu et al., 2012; Palmer et al., 2014; Beck et al., 2018). The approach herein couples extensive erosion pin data from throughout the state with aerial infrared photographs from the mid-1980s and late 2000s to identify emergent patterns of bank erosion for higher order systems.

3.2.2 Regional Setting

The bank erosion studies examined in this section were grouped by the different Major Land Resource Areas, or MLRAs, in the state. MLRAs are geographically associated landscapes delineated by the Natural Resources Conservation Service to characterize regions based on similar soils, landscape features, precipitation, and temperature. There are 204 MLRAs in the United States, ranging in size from less than 2000 km² to more than 240,000 km². Iowa is part of 10 MLRAs, which are similar to Iowa landform regions (Prior, 1991) and ecoregions (Griffith et al., 1994). Herein the eight major MLRAs were considered in the analysis (Figure 3.1).

The surficial geology of Iowa is dominated by Pleistocene glacial deposits consisting of fine-textured glacial till and loess of varying ages (Prior, 1991). The Wisconsin-age Des Moines Lobe represents the most recent glacial advance into Iowa around 12,000 years ago (MLRA 103 – Central Iowa and Minnesota Till Prairies). The low-relief topography of the region stands in contrast to the hillslope-dominated terrain found in the western and southern parts of the state. MLRA region 107B (Iowa and Missouri Deep Loess Hills) is dominated by thick loess deposits,

whereas MLRA regions 108C (Illinois and Iowa Deep Loess and Drift, West-Central Part), 108D (Illinois and Iowa Deep Loess and Drift, Western Part), and 109 (Iowa and Missouri Heavy Till Plain) in southern and southeast Iowa consist largely of rolling landscapes with a thinning layer of loess over pre-Illinoian till. The topography of MLRAs 104 (Eastern Iowa and Minnesota Till Prairies) and 107A (Iowa and

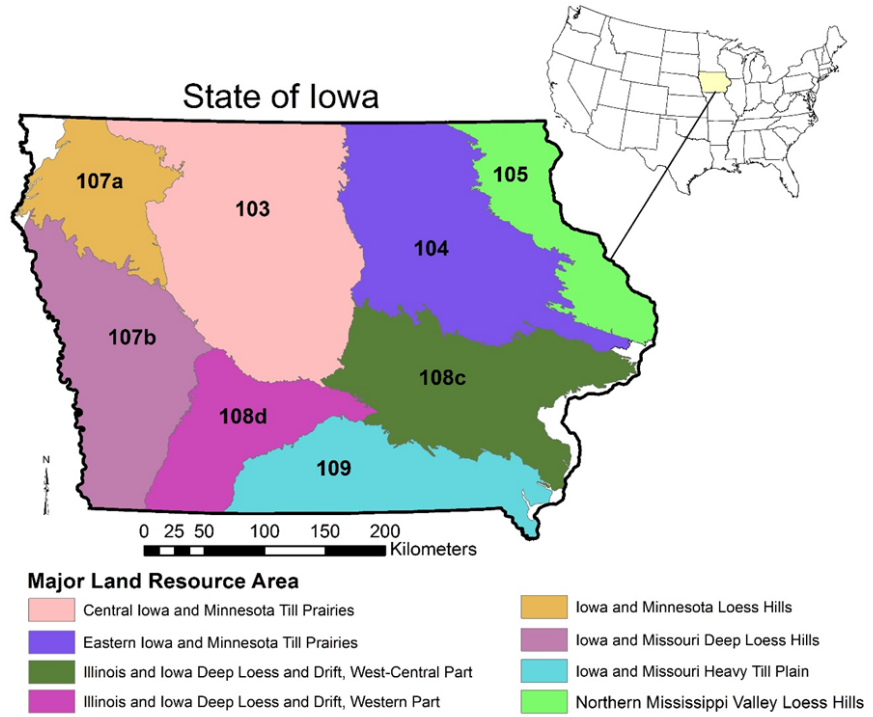


Figure 3.1. Location of MLRA regions in Iowa.

Minnesota Loess Hills) slope less due to the loess cover over recent glacial sediment (107A), as well as extensive erosion (104). The landscape and river corridors in northeast Iowa for MLRA region 105 (Northern Mississippi Valley Loess Hills) are dominated by thin soils overlying fractured Paleozoic bedrock.

3.2.3 Erosion Pins

Erosion pins have been used by several researchers to assess bank recession in 3rd to 4th order streams in Iowa (Zaimes et al., 2006; Tufekcioglu et al., 2012; Palmer et al., 2014; Beck et al., 2018; Williams, 2019). In total, erosion pins are available for 385 streambanks in Iowa (Table 3.1). The erosion pin methodologies used in these studies are comparable as they have been conducted by similar groups of researchers from the Department of Natural Resource Ecology and Management at Iowa State University.

Briefly, stream surveys were conducted to identify the eroding streambanks within a study reach. A subset of the eroding banks was randomly selected for pin installation. The installed pins measured 762 mm in length and 6.2 mm in diameter. They were installed along the bank face in a grid spaced vertically at 1/3 and 2/3 of the bank height, and horizontally one meter apart along the entire length of the selected reach. Beck et al. (2018) modified the arrangement of pins to account for variations in alluvial stratigraphy by installing pins at the midpoints of exposed stratigraphic units.

The exposed pin lengths were measured using a ruler. An increase in the exposed length from the previous measurement was attributed to erosion, whereas a decrease in length was assumed to indicate deposition. The frequency of pin measurements varied among study sites and projects, but herein the compiled pin data were aggregated to provide annual erosion rates.

Table 3.1. Summary of annual streambank recession rates in Iowa measured with erosion pins.

Study	MLRA	Years of monitoring	Number of banks in study	Recession rate (cm ⁻¹ yr ⁻¹)
Beck (2018)	108C	2016	10	12.3
		2017	10	6.3
		2018	10	18.6
Williams (2019)	103	2011	28	-1.23
		2012	35	-0.40
		2013	34	3.90
		2014	35	4.63
		2015	33	21.36
		2017	25	-0.50
Palmer et al. (2014)	108C	2018	24	30.97
		2005	10	0.4
		2006	10	-0.6
		2007-08	10	19.2
		2009	10	34.2
		2010	10	27.0
Tufekcioglu et al. (2012)	109	2011	10	13.6
		2006	13	11.7
		2007	13	26.6
Zaimes et al. (2006)	103	2008	13	26.3
		2001	5	10.3
		2002	5	9.5
	104	2003	5	20.2
		2001	4	5.8
		2002	4	9.2
109	2003	4	11.9	
	2001	5	8.6	
	2002	5	2.2	
		2003	5	15.1
<i>Average</i>				12.4
<i>St dev</i>				10.3
<i>Median</i>				11.0

3.2.4 Aerial Imagery Analysis of Stream Migration

To expand upon the reach-scale erosion-pin estimates, long-term annual average streambank recession rates in the 3rd to 6th order streams in Iowa were estimated using changes in stream migration occurring over a 25-year period. Color infrared photographs are available for Iowa for the mid-1980s and late 2000s (note: photograph dates are slightly different across the state). The changes in stream bank positions between these two time periods were used to estimate long-term bank migration.

Segments in 3rd to 6th order streams in each MLRA were divided into reaches that corresponded to 30 times the average channel width to account for full meander belts. From these reaches, 100 stream centerline segments were randomly selected in the eight MLRA regions. For each selected segment, a stream centerline was digitized from both the 1980s and 2000s aerial images starting and ending at the segment's endpoints. The two line segments were combined and converted to polygons. The area between the lines was calculated as the area over which the stream segment migrated over the ~25-year period. Average migration areas over the period were estimated by dividing the polygon area by the segment length and annual recession rates were determined by dividing the average migration areas by the number of years. Examples of the analysis for typical 3rd order and 6th order streams are shown in Figures 3.2 and 3.3, respectively.

Although we analyzed a subset of 100 stream segments per stream order in each MLRA, some streams were obscured by overhanging vegetation or flooding and migration rates could not be determined. Hence the numbers of values reported in Table 3.2 are less than 100 per order per MLRA. In total, 2,111 stream segments were visible out of a possible 3,200 reaches stream migration (8 MLRAs x 4 stream order x 100 reaches).

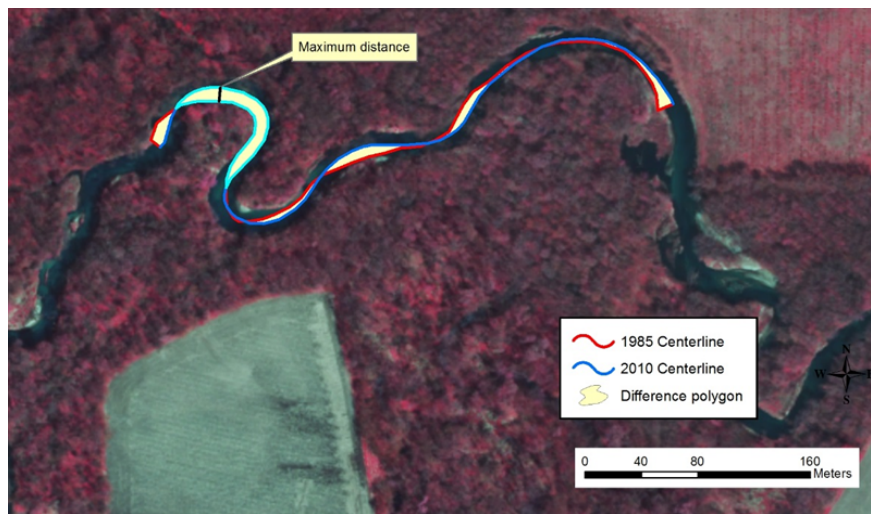


Figure 3.2. Stream migration measured in a third-order watershed.

3.3 Results and Discussion

3.3.1 Erosion Pin Recession Rates

Since the early 2000s, hundreds of erosion pins were installed to monitor streambank recession across Iowa. Results from five studies led by researchers at Iowa State University are reported in Table 3.1, but it should be noted that the universe of pinned streambanks is actually much larger than this, as the data included in Table 3.1 are only for those banks with regular long-term measurements. Data included herein represent the most comprehensive set of annual streambank erosion estimates available for Iowa or similar regions in the glaciated U.S. Midwest with similar hydrology.

As might be expected, published results from the pin studies show wide variability in annual recession rates, ranging from -1.2 cm/yr (deposition) to 34.2 cm/yr with an average recession rate of 12.4 ± 10.3 cm/yr, with a median value slightly less (11.0 cm/yr). It is important to recall that erosion pins were installed in banks that were previously identified as severely eroding using USDA-NRCS visual assessment protocols during an initial stream assessment. Hence, the variability in recession mainly reflects variations measured in bare and exposed banks, not simply eroding versus non-eroding segments of the channel.



Figure 3.3. Stream migration measured in a sixth-order watershed.

Walnut Creek in MLRA 108C has been the subject of intense streambank erosion monitoring since 2005 (Palmer et al., 2014; Beck et al., 2018). Combining both published and non-published results provides more than a decade of streambank erosion estimates within the same watershed. The box plot in Figure 3.4 shows both the range of variation measured in the same year among 10 streambank sites, as well as annual patterns indicating little bank erosion occurring in 2005, 2006, and 2012, and significant bank erosion occurring in 2009 and 2010. This variation is encompassed in an overall average value of 10.7 cm yr^{-1} for bank erosion occurring in the same watershed over an 11-year period.

So what causes the annual variations in bank recession rates among erosion pin sites? Iowa researchers have attributed the variations in recession rates to variations of riparian land cover (Zaimes et al., 2004; 2006), cattle grazing (Tufekcioglu et al., 2012), hydrology (Palmer et al., 2014), and alluvial stratigraphy (Beck et al., 2018). These factors are consistent with mechanistic processes controlling bank erosion observed at other sites around the world (e.g., Lawler, 1992a; Simon & Collison, 2002; Pollen & Simon, 2005; Fox et al., 2007). However, some variations in erosion pin data are also due to measurement limitations including how to account for missing or buried pins, as well as the documented underestimation of large planar and rotational failures using pins (Hooke, 1979; Lawler 1992; Couper et al., 2002; Palmer et al., 2014). Additionally, reach- or basin-scale dynamics reflect local and regional variations in topography, geology and climate, thus inhibiting intra- or inter-basin comparison of recession

rates (Palmer et al., 2014). Despite these challenges, the erosion rates seemingly converged at a long-term annual rate of approximately 11 cm yr⁻¹ for 3rd - 4th order streams.

3.3.2 Recession Rates from Aerial Imagery

At a much larger spatial scale, average annual bank recession rates estimated from changes in channel migration increased with increasing stream order in all MLRAs over an ~25-yr period, (Table 3.2). Mean annual recession rates increased from 12.4 cm/yr in 3rd order streams to 18.1, 31.9, and 53.8 cm/yr in 4th, 5th, and 6th order streams, respectively. Maximum recession rates represented

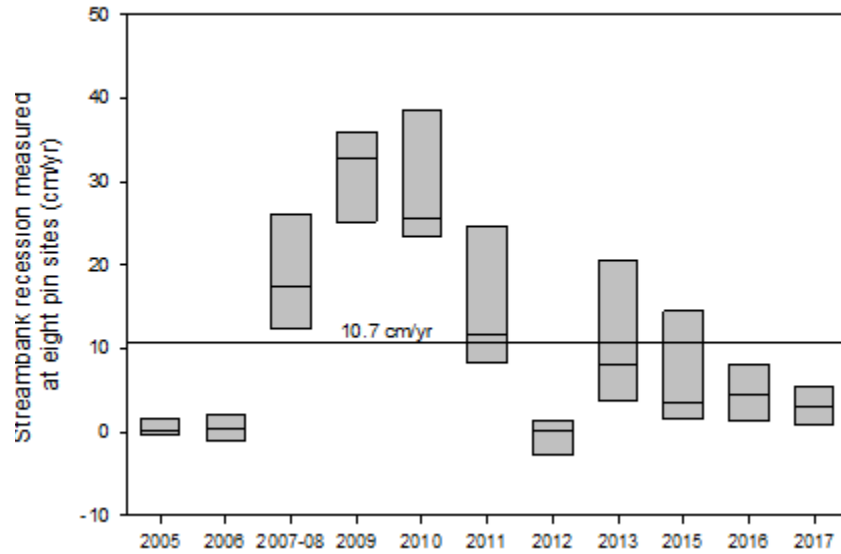


Figure 3.4. Annual streambank recession rates measured in Walnut Creek, Iowa based on data reported in Palmer et al. (2014) and Beck et al. (2018).

by the maximum change in channel migration within a segment were approximately 3.6 to 4.4 times greater than the mean rate (Table 3.2). Overall, measured recession rates in Iowa streams are consistent with other studies using aerial imagery (e.g., Beeson & Doyle, 1995; Miller et al., 2014; Purvis & Fox, 2016).

Having greater mean values of annual recession in larger streams is consistent with having greater discharge from larger watershed areas and higher stream power (Hooke, 1980). Both scour and lateral erosion increase with stream size as a function of discharge, drainage area, and channel dimensions (U.S. Department of Transportation, 2012). Hooke (1980) found that watershed size explained more than 50% of the variation in mean bank erosion rate and 39% of the variation in maximum rates. Herein, the effects of watershed size are captured using stream order, which has a functional relation with watershed size in similar hydroclimatic regions (Leopold & Wolman, 1957).

In general, recession rates were higher in MLRA regions 104 and 105, and they were lower in MLRA regions 108C and 109 (Table 3.2). These differences are likely due, in part, to differences in geology and the composition of the streambank sediments. The loamy riparian soils of MLRA 104 and the sand dominated floodplains of northeast Iowa in MLRA 105 (Moustakidis et al., 2019) have less cohesion than the streambank soils of southern and

southwest Iowa which are dominated with silt and clay. Cohesive channel banks are less susceptible to retreat (Couper, 2003; Julian & Torres, 2006) as the added cohesion provides more resistance (Hooke, 1980). Riparian soils along lower order streams in southern Iowa (MLRAs 108C and 109) are dominated by fine-textured sediments, although the riparian zones become increasingly sandy and gravelly in larger 6th order river systems (Schilling et al., 2018). Other differences in bank recession rates among MLRAs may be due to factors such as width-depth ratios (Hooke, 1980), planform geometry (Odgaard, 1987), and landscape changes from channelization (Simon, 1989), agriculture (Knox, 1977), and urbanization (Trimble, 1997).

Using aerial imagery allows for an integrated analysis of bank recession over a much longer period and much larger area than erosion pins. For example, Tomer & Van Horn (2018) recently analyzed the South Fork Iowa River using aerial imagery to quantify channel changes and sediment movement from the 2008 flooding. Although Fox et al. (2016) points out that errors in bank recession estimates could occur if the temporal or spatial resolution of the images are not sufficient. In this study, we were not able to analyze some stream segments because the stream centerline could not be identified from the 1980s photo due to dense vegetation or because the segment was under flood condition.

3.3.3 Estimating Bank Recession Rates in Iowa

While a single bank recession rate cannot be applied to all of Iowa's stream miles, there are some generalities that can be made based on this analysis of erosion pins and stream migration rates (Figure 3.5). First, at the scale of individual streambanks, bank recession rates in Iowa vary considerably annually. Based on studies using erosion pins at sites throughout Iowa, annual recession rates have ranged from net deposition to erosion in excess of 60 cm when the pins were completely lost (e.g., Zaimes et al., 2006; Tufekcioglu et al., 2012). Considering the annual rates derived from the pin studies to be mainly applicable to commonly measured 3rd order streams suggests that a wide disparity in annual recession rates may occur in any given year (Figure 3.5). This was further supported from long-term annual monitoring of erosion pins in the Walnut Creek watershed where monitoring showed highly variable recession rates (Figure 3.3).

On the other hand, aerial imagery analysis of stream migration across a longer period suggests that mean bank recession rates in Iowa scale with stream order (Figure 3.5). Annual bank recession of about 12 cm/yr in 3rd order streams systematically increased to nearly 60 cm/yr in larger 6th order rivers. Extrapolation of the trend suggests average annual recession rates less than 10 cm/yr in small 1st and 2nd order channels. The bank recession curve intersects the pin-measured rates at approximately the mean of the pin data (12.4 cm/yr). Hence, there would appear to be some predictability of bank recession rates at longer timeframes for Iowa's streams

and rivers. Simply applying the long-term recession rates per stream order to the stream miles in Iowa highlights the threat of bank erosion to bridge infrastructure safety.

3.4 Conclusions

In this study, we compiled streambank erosion data from Iowa erosion pin studies to determine long-term stream migration rates and to assess how annual bank recession rates vary by stream order. Results suggest that while annual recession rates vary considerably at the scale of individual banks, bank recession rates scale at longer time intervals across a range of stream orders. More bank recession is occurring in larger streams and rivers from greater discharge from larger watershed areas and an increase in stream power. Variations in bank recession rates were observed in Iowa MLRA regions mainly due to differences in geology and the composition of the streambank sediments. Overall, study results provide temporal and spatial context for evaluating streambank recession in Iowa and the glaciated Midwest. In summary, a deeper understanding of the variability, both spatially and temporally, across the state is needed.

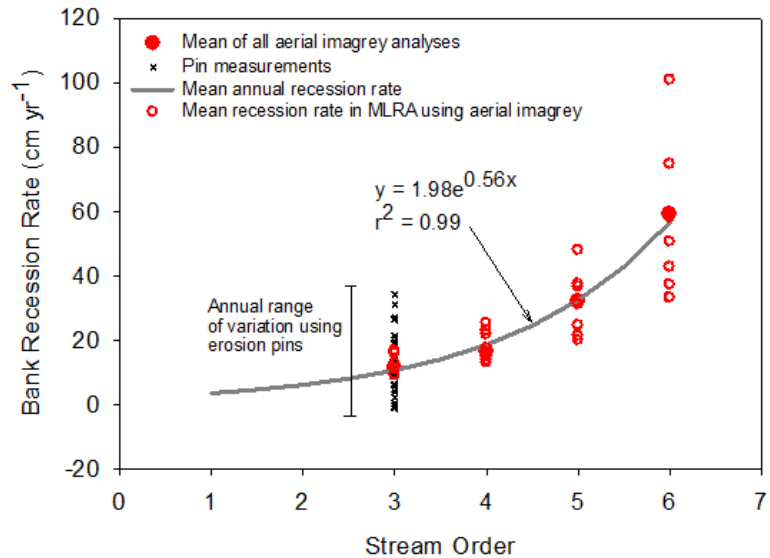


Figure 3.5. Comparison of annual pin-measured streambank recession rates in 3rd order channels to mean channel migration rates for 3rd to 6th order rivers estimated using aerial imagery.

3.5 Products

This section has been developed into a manuscript submitted for peer-review to the *Journal of Hydrology Regional Studies*. It is currently under review. The manuscript is entitled “**An assessment of streambank recession rates in Iowa**” and co-authored by Keith Schilling and Calvin Wolter (investigators of the project team), as well as Jason Palmer of the Iowa Department of Natural Resources and the following members of the Department of Natural Resource Ecology and Management at Iowa State University: William Beck, Forrest Williams, Peter Moore, and Thomas Isenhardt.

Table 3.2. Summary of annual streambank recession by stream order and MLRA estimated using changes in channel morphology over 25 years.

Mean rate (cm/yr) over 25 years												
	Order 3			Order 4			Order 5			Order 6		
MLRA	Mean	St Dev	Count									
103	12.8	8.3	74	16.2	7.7	81	36.5	32.6	64	42.7	38.5	30
104	15.9	11.5	84	22.9	12.5	81	24.5	16.0	61	37.2	21.9	39
105	16.7	9.1	83	21.7	13.1	87	37.4	24.2	64	100.8	101.1	47
107A	11.2	12.6	89	25.2	21.4	82	47.9	38.4	55	58.1	31.4	34
107B	11.1	5.8	82	17.4	11.9	88	36.5	41.8	66	74.7	77.9	44
108C	9.0	4.0	83	13.0	6.6	81	19.9	12.8	64	33.2	20.4	44
108D	11.1	4.6	73	13.7	8.3	72	31.0	27.7	59	50.5	42.9	42
109	11.3	6.0	79	14.8	11.7	79	21.3	13.7	63	33.1	28.8	37
average	12.4	7.7		18.1	11.6		31.9	25.9	62	53.8	45.4	

Maximum rate (cm/yr) over 25 years												
	Order 3			Order 4			Order 5			Order 6		
MLRA	Mean	St Dev	Count									
103	53.3	38.8	74	62.0	35.4	81	156.5	130.0	64	178.8	162.0	30
104	67.9	52.2	84	87.7	43.3	81	123.5	101.7	61	179.2	141.6	39
105	49.7	23.6	83	77.0	53.1	87	148.9	109.1	64	497.8	522.0	47
107A	37.3	36.4	89	84.0	64.9	82	183.3	137.6	55	299.0	195.7	34
107B	37.9	17.8	82	58.5	44.2	88	126.6	121.1	66	268.3	217.8	44
108C	33.5	16.9	83	50.3	33.1	81	77.7	67.7	64	165.3	131.7	44
108D	43.0	20.1	73	49.6	32.8	72	113.4	94.3	59	184.2	148.5	42
109	44.5	25.5	79	56.9	45.6	79	95.2	73.4	63	119.1	90.3	37
average	45.9	28.9		65.8	44.1		128.1	104.4		236.5	201.2	

SECTION 4: QUANTIFYING THE EXTENT OF ERODING STREAMBANKS IN IOWA

4.1 Goal Statement

Streambank contributions to annual sediment loads are highly variable and episodic, ranging from <10% to 96% of the annual loads (e.g., Wilson et al., 2008; Belmont et al., 2011; Schilling et al., 2011; Palmer et al., 2014). Moreover, processes controlling streambank erosion differ within and among watersheds (Fox et al., 2016). Due to such variability, mapping the spatial distribution of eroding streambanks at a basin scale is exhaustive and time-consuming and thus is rarely done.

Herein, we report a new methodology to identify eroding streambanks at a regional scale using high resolution LiDAR elevation data. The steps were to 1) develop the methodology for identifying severely eroding streambanks in Iowa remotely; 2) validate the estimated bank erosion against intensive field mapping campaigns in two watersheds; 3) quantify the extent of eroding lengths and identify spatial patterns at watershed and landscape scales; and 4) assess the limitations and implications of the approach for future watershed-scale assessment of streambank stability at bridge crossings in Iowa.

4.2 Methodology

4.2.1 Methodological Overview

The broad-scale assessment methodology for identifying potential severe bank erosion discussed here uses a new approach involving the slopes between adjacent cells in a high-resolution LiDAR coverage map to identify severe erosion for quantifying the relationship between streambank angles and heights. The approach is calibrated and validated using intensive field mapping campaigns in two Iowa watersheds. It is applied to the 3rd - 6th order streams in the state. Despite certain limitations, the approach provides a first-order approximation of eroding streambank lengths in Iowa's rivers and streams.

4.2.2 Rathbun Lake Watershed Streambank Erosion Mapping

Intensive field mapping in the Rathbun Lake watershed was used to develop and calibrate the LiDAR-based method for estimating eroding streambank extent. The Rathbun Lake watershed encompasses over 350,000 acres in MLRA 109 of south-central Iowa, where most of the soils are silty clay loams, silt loams, and clay loams formed in loess and pre-Illinoian till.

A random subset of 800-m stream segments was selected from a National Hydrologic Dataset (NHD) of stream centerlines purged of any segments located above detention basins or

small lakes. These stream segments accounted for roughly ten percent of the total stream length in 2nd through 5th order streams and the random subset was assumed to represent overall erosion conditions throughout the larger watershed (Figure 4.1). The 800-m segments were selected by placing nodes at 100-meter intervals along the NHD stream centerlines and using the random selection tool in ArcGIS to randomly select the center point for each reach.

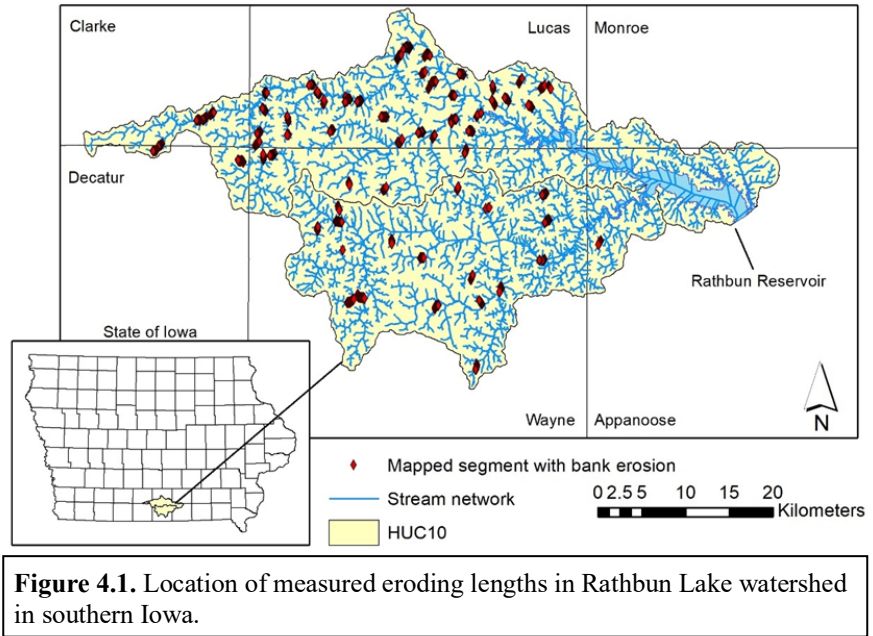


Figure 4.1. Location of measured eroding lengths in Rathbun Lake watershed in southern Iowa.

Field surveys mapped severely and very severely eroding streambanks within the 800-m segments using the visual assessment criteria developed by the Natural Resources Conservation Services (Newton et al., 1998). This visual assessment classifies banks that are predominantly bare, with overhanging vegetation and exposed roots, as severely to very severely eroding. The locations, height, and length of each identified bank were recorded using a Trimble Nomad 900 (2- to 4-m accuracy).

4.2.3 Delineating Eroding Streambank Extent in Rathbun Lake Watershed

We used the field mapping conducted in the Rathbun Lake watershed to develop a GIS routine that estimates the extent of severe to severely eroding streambanks in stream reaches based on LiDAR streambank angles and bank heights. The data sources for this analysis were a 1-m digital elevation model (DEM) and a 1-m slope grid, along with coverages of stream centerline, edge-of-water, order, and sinuosity, which are all available at the Iowa Geodata website (<https://geodata.iowa.gov/>).

The bank angle between adjacent 1-m DEM grid cells was determined by the bank height and grid size (z-dimension, Figure 4.2). Steeper bank angles will occur at progressively higher stream bank heights and it was assumed herein that steep bank angles (slope between adjacent cells) would indicate severe streambank erosion. However, since the x-distance between adjacent cells was always 1 m, lower bank heights in smaller order streams would have lower bank angles indicative of severe bank erosion. Therefore, we used the field mapping data in the

Rathbun Lake Watershed to develop a relation of bank angles to streambank heights (i.e., slopes between adjacent cells) to determine the best slopes that match the extent of eroding banks (Figure 4.3).

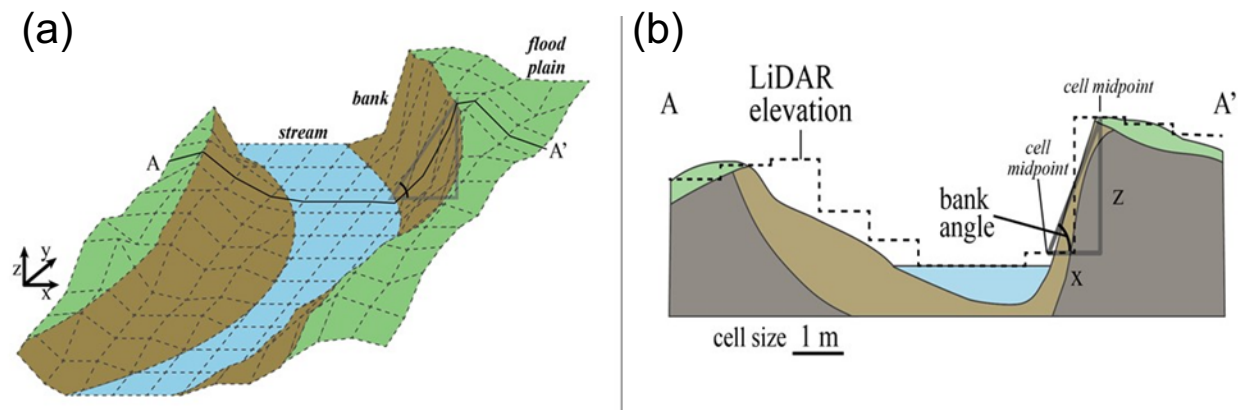


Figure 4.2. Conceptual schematic of modeling approach to estimate severely eroding streambanks. (a) LiDAR grid superimposed on a stream; (b) cross section of streambank showing the bank angle calculation.

First, a series of slope grids was generated for the watershed using cell-to-cell slope ranges of 40-45%, 45-50%, 50-55%, 55-60%, 60-65%, 65-70% and >70%. A stream centerline and edge-of-water buffer of 20 m was used to clip each series of slope grids for the stream network and merge them into one coverage. The slope grids were converted into line coverages using the Vectorization command in ArcScan to create bank segments with the above slopes.

Next, the field mapping data for the 800-m long segments were used to quantify the total length of eroding streambanks within each severely eroding segment. The measured streambank slopes were plotted against the percentage of eroding streambank in each segment to find the best agreement between measured bank height and total eroding length. For example, for bank heights greater than 3.2 m, a bank slope greater than 70% would identify an eroding stream length mapped in the channel (Figure 4.3). For lower stream bank heights, the slopes between adjacent cells would be less and the field mapping data was used to identify a lower slope threshold that would correspond to eroding streambank lengths. Hence, for bank heights from approximately 1.7 to 2.0 m, slopes of 50% would correspond to a severely eroding streambank (Figure 4.3). It is important to recognize that the overall goal for this study was to develop a method to estimate how much streambank erosion is occurring across broad geographical areas (i.e., the “extent”) and not necessarily identify the exact location of severe bank erosion.

4.2.4 Estimating Eroding Streambanks in Iowa

To scale this procedure to the state level, bank heights were needed for all streams in Iowa. To obtain bank heights for all these streams, stream order segments were split every 100-m and the end points were buffered by the appropriate stream width (1/2 the mean value plus 1 standard

deviation). Zonal statistics were performed on the buffered points to obtain the range in elevation at each site which was then used as the bank height. The mean and standard deviation of bank heights were calculated for each stream order within a MLRA and applied to all segments of those stream orders in the MLRA.

As done for the Rathbun Lake watershed analysis, streambank slope grids in Iowa's 3rd to 6th order streams were generated for the entire state. Although 1st and 2nd order streams comprise most of the linear kilometers of Iowa's stream network (Schilling et al., 2018), the channel dimensions of these smaller streams are obscured by trees and overhanging vegetation. Thus, bank slopes could not be determined reliably and the methodology could not be applied to these low-order streams.

The grids were generated and clipped using the buffered state-wide stream centerline and edge-of-water coverages. The grids were converted to lines using the Vectorization command and a centroid of each 100-m segment was created and buffered at 10 m. Zonal statistics were run using the buffered points and 1-m DEM to identify the bank height to use for the segment (assuming that bank heights remained

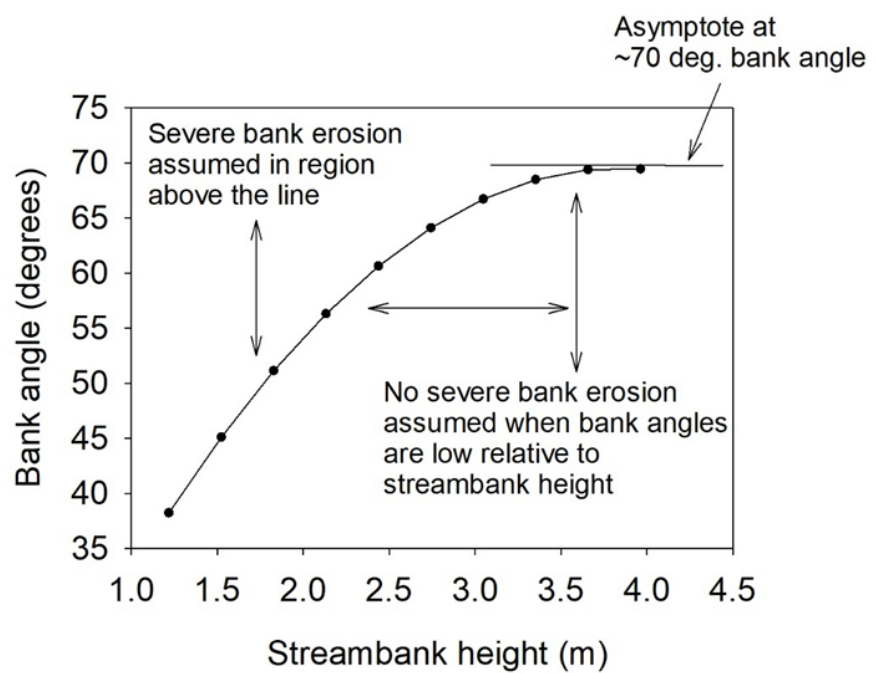


Figure 4.3. Relation of streambank heights to bank angle of adjacent 1-m LiDAR elevation cells in the Rathbun Lake watershed.

constant within the segment). Thus, for each cell position in the slope grid line, a comparison of the slope value to bank height would indicate whether or not severe bank erosion may be occurring based on the relation in Figure 4.3. Slope values greater than the threshold shown in Figure 4.3 for a particular bank height would be considered eroding.

4.2.5 Ancillary Data

Ancillary data of stream sinuosity and stream gradient were also developed for the stream network in the MLRAs to test as potential factors contributing to spatial bank erosion patterns. For both factors, all stream lengths were divided into segments corresponding to 30 times the

channel width. Stream lengths from both end points of the segments were determined and divided by the straight-line length to calculate sinuosity. Stream gradient was determined by selecting the elevation at the end points of each stream segment, calculating the elevation difference and then dividing by the length of the segment. The ancillary data were summarized by MLRA to assess their relation to regional summaries of eroding length values.

4.3. RESULTS

4.3.1 Model Validation

The watershed-scale extent of streambank erosion estimated using the LiDAR-based procedure was validated in two watersheds where field mapping of eroding streambanks has been conducted. Walnut Creek is a 4th order stream in MLRA 108D, where a channel bank survey was first completed in 1998 (Schilling & Wolter, 2000) and subsequent surveys were conducted nearly annually since then (Palmer et al., 2014; Beck et al., 2018). Similar eroding bank surveys were also completed in the 3rd order Onion Creek in MLRA 103 (Des Moines Lobe region) as part of Iowa State University thesis projects (Leate, 2013; Williams, 2019). Field mapping in both watersheds involved using GPS to identify the beginning of an eroding bank segment and then include the length of the eroding segment as a numeric value in the spatial database.

In Walnut Creek, the LiDAR-based streambank erosion model estimated 11,600 m of eroding streambanks (Figure 4.4). This length was higher than reported in 2010 field mapping (8,200 m) but both the model and field mapping program identified most of the same critical eroding segments. Likewise, in Onion Creek, the total eroding streambank length estimated using the model (11,675 m) was higher than the field mapping data collected in 2011 (7,600 m). The validation process suggests that the model may be overpredicting eroding streambank lengths compared to field mapping.

However, for both streams, it should be noted that the LiDAR-estimated eroding lengths were based on channel conditions mapped in 2008 when the LiDAR flights were done and not coincident with the time period of field mapping. For example, annual field mapping conducted in Walnut Creek indicates that the linear extent of streambank erosion can change over time with some streambanks previously characterized as “severely eroding” at one point in time undergoing a healing process (Beck, 2018). Beck (2018) reported that the percentage of banks deemed to be severely eroding in Walnut Creek ranged from approximately 11% to 40% over a 20-year period as streambanks respond to large storm events. During periods of reduced streamflow, colluvial material amass at bank toe regions, reducing bank angles and allowing for the establishment of vegetation. It is possible that several high-flow events in Walnut Creek between 2008-2010 (Palmer et al., 2014) accentuated the severity of streambank erosion in the

watershed at the time of the LiDAR flights. Streambank surveys were not conducted during this active period, but when measured in the fall of 2010, there was still a 22% increase in eroding bank lengths from 2004 (drought conditions) to 2010 (Palmer et al., 2014). Conditions in Onion Creek have been monitored less frequently than Walnut Creek but the spatial extent of eroding streambank lengths also changes annually (Leate, 2013). In Onion Creek, an added complication was the presence of overhanging vegetation that partially obscured the high-resolution channel elevation data. Overall, while the LiDAR-mapping procedure identified many of the same streambanks mapped as severely eroding

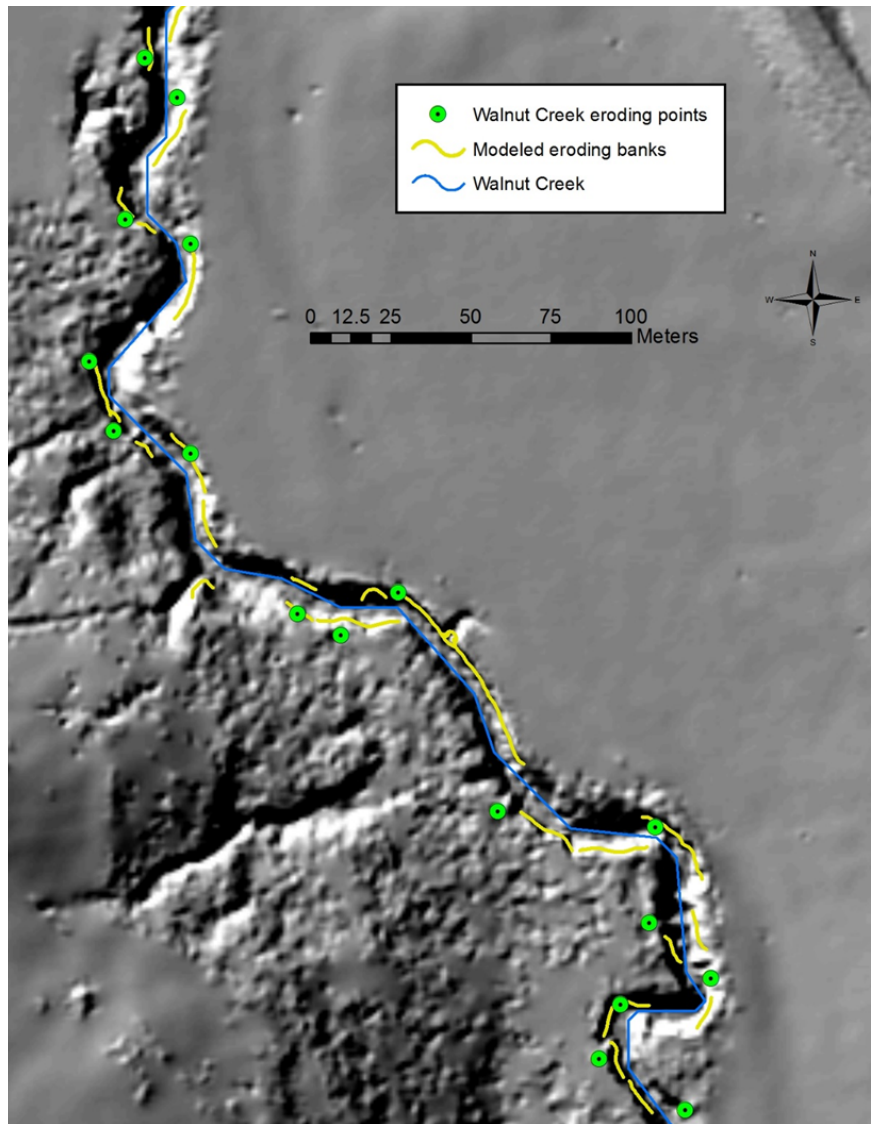


Figure 4.4. Spatial correlation of the location of the beginning of a severe bank erosion segment mapped in Walnut Creek watershed with the linear extent of severe bank erosion estimated using the LiDAR-based model.

in the field studies, the timing of the field mapping relative to the LiDAR elevation data complicated any direct comparison. LiDAR flights conducted soon after high discharge events that scour the channel and the banks will document steeper bank angles and produce greater eroding bank lengths using the procedures we report herein. Since field mapping data were only available for two small watersheds in the state, additional field mapping of eroding banks is needed to confirm the estimates of eroding lengths estimated in this study.

4.3.2 Eroding Streambanks

Using the above approach, 35,200 km of streambanks along 3rd to 6th order rivers are identified as severely eroding in Iowa (Figure 4.5). The total stream kilometers evaluated in this study was 85,970 km which account for streambanks on both sides of the river. This suggests that approximately 41% of the streambanks in Iowa are severely eroding.

However, spatial patterns of eroding bank lengths varied considerably by watershed, region and stream order.

By summing the total length of eroding banks in a watershed or MLRA, an eroding bank density was calculated to normalize eroding bank length by watershed area. Eroding length densities ranged from 645 m/km² in a MLRA 107B watershed in western Iowa to 24 m/km² in the West Fork of the Cedar River in eastern Iowa, with a low value of 11 m/km² found in a small portion of the Blue Earth watershed in northern Iowa (Figure 4.6).

Ten 8-digit HUCs, mostly found in southern and southwest Iowa, had more than 500 m/km² of eroding streambank (Figure 4.6). In contrast, 13 8-digit HUC watersheds had eroding lengths <100 m/km².

Spatial patterns of streambank erosion were summarized by MLRA (Table 4.1). Streambank erosion density exceeded approximately 450 m/km² in MLRAs 107B, 108D and 109, but were less than 67 m/km² in MLRAs 103 and 104 (Table 4.1). Overall, across the state, the average eroding bank density was estimated to be 238 m/km².

4.3.3 Eroding Lengths by Stream Order

Eroding streambank lengths varied by stream order within the MLRAs (Table 4.2). In the more recently glaciated Des Moines Lobe (MLRA 103), approximately 13% of 3rd order streambanks were eroding, whereas in the Loess Hills (MLRA 107B), more than 61% of 3rd order

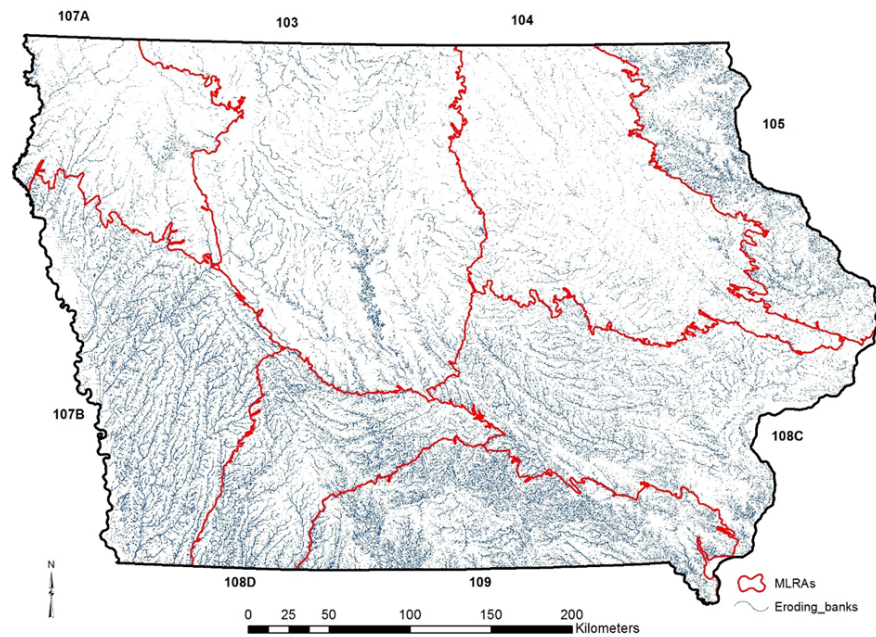


Figure 4.5. Location of severely eroding streambank lengths in 3rd - 6th order streams of Iowa.

streambanks are eroding. At higher stream orders, the eroding bank percentage remained highest in MLRA 107B and it increased to over 84% in 6th order rivers in the region. Higher eroding bank percentages were also estimated for MLRAs 108D and 109, where 35 to 77% of streambanks were considered eroding. Less streambank erosion at higher order streams was observed in MLRA 104

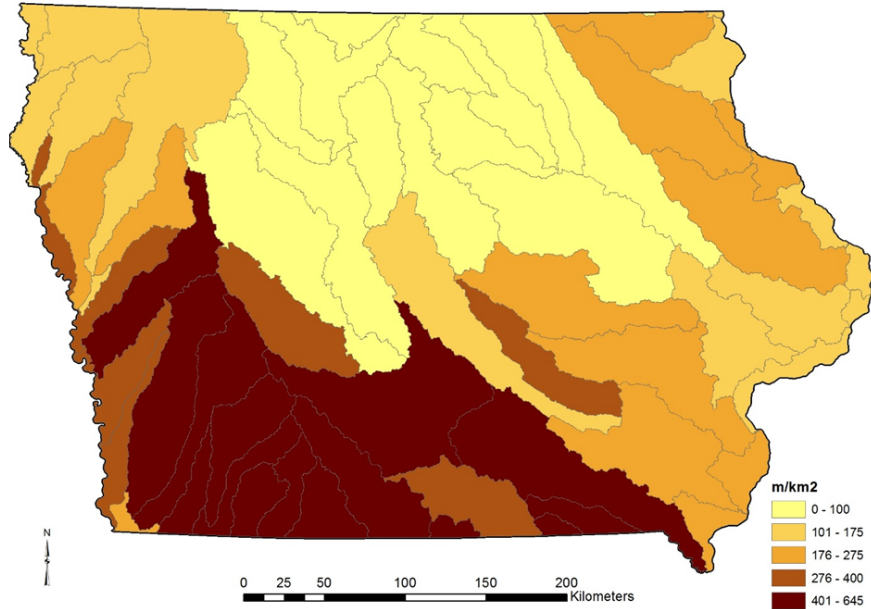


Figure 4.6. Density of eroding lengths in HUC-8 watersheds in Iowa (in meters of eroding length per km² of watershed area).

where the eroding streambank percentage ranged from 15.4 to 18.5% across four stream orders (Table 4.2). As a summary of all stream kilometers in Iowa, the percentage of severely eroding streambanks increased with stream order. Approximately 32% of 3rd order streams in Iowa were considered to be severely eroding compared to 48%, 53% and 58% of 4th, 5th and 6th order streams, respectively.

As expected, since streambank erosion was estimated, in part, from bank slopes, across all stream orders and MLRAs, the fraction of stream kilometers experiencing severe bank erosion was significantly related to bank height (Figure 4.7). The higher the stream banks, the greater proportion of channel length was estimated to be severely eroding. In contrast, streambank erosion was only nominally related to stream sinuosity across stream orders and MLRAs ($p=0.06$). Stream sinuosity varied within a relatively narrow range among all regions (1.2 to 1.5) and did not vary systematically by stream order or region. Channel gradient was considerably larger in 3rd order streams and decreased systematically with increasing stream order in most MLRAs (Table 4.2), but the relation of eroding stream length to stream gradient was not statistically significant ($p>0.1$).

4.4 DISCUSSION

Streambank erosion is considered to be a major source of sediment to rivers and streams (e.g., Fox et al., 2016) but studies quantifying the extent of severe erosion occurring at a watershed scale are limited to select, small watersheds (Schilling & Wolter, 2000; Tufekcioglu et al., 2012;

Palmer et al., 2014; Preacher et al., 2018). In this study, we calibrated field mapping of severe bank erosion to LiDAR-derived streambank heights, and validated the bank erosion model to intensive field mapping in two representative watersheds, to develop a LiDAR-based model that could estimate the extent of streambank erosion occurring throughout the state.

Table 4.1. Summary of eroding streambank lengths and watershed density by MLRA.

MLRA No.	MLRA Name	Area of MLRA (km ²)	Eroding length (m)	Eroding density (m/km ²)
103	Central Iowa and Minnesota Till Prairies	31,400	2,089,684	67
104	Eastern Iowa and Minnesota Till Prairies	24,129	2,089,684	65
105	Northern Mississippi Valley Loess Hills	10,544	2,633,942	250
107A	Iowa and Minnesota Loess Hills	11,793	1,489,320	126
107B	Iowa and Missouri Deep Loess Hills	19,957	8,897,432	446
108C	Illinois and Iowa Deep Loess and Drift, West-Central Part	21,717	5,758,478	265
108D	Illinois and Iowa Deep Loess and Drift, Western Part	11,541	6,025,678	522
109	Iowa and Missouri Heavy Till Plain	14,618	6,728,886	460

Overall, we estimated that approximately 35,200 km of streambanks are actively eroding in the state. Bank erosion is considered a “natural geomorphic process” (Florsheim et al., 2008), and typically occurs at greater frequency and magnitude at the outside bends of meandering streams (e.g., Leopold & Wolman, 1957). As such, a typical percentage of eroding stream lengths in a natural meandering river would be on the order of ~20%. Across all rivers and streams in Iowa, the percentage of eroding bank lengths was much greater (41%), suggesting that streambank erosion may be occurring at an excessive rate in the state. However, study results indicate that while streambank erosion appears to be widespread across the state, regional differences were strikingly evident.

4.4.1 Regional Patterns

Longer stretches of streambank erosion per watershed area are occurring in southwest and southern Iowa than other portions of the state (Figure 4.7), with eroding lengths ranging from 446 to 522 m/km² in their MLRA regions, and 35-84% of streambanks considered to be severely eroding (Table 4.1). The geology of western Iowa is dominated by thick deposits of highly erodible, wind-blown silt (loess) that is vulnerable to fluvial surface and mass erosion (Bradford

& Piest, 1977; Thomas et al., 2004). Fluvial surface and mass erosion tend to occur along the entire length of channel (Figure 1.2). Thomas et al. (2004) also reported that mass failure was responsible for channel widening of more than 70% in the deep loess region. Although the loess thins moving across southern Iowa, the region is dominated by rolling hills with the loess overlying older weathered glacial deposits.

Historical row crop cultivation in the region, removal of riparian vegetation and channel straightening in the region led to widespread channel instability since the turn of the 20th Century (Simon & Rinaldi, 2000; Schilling et al., 2011). Most stream channels in the western and southern Iowa regions are deeply incised. This was reflected in bank heights measured in this study, where, for example, bank heights of 3rd order streams in the Deep Loess region (107B) are nearly 4 m high and increase to 6.1 m in 6th order channels (Table 4.2). Likewise, bank heights exceed 3-5 m in

southwest and southern Iowa MLRAs. Channel incision results in higher and often steeper streambanks that are susceptible to streambank erosion and mass failure (Simon & Rinaldi, 2000). During high flow events in incised channels, streamflow is confined within the channel and scours the streambanks over the entire bank height. Steep streambanks often become saturated during

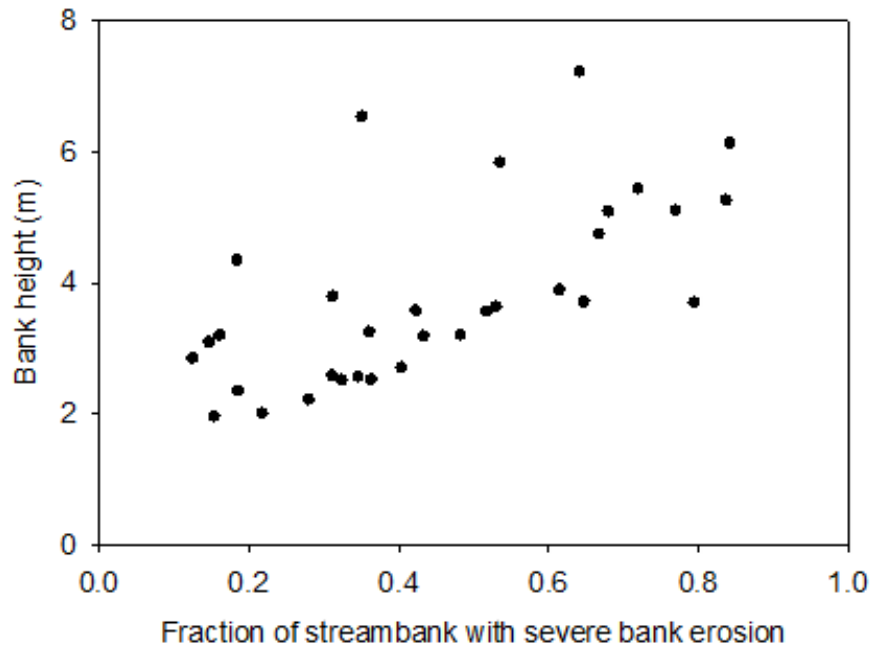


Figure 4.7. Relation of the fraction of streambank in 3rd - 6th order streams in Iowa MLRAs to the average bank heights.

bankfull events and are subject to mass failure when stream flow recedes and they are no longer supported by the flow in the channel (Simon & Collison, 2002). Simon & Rinaldi (2000) examined channel instability in the loess area of the U.S. Midwest and specifically analyzed data from West Tarkio Creek which flows from southern Iowa into Missouri. They reported that the relation of channel bank height to bank angle can be used to assess streambank instability and noted that many sections of the river should be considered “at risk” or “unstable” based on channel geometry and shear-strength conditions. These conditions are reflected in the mapping of widespread streambank erosion in southwest and southern Iowa MLRA regions.

Table 4.2. Summary of streambank erosion by MLRA, stream order and relation to landscape properties.

MLRA	Property	Order 3	Order 4	Order 5	Order 6
103	<i>% streambanks eroding</i>	12.6	32.5	31.3	35.2
	<i>Bank Height (m)</i>	2.84	2.51	3.78	6.52
	<i>Sinuosity</i>	1.38	1.46	1.38	1.34
	<i>% slope of channel</i>	0.20	0.10	0.09	0.29
104	<i>% streambanks eroding</i>	15.4	18.6	14.8	18.5
	<i>Bank Height (m)</i>	1.95	2.34	3.08	4.34
	<i>Sinuosity</i>	1.38	1.46	1.38	1.34
	<i>% slope of channel</i>	0.17	0.10	0.08	0.12
105	<i>% streambanks eroding</i>	28.1	40.4	53.6	64.2
	<i>Bank Height (m)</i>	2.21	2.69	5.83	7.21
	<i>Sinuosity</i>	1.38	1.46	1.38	1.34
	<i>% slope of channel</i>	0.61	0.28	0.19	0.12
107A	<i>% streambanks eroding</i>	21.9	31.2	36.1	16.2
	<i>Bank Height (m)</i>	2.00	2.57	3.24	3.19
	<i>Sinuosity</i>	1.38	1.46	1.38	1.34
	<i>% slope of channel</i>	0.29	0.14	0.09	0.08
107B	<i>% streambanks eroding</i>	61.6	83.8	79.5	84.3
	<i>Bank Height (m)</i>	3.88	5.25	3.69	6.12
	<i>Sinuosity</i>	1.38	1.46	1.38	1.34
	<i>% slope of channel</i>	0.46	0.21	0.13	0.11
108C	<i>% streambanks eroding</i>	36.4	48.3	53.1	42.3
	<i>Bank Height (m)</i>	2.51	3.20	3.63	3.57
	<i>Sinuosity</i>	1.38	1.46	1.38	1.34
	<i>% slope of channel</i>	0.29	0.16	0.10	0.07
108D	<i>% streambanks eroding</i>	43.4	64.8	77.0	72.0
	<i>Bank Height (m)</i>	3.18	3.70	5.09	5.43
	<i>Sinuosity</i>	1.38	1.46	1.38	1.34
	<i>% slope of channel</i>	0.52	0.25	0.16	0.14
109	<i>% streambanks eroding</i>	34.6	51.8	66.8	68.1
	<i>Bank Height (m)</i>	2.56	3.55	4.73	5.09
	<i>Sinuosity</i>	1.38	1.46	1.38	1.34
	<i>% slope of channel</i>	0.46	0.24	0.16	0.12

Across northern Iowa, including the recently glaciated Des Moines Lobe (MLRA 103) and the Iowan Erosion Surface (MLRA 104), the topography is flatter, soils are coarser, and bank heights are lower. Among all stream orders, the percentage of streambanks with eroding banks ranged from 15 to 35% and the eroding length density was 67 and 65 m/km², respectively (Table 4.1). Although watersheds in the regions contain more intense agricultural row crop production (>70-80% corn and soybeans) compared to southern Iowa, basin slopes are less. Schilling & Wolter (2005) reported that basin slopes in Des Moines Lobe watersheds were typically 1.5% compared to ~7% in southwest Iowa watersheds. The channel slopes of 3rd order streams in MLRAs 103 and 104 were approximately 1/3 of the slopes in southwest Iowa.

In MLRA 105, streams flow over shallow carbonate bedrock that limits downcutting and channel incision despite high channel slopes (slope of 0.61 in 3rd order streams; Table 4.2). Although bank heights increase with increasing stream order and the proportion of severely eroding streambank lengths also increases, in larger order streams, riparian zones contain both steep rock outcrops and sand-dominated floodplains (Moustakidis et al., 2019). The combination of these two conditions brings uncertainty into the assessment of eroding bank lengths in the northeast Iowa region.

4.4.2 Relation to Explanatory Factors

Across all MLRAs, eroding bank lengths increased with increasing stream order (Table 4.2). Approximately 31% of streambanks in 3rd order streams had eroding banks whereas 6th order streams had more than 50% of their banks estimated to be eroding. Larger rivers receive discharge from larger watershed areas, and this increase in discharge with scale increases stream power which contributes to more bank erosion (Knighton, 1999). The U.S. Department of Transportation (2012) similarly noted that the potential for river scour and lateral erosion increases with stream size, with discharge being a function of stream size, drainage area and channel dimensions. Stream power is also a function of slope, but in this study, eroding bank lengths were not related to channel slope ($p > 0.1$).

Channelization is understood to contribute to river downcutting and accelerate streambank erosion (Simon & Rinaldi, 2000). For example, channelization in the Ligoire River, France, resulted in incision of 0.4 m and bank erosion of 0.2 m over ~60% of the channel over a 42-year period (Landemaine et al., 2015). In Iowa, channelization occurred primarily in the first half of the 20th Century and it likely had similar effects on streambed and bank conditions shortly thereafter. However, in this study, which is conducted more than a century after much of the channelization was performed, we found little spatial relation between eroding bank lengths and sinuosity ($p = 0.06$). Indeed, the uniform range of sinuosity observed across the state (1.2 to 1.5) suggests that most rivers in the state have been impacted to some extent by channelization. Some criteria indicate that rivers with a single channel sinuosity of 1.5 or more are defined as natural meandering rivers (Leopold & Wolman, 1957). In their mapping of Walnut Creek in Iowa, Schilling & Wolter (2000) reported that severe bank erosion was often less in channelized reaches and greater in meandering reaches of the same 4th order stream. More intense bank erosion was observed in meandering segments downstream of channelized segments, as the increased stream power from straightened segments was diverted into the streambanks in the meandered segments. Hence, while sinuosity may not be an overriding variable in predicting the occurrence of bank erosion, variations in sinuosity among channelized and meandering segments

of Iowa streams and rivers may be major factor contributing to widespread bank erosion in Iowa rivers.

4.4.3 Limitations

Our first-order approximation of eroding streambank lengths in Iowa's rivers and streams comes with limitations. First, we based the eroding length model on LiDAR elevation data collected statewide from 2007-2010, so the elevation data used in this study are about a decade old. Since, the spatial maps of eroding streambanks used to calibrate and validate the bank erosion model were done more recently, the timing of field mapping was not synced with collection of the LiDAR elevation data. In some cases, eroding streambanks can heal, or in other cases, new bank erosion can emerge where it did not exist before (Palmer et al., 2014). Although the validation monitoring of eroding bank lengths in Walnut and Onion Creeks indicated that the bank erosion model was reasonable, we acknowledge that the results should not be used for site-specific classification. For site-specific river assessments, actual field mapping of eroding streambanks would be needed (e.g., Tufekcioglu et al., 2012, Beck et al., 2018; Preacher et al., 2018).

A second major limitation is the lack of quantification of eroding lengths in 1st and 2nd order channels. Smaller channels are vastly more numerous in watersheds than higher-order streams and rivers (Schilling et al., 2018). However, LiDAR resolution was not sufficient for delineating bank heights or widths with needed accuracy to calculate streambank angles in these small channels. In particular, overhanging vegetation interfered with channel assessments. For this study, we focused exclusively on eroding lengths in 3rd to 6th order channels and normalized eroding length fractions to this subset of Iowa streams and rivers. Given the trend of decreasing percentages of eroding bank lengths with lower stream orders, it would not be unreasonable to assume that less bank erosion (as a fraction of the total stream length) is occurring in 1st and 2nd order channels.

Another limitation would be the use of the mapping data from the Rathbun Lake Watershed to calibrate a statewide bank erosion model. As noted above, field mapping of eroding streambank lengths is not often conducted, and when it is done, mapping is typically performed primarily within a single 3rd to 4th order watershed (e.g., Schilling & Wolter, 2000; Willet et al., 2012; Palmer et al., 2014; Beck et al., 2018; Preacher et al., 2018). However, the field mapping work utilized in this study was rare in that it was done across a scale of stream orders. In the future, work should be done to develop regional-specific relations of eroding bank lengths across a range of stream orders in other regions of the state.

Finally, we note that there are many factors and processes that contribute to spatial patterns of severe streambank erosion in watersheds and acknowledge that simply mapping the

occurrence of severe bank erosion does not shed light on potential causal factors. In this study, we considered the spatial relation of severe bank erosion to channel sinuosity and slope but streambank erosion processes typically involve (surface and mass) fluvial erosion, mass wasting and subaerial processes (Fox et al., 2016). Additional work is needed to correlate the spatial mapping results to site-specific processes to shed light on the relation of watershed-scale patterns of severe bank erosion to causal factors occurring at a local scale.

4.4.4 Implications

During the latter half of the 20th century, upland soil conservation practices have been reducing sediment erosion from agricultural cropped fields (Jones & Schilling, 2011). For example, a significant reduction in sediment delivery in the Raccoon River in Iowa for the 1916 to 2009 period, with suspended sediment loads peaking in the early 1970s and then steadily declining throughout the 1980s to present (Jones & Schilling, 2011). Widespread adoption of land management practices such as terraces, conservation tillage, and contour cropping implemented under USDA conservation programs were thought to be primarily responsible for the sediment reductions (Villarini et al., 2016).

However, Iowa stream channels have been severely impacted by agricultural intensification over the last 150 years and have accumulated a legacy of historical alterations and hydrologic impacts (Jones & Schilling, 2011). Stream channels will continue to evolve over time as they adjust to historic alterations in channel morphology and flow (Simon & Rinaldi, 2000). The degree of state-wide streambank erosion we estimated in this study is consistent with recent studies indicating that streambank erosion is a major contributor to watershed sediment loads (e.g., Wilson et al., 2008; Palmer et al., 2014; Beck et al., 2018). Study results suggest that streambank erosion will likely be a challenge for bridge infrastructure for decades to come (Schilling et al., 2011).

4.5. Conclusions

In this study, we calibrated field mapping results to LiDAR derivative data to provide a first-order estimation of severely eroding streambanks in 3rd - 6th order streams and rivers found in Iowa. Streambank erosion represents a major challenge for Iowa with results suggesting that over 35,200 km of streambanks may be severely eroding, or approximately 41% of all 3rd - 6th order streams. The extent of streambank erosion was not uniform across the state with more erosion occurring in hillier western and southern Iowa compared to flatter and more recently glaciated northern Iowa. Streambank erosion was related to greater bank heights and was more prevalent (as a percent of the total stream length) in larger 5th and 6th order rivers. Overall,

despite limitations in the study related to the collection and extrapolation of the LiDAR dataset, study results provide new evidence for the magnitude of the streambank erosion problem in Iowa. Even though Iowans have made substantial progress in reducing sediment contributions from upland agricultural areas over the last half-century, it is clear from this study that contributions from streambank erosion will likely be a challenge for decades to come.

4.6 Products

This section has been developed into a manuscript submitted for peer-review to the *Journal of the American Water Resources Association (JAWRA)*. It is currently under review. The manuscript is entitled “***Quantifying the Extent of Eroding Streambanks in Iowa***” and co-authored by Keith Schilling and Calvin Wolter (investigators of the project team), as well as Jason Palmer of the Iowa Department of Natural Resources.

SECTION 5: IN-SITU AND LABORATORY MEASUREMENTS OF PARAMETERS INFLUENTIAL TO BANK EROSION

5.1 Goal Statement

There are many factors and mechanisms that contribute to the spatial patterns of streambank erosion in watersheds, which are not apparent when mapping occurrences of severe bank erosion, as in Section 4. Additional work is needed to correlate the spatial observations with site-specific information for identifying watershed-to-region-scale patterns of severe bank erosion and their causal factors.

This section discusses the in-situ and laboratory measurements of hydraulic and geotechnical parameters that are influential to bank soil strength and erodibility. The in-situ measurements were conducted at representative sites that were identified through the regional analyses in Section 4. Additionally, intact soil samples from these representative sites were brought back to the laboratory for conducting controlled measurements of the critical shear stress and corresponding erodibility coefficient.

The strength and erodibility parameters are utilized in the subsequent section with complementary modeling exercises to capture more fully the spatial and temporal variability of bank erosion in Iowa. Understanding the range that these parameters can exhibit over a wide range of flows is essential for determining the likelihood of erosion and the degree of bank recession at a site, as streambank erosion mechanisms can vary both within and among watersheds (e.g., Palmer et al, 2014; Wilson et al., 2014).

5.2 Methodology

5.2.1 Methodological Overview

In Section 4 of this report, it was shown that patterns of streambank recession are apparent in the different MLRAs of the state. Building on that finding, stream reaches in the different MLRAs have been selected near bridge crossings on county roads, as well as state and U.S. highways, for a more detailed examination of the erodibility and strength parameters within the local soils. The use of representative sites reduces the number of soil samples and monitoring locations (as well as corresponding time and labor) needed to assess bank soil erodibility across the state and facilitates the development of a broader (i.e., regional) model to predict bank erosion severity.

At each representative site, in-situ measurements of the soil's mechanical strength for estimating mass failure using a cone penetrometer and a Torvane shear tester are presented. Additionally, changes in soil moisture, flow discharge, and stream flashiness are identified using historical data from Iowa State University's network of observation stations located at

the Research and Demonstration Farms and the U.S. Geological Survey stream gaging stations to help assess the temporal changes in the mechanical strength.

Soil samples from the representative sites have been analyzed for texture, organic matter, bulk density, and Atterberg Limits, which will be used in empirical relationships with the critical shear stress to assess the strength and erodibility parameters for shear-driven erosion. Additionally, larger soil blocks placed in a conduit flume measure directly the critical shear strength and erodibility values for surface fluvial erosion. Photo-electric erosion pins (PEEPs) are also used to monitor recession during a series of storm events.

5.2.2 Identify Representative Stream Reaches for Field Monitoring

Within the different MLRAs, potential bridge crossings sites (Figure 5.1) were identified using historic aerial photographs that showed severe erosion coupled with knowledge from the past studies mentioned in Sections 3 and 4. The number of potential sites were further reduced by considering only the dominant soil types in the different MLRAs. In the end, sites along six different streams were selected.

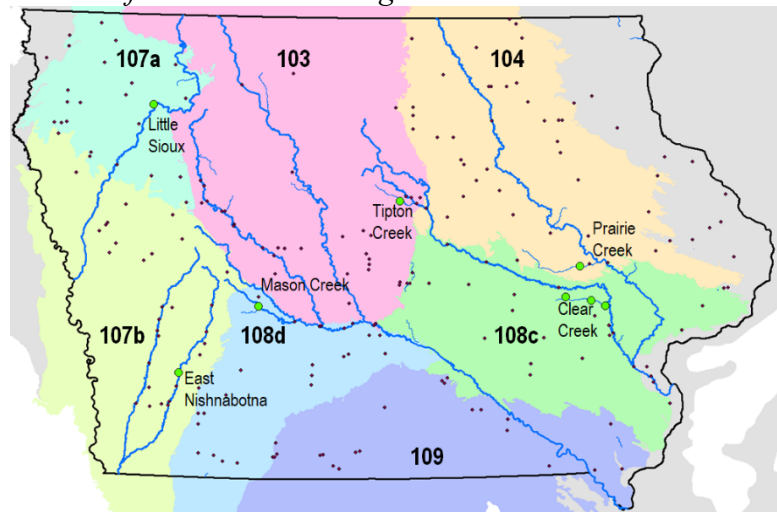


Figure 5.1. Map of representative sites. Black circles are all potential sites and green circles are the representative sites. Colored polygons represent the MLRAs. Blue lines represent pertinent streams.

5.2.3 In-situ Measurements and Ancillary Data for Mechanical Soil Strength Estimates

5.2.3.1 In-situ Methods

A soil's resistance to structural failure depends on cohesive forces and friction between particles. The soil's mechanical strength is a measure of this resistance, which is related to the internal friction angle of the soil, i.e., Mohr-Coulomb theory (Bryan, 2000). Because large soil blocks are susceptible to physical disturbances and potential chemical alterations during sampling, transport, and storage, in situ techniques to measure a soil block's stability are often utilized (Grabowski, 2010).

Vane shear testers are common instruments to estimate the undrained shear strength of the soil (Bryan, 2000). As the streambank soils in Iowa are predominantly cohesive and semi-

cohesive soils, they do not drain easily and may develop excess pore pressures due to the applied load, so the undrained shear strength is applicable here (Springston, 2007).

The shear strength measured with the Torvane shear tester relates to the structural and hydric state of the soil. This is different from the shear strength which relates to the detachment of particles at or near the soil surface under shearing flows (Torri et al., 1987). Nonetheless, mechanical shear strength has been related to Atterberg limits (Widodo et al., 2012) and used to estimate critical shear stress and erodibility (Mehta & Parchure, 2000).

The use of a Torvane shear tester at the representative sites followed standard methods (i.e., ASTM D 2573-72). It was inserted into the bank soil until the vanes were just covered (Figure 5.2a). The dial was rotated at a constant rate of approximately 1 revolution per minute until the soil broke apart. The strength was determined as a function of the torque applied at failure and the diameter of the vane.

The integrated strength over depth (~30 cm) was also measured with a cone penetrometer (Figure 5.2b) to provide a measure of bulk erodibility (Grabowski, 2014). The penetrometer consisted of a 60°, 2-cm diameter cone attached to a 3-cm diameter rod. The rod was pushed into the ground manually at a rate of about 1 cm/sec and the pressure of pushing the rod into the soil was measured on the Bourdon gage. The rate of 1 cm/sec is such that the penetration resistance ideally corresponds to shear strength under a static load, so point resistance and the effects of the friction are measured simultaneously (Grabowski, 2010).

5.2.3.2 Changes in Moisture

Mass failure occurs when processes acting on a streambank lower the soil strength below the soil block's weight (Rinaldi & Nardi, 2013). Increases in the moisture content of the soil both reduce



Figure 5.2. Torvane and penetrometer measurements. (a) Using the Torvane shear tester and (b) cone penetrometer along 2 Iowa streams.

the soil's strength and increase its weight, causing a soil block to slip and fail (Bryan, 2000). As an example, shear strength values have been observed to drop from 10 kPa to 1 kPa as moisture increases from 20% to 35% (Leonard & Richard, 2004).

Since the moisture content of a soil is a dynamic parameter, understanding its intra-annual variability and how that variability affects mass failure is essential. The historical intra-annual changes in soil moisture were identified using Iowa State University's network of observation stations (<https://mesonet.agron.iastate.edu/agclimate/#tmpf>). The stations within the network have changed over the years, but data from this network date back to 1986. Moisture data are monitored using water content reflectometers, which consist of two 12-cm-long stainless-steel rods connected to a printed circuit board that measures dielectric permittivity, volumetric water content, and bulk electrical conductivity.

5.2.3.3 Stream Flashiness

Stream flashiness reflects how quickly and how often flow depth changes in response to storm events. Although flashiness variability is predominantly related to precipitation, non-stationarity is also driven by land-use changes, such as the conversion of prairie-forests to agriculture and then to urban areas (Fongers, 2008). The rapid lowering of water removes the confining pressure of high flows increasing the likelihood of collapse of saturated bank soils (e.g., Mongollon et al., 2016; Zaimet et al., 2019).

The Richard-Baker Flashiness Index (Baker et al., 2004) was determined for the representative streams in this study using the sum of the differences between flows on two consecutive days divided by the total daily average flow. Larger fluctuations result in a higher Flashiness Index value, while a stable stream flow will have a value closer to zero. The flow values were obtained from the U.S. Geological Survey stream gage data over the period of record for the representative streams.

5.2.4 Laboratory Measurements of Streambank Soil Samples from the Representative Reaches

5.2.4.1 Sample Collection

Two types of soil samples were collected at sites along the representative streams. The first sample type consisted of surface material from the crest, midsection, and toe of streambanks exhibiting erosion. Multiple 5-cm x 5-cm x 5-cm scoops were collected at each location to ensure enough material was available for the series of soil assessment analyses. The examined soil properties included the following: texture; organic matter content; bulk density; water content; Atterberg limits; pH. The second sample type consisted of intact soil blocks also from

the crest, midbank, and toe of the eroding banks at a site (Figure 5.3). These soil samples were placed in a conduit flume for measuring critical shear stress and erodibility coefficients.

The majority of the soil samples were extracted between July 31 – August 1, 2015. This was 4 days after a frontal band of thunderstorms moved across the entire state that produced >1.0-inch of rain to eliminate soil desiccation effects. An additional set of soil block samples from two of the sites were collected on December 14, 2014. Soil temperatures rose from -1 °C to +5 °C on that day. These samples were analyzed to quantify the effects of a freeze-thaw cycle on the critical shear stress.



Figure 5.3. A soil block being excavated from a streambank for that determining critical soil strength and erodibility.

To ensure repeatability, a consistent extraction protocol was used to obtain and preserve the soil samples. The vegetation along the bank face was cut to the soil surface but leaving the roots intact to preserve the soil structure. Blocks of soil (length = 35 cm; width = 20 cm; height = 15 cm) were isolated by excavating the surrounding soil. The blocks were removed using long soil blades and a wire saw. They were then wrapped in aluminum foil and shrink wrap to maintain their shape and moisture level content during transport and storage. The samples were stored in the laboratory at a constant room temperature of 20° C before analysis.

5.2.4.2 Geotechnical Measurements

Standard methods of the American Society for Testing and Materials and other geotechnical methods were used to evaluate the soil characteristics. The soil samples were weighed wet, air-dried at room temperature under low humidity for one week, and re-weighed to estimate water content. The bulk density for each sample was determined by dividing the dry weight with the volume of the sample (125 cm³, based on the scoop dimensions).

To determine texture, the dried samples were lightly crushed and passed through a nest of pre-weighed sieves (i.e., No. 10, 20, 40, 60, 100, 140, 200; Figure 5.4a) to determine the sand content (ASTM D422). The silt-clay particle size distribution was determined using a standard hydrometer test (ASTM D422-63). Approximately 50-g of the soil less than 0.074 mm was dispersed in 125 mL of a 35.7 g/L mixture of sodium hexametaphosphate (NaPO₃)₆ for 12 hours.

Hydrometer measurements were recorded at set intervals over a two-day period to determine the gradation of fine soil particles (Figure 5.4b).

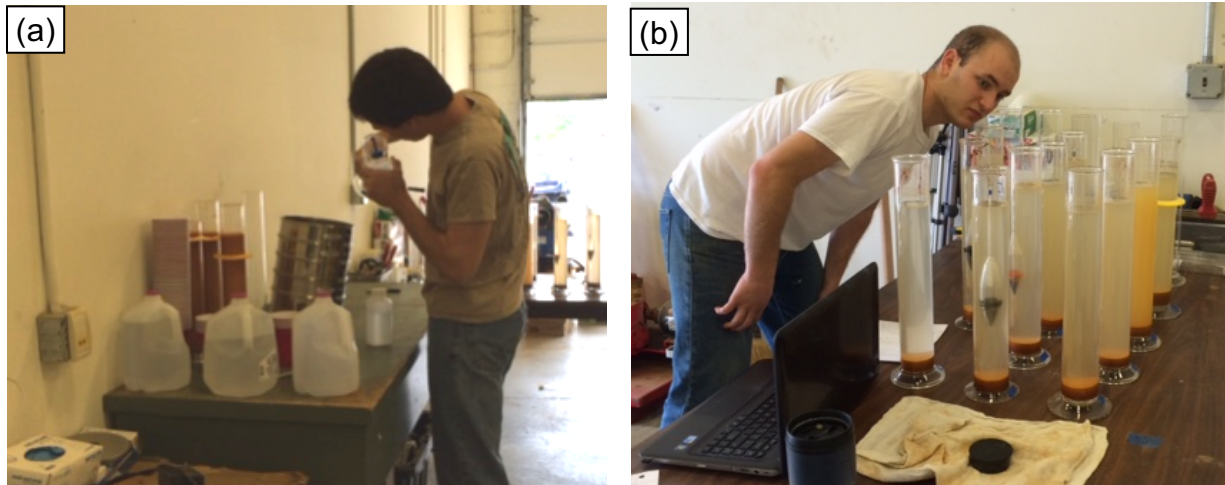


Figure 5.4. Sieving and hydrometer particle size analysis. (a) A nest of sieves was used to determine coarse particle sizes, (b) while the hydrometer method was used to determine the fine particle sizes.

The Liquid Limit (*LL*) and the Plastic Limit (*PL*) of the soil samples were estimated using the Casagrande Cup method and the standard plastic limit test (ASTM D4318). In addition, the Plasticity Index, *PI*, was estimated as the difference between the *LL* and the *PL*, or $PI = LL - PL$. The organic carbon was measured using a visible near infrared spectrometer calibrated for the soils in Iowa following the protocols of the NRCS Rapid Carbon Assessment protocol (Zhou et al., 2020). The pH of each sample was measured in a 1:2 mixture with distilled water.

5.2.4.3 Conduit Flume Runs to Quantify Critical Shear Stress and Erodibility

The critical shear stress and corresponding erodibility of the collected samples were measured under controlled flow conditions in a recirculating, water-and-sediment, conduit flume (Figure 5.5). The flume has a 10-cm x 5-cm, rectangular cross-section and a 305-cm useful length. The flume can reproduce the shearing action of stream flow to generate surface fluvial erosion (Sutarto et al., 2014); moreover, the conduit design can provide a wider range of applied shear stresses than open-channel flumes as the flow is pressurized, which helps replicate mass fluvial erosion conditions (Papanicolaou et al., 2017).

The details regarding sample preparation and flume operation are comprehensively detailed in Sutarto et al. (2014) and are summarized here. A 30-cm long x 10-cm wide x 5-cm deep subsection of each soil block was placed in the sample tray of the conduit flume. The tray

(Figure 5.5) is connected to the flume with jack screws, so the soil surface can be positioned flush with the flume bed. It is located 215 cm downstream of a diffuser. This distance is sufficient to allow a mature boundary layer to develop in the flow before it reaches the sample (e.g., McNeil et al., 1996). The flume bed and the top of the conduit between the diffuser and the sample box are covered with fine sandpaper (roughness, ϵ , = 0.0002 m) to replicate the surface micro-roughness of the soil and reduce the effects of a roughness change on the flow.

The flow rate was adjusted with a variable speed controller to produce different applied shear stresses. The operational flow rate of the flume ranged from 0.0025 to 0.0117 m³/s, which corresponded to bulk velocities of 0.5 to 2.3 m/s and applied shear stresses of 1 to 19 Pa. At least 5 different applied stresses were used for each sample.

For each soil sample, water and suspended sediment were collected 10 minutes after the stress-level change to allow time for the flow to develop. The water-sediment mixture was

retrieved through tubes projecting into the flow just downstream of the sample tray. Two liters were collected per stress-level, which were filtered through 1.0- μ m glass microfiber filters. The filters and collected sediment were oven-dried overnight and re-weighed.

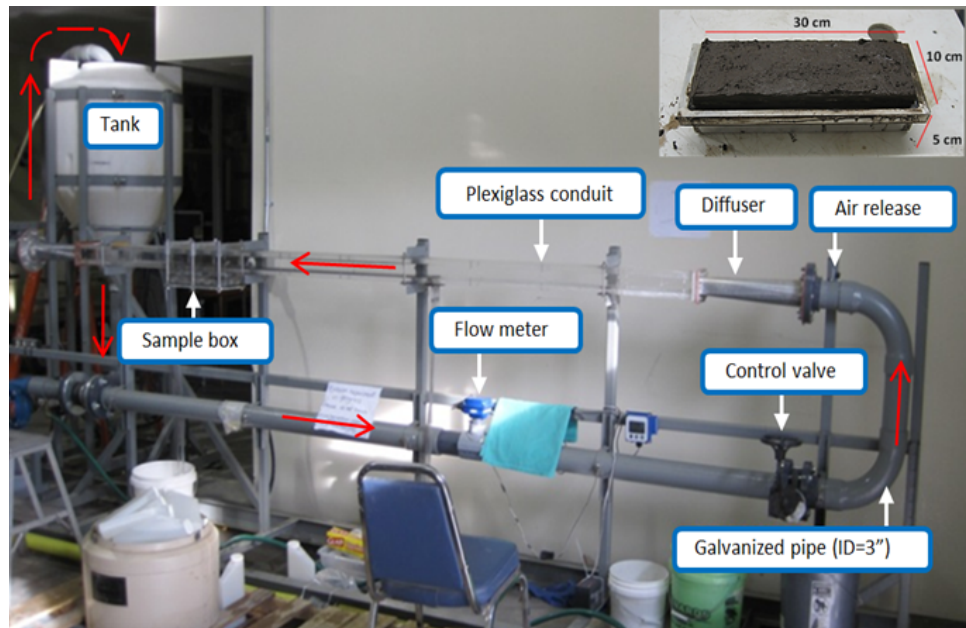


Figure 5.5. The conduit flume to measure critical soil strength and erodibility for surface fluvial erosion.

The erosion rate, E (kg/m²/s), at each stress level was quantified as follows:

$$E = \frac{\Delta C_{avg} * Q}{A_s} \quad (5.1)$$

where ΔC_{avg} is the difference in concentrations between two consecutive stress levels; Q is the volumetric flow rate; and A_s is the surface area of the soil sample (0.03 m²). The critical shear strength for each sample was determined by plotting the applied stresses and corresponding erosion rates and extrapolating a best fit line to $E = 0$ (Papanicolaou et al., 2007).

5.2.5 Photo-Electric Erosion Pin Measurements

Photo-Electric Erosion Pins were used to quantify a series of fluvial erosion events along entire bank profiles at representative sites. The installation and operation of the PEEP measurements are detailed in Papanicolaou et al., (2017).

PEEP sensors (Figure 5.6) have a series of photo-voltaic or photo-resistance diodes that are spaced at a fixed distance (i.e., 1.65 cm). PEEPs are initially inserted into the bank face so that the diodes are buried. As the bank face erodes, a number of diodes become exposed to the sunlight relative to the amount of the erosion. The sunlight either provides a voltage signal relative to the number of exposed diodes which is transmitted to a datalogger or causes resistance to decrease allowing a supplied voltage to pass to the datalogger also relative to the number of diodes exposed. The voltages were logged every 15 seconds and averaged every 15 minutes (e.g., Mitchell et al., 2003; Horn & Lane, 2006; Lawler, 2008; McDermott & Sherman, 2009; Zaimes & Schultz, 2015).



Figure 5.6. The photo-electric erosion pin.

5.3 Results & Discussion

5.3.1 Representative Stream Reaches

Six stream reaches were selected to represent the different MLRAs in the state in terms of geomorphic, geotechnical, and hydraulic characteristics (Table 5.1). The sites include Tipton Creek, a tributary of the Upper Iowa River in Hardin County; Prairie Creek, a tributary of the Middle Cedar River in Linn County; Clear Creek, a tributary of the Lower Iowa River in Iowa & Johnson Counties; the Little Sioux River in Obrien County; the East Nishnabotna River in Pottawattamie County; and the South Raccoon River in Guthrie County. Table 5.1 contains the pertinent site information including the represented MLRA and the stream order.

5.3.2 In-situ Measurements of Soil Strength and Ancillary Hydraulic Data

5.3.2.1 Torvane and Penetrometer Measurements

At the representative sites, both penetrometer and Torvane shear strength measurements were conducted at the crest, midbank, and toe locations along the bank face. The Torvane measurements of undrained shear strength ranged from 5-25 kPa, while the penetrometer

measurements of soil penetration resistance (i.e., integrated soil strength over a depth of 30 cm) ranged from 500 to 1750 kPa. With the depth-integrated measurement being larger than the surface value, this confirms an increase in soil strength as the soil compacts.

Table 5.1. Representative sites.

	MLRA	HUC-8 Watershed	Stream	Order	County	Road	Latitude/ Longitude
103	Central Iowa & Minnesota Till Prairies	Upper Iowa	Tipton Creek	3	Hardin	US 65 & 250th St	42.33959 -93.30962
104	Eastern Iowa & Minnesota Till Prairies	Middle Cedar	Prairie Creek	4	Linn	US 151 & Prairie Ave	41.92325 -91.78408
107A	Iowa & Minnesota Loess Hills	Little Sioux	Little Sioux River	6	Obrien	IA 10	42.92926 -95.43005
107B	Iowa & Missouri Deep Loess Hills	East Nishnabotna	East Nishnabotna River	4	Pott	IA 92 & 535th St	41.23499 -95.16243
108C	Illinois & Iowa Deep Loess & Drift (west-central)	Lower Iowa	Clear Creek	3	Iowa	US 151 & 190th St	41.72946 -91.90889
108D	Illinois & Iowa Deep Loess & Drift (west)	South Raccoon	South Raccoon River	5	Guthrie	IA 25	41.66409 -94.50399

An increasing linear trend was observed across sites when comparing the corresponding Torvane and penetrometer measurements (Figure 5.7). The correlation between the surface and the depth integrated values suggests homogeneity in bank properties for at least the top 30 cm, which has been observed in other studies from Iowa (e.g., Sutarto et al., 2014). The samples from the East Nishnabotna stream bank exhibited higher strength values than the other sites, suggesting it was more compacted. The values for the South Raccoon River, as well as Tipton and Prairie Creeks all plot similarly. Yet, these values plot in a descending order from the crest to the toe. This result was

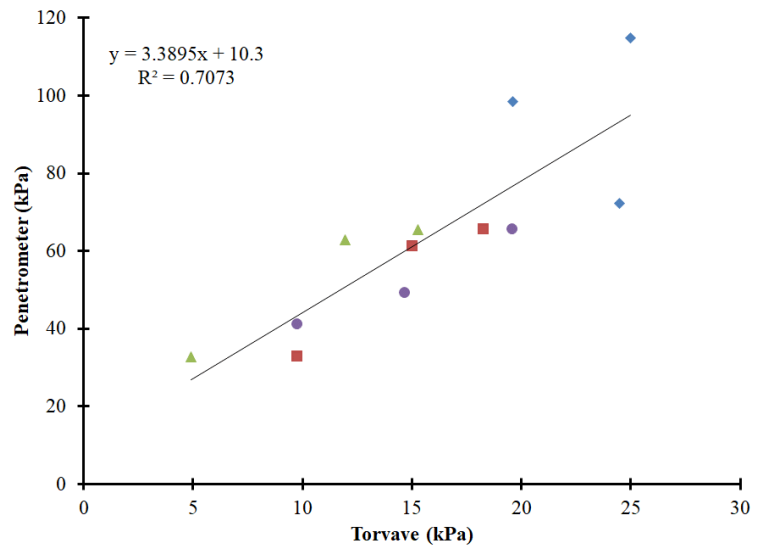


Figure 5.7. Corresponding measurements from a cone penetrometer and Torvane shear stress tester. Blue diamonds are values from the East Nishnabotna River; Green triangles are values from the South Raccoon; Red squares are from Tipton Creek; Purple Circles are from Prairie Creek.

contrary to the expected trend where the toe of the bank is the most consolidated (Sutarto et al., 2014).

A positive correlation between c' and clay content was established, where higher clay content correlated with higher cohesion. Compacted clay has less available pore spaces and hence higher bulk density. Higher bulk density values in most cases indicate higher effective stresses (e.g., Ayers, 1987; Bardet et al., 2011). The highest c' values were from Tipton Creek (MLRA 103) at 39 kPa, due to relatively high clay content. The values for Prairie Creek (MLRA 104) and the East Nishnabotna (MLRA 107B) had values near 25 kPa. The Clear Creek (MLRA 108C) values were near 11 kPa, while for the South Raccoon (108D) samples, the c' was only 0.5 kPa. Yang et al. (2005) reported c' values in the range of 2.7 to 12 kPa for glacial till soils with a texture of silt clay loam extracted across six counties in southern Iowa.

5.3.2.2 Soil Moisture Changes

Soil moisture is variable throughout the year and Figure 5.8 shows the average annual soil moisture fluctuations per MLRA from 2013 through 2019. Moisture values for all MLRAs peak in May and June corresponding with the seasonal rainfall peak for Iowa. MLRA 104 in northeast Iowa experienced the highest levels of soil moisture throughout the year. It is followed by MLRA 108D.

These would be the most at-risk regions for having saturated banks during the most intense rainstorms, (and potentially the flashiest storm events) highlighting the risk for mass failure. MLRA 104 would also be the most likely region to

have high moisture in the stream banks during the freeze-thaw periods of late fall and early spring. High moisture levels during freeze-thaw periods have been shown to weaken the soil structure considerably (Mostaghimi et al., 1988). Incidentally, MLRA 104 saw the largest recession rates marked by the aerial imagery results (Table 3.2).

Table 5.2 shows the number of freeze-thaw cycles per year since 2013. These data were derived from Iowa State University soil moisture network which has co-located soil temperature

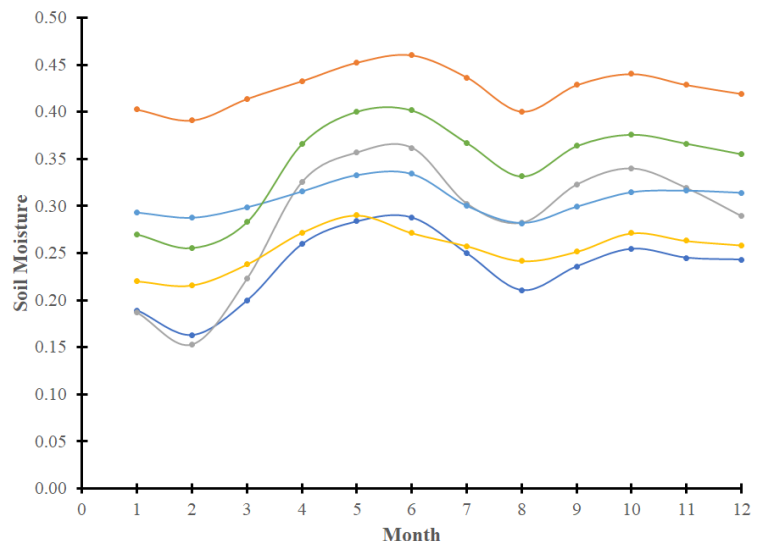


Figure 5.8. Average annual soil moisture measurements. Dark blue line is MLRA 103; Orange line is MLRA 104; Grey line is MLRA 107A; Yellow line is MLRA 107B; Light blue line is MLRA 108C; Green line is MLRA 108D.

monitoring. MLRA 103 had 2 more freeze-thaw cycle per year (13 cycles/year) over MLRA 108C (11 cycles/year). With freeze-thaw cycles considerably weakening the critical shear strength (Ferrick & Gatto, 2005), MLRA 103 is most at-risk of having a large erosion event in early spring.

Table 5.2 Freeze-Thaw Cycles

MLRA	2013-2014	2014-2015	2015-2016	2016-2017	2017-2018	2018-2019	2019-2020
103	7	17	8	14	21	22	5
104	0	2	1	2	7	4	7
107A	6	8	5	6	11	15	1
107B	11	0	3	4	8	9	3
108C	8	17	16	8	10	11	4
108D	10	18	2	8	10	9	0
109	9	17	9	8	10	10	2

5.3.2.3 Stream Flashiness

Stream flashiness can be a key mechanism leading to mass failure of saturated stream banks. A rapid rise and fall in stage during a storm event most likely would occur faster than the draining of the stream banks. Without the confining pressure of the high flows, these banks have a higher chance of collapse. Table 5.3 list the USGS gaging stations used for the representative sites in this study. Systems with smaller drainage areas tend to be flashier than larger systems because the upland runoff has a shorter distance to travel thereby reaching the stream more quickly (Figure 5.10). The same is true for systems with higher levels of impervious surfaces or subsurface drain tiles. Finally, channelization of the streams allows the water to move more quickly through the channel, which would increase the flashiness of the stream. The smaller systems of Prairie Creek and Clear Creek had high flashiness indices (>0.45). However, the larger systems of the South Raccoon and East Nishnabotna had unexpectedly high flashiness indices (~0.33) compared to the other larger systems of the Little Sioux and the South Fork of the Iowa River (<0.27), which may be attributed to channelization.

Table 5.3. USGS sites near the sampling locations.

Site Number	Site Name
USGS 05454300	Clear Creek near Coralville, IA
USGS 05454220	Clear Creek near Oxford, IA
USGS 05484000	South Raccoon River at Redfield, IA
USGS 05451210	South Fork Iowa River NE of New Providence, IA
USGS 05464695	Indian Creek at Marion, IA
USGS 06604440	Little Sioux River at 300th St near Spencer, IA
USGS 06809210	East Nishnabotna River near Atlantic, IA

5.3.3 Measurements of Critical Shear Strength against Surface Fluvial Erosion and Erodibility

5.3.3.1 Geotechnical Measurements

On a whole, the soil textures of the representative sites ranged from sandy loam to loam and then silty clay and clay loams (Table 5.4). The organic matter ranged from 1-5%. The plasticity index *PI* range from 12 to 19 and the prevalent clay type was illite (Clay Mica) and smectite. The bulk density values measured using the scoops show fairly consistent values. This supports the homogeneity suggested by the Torvane and integrated penetrometer measurements (Figure 5.7). Higher variability was observed at the crest and midbank than at the toe which was attributed to deposition of coarser, sand-sized bed material during overbank conditions (Wilson et al., 2012; Sutarto et al., 2014).

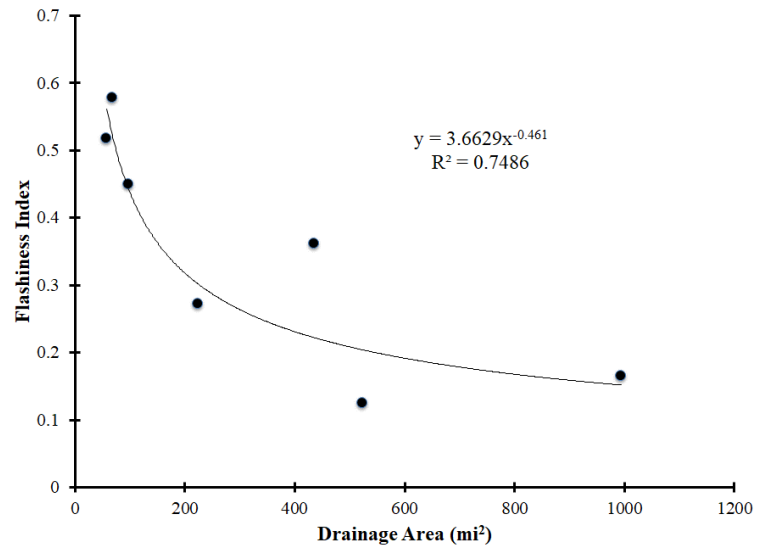


Figure 5.9. The Richards-Baker Stream Flashiness Index per drainage area.

Table 5.4. Soil characteristics of surface samples collected at each representative site.

MLRA	Sand	Silt	Clay	Organic Matter	Bulk Density	Water Content	Plasticity Index	Liquid Limit	pH
103	22.0	47.0	31.0	7.0	1.15	21.6	21.0	55.0	6.7
104	9.4	67.1	23.5	3.5	1.45	18.2	10.0	32.5	6.5
107A	30.0	47.0	23.0	4.5	1.39	18.5	15.0	43.0	7.0
107B	9.1	66.1	24.8	2.7	1.36	16.8	15.9	40.6	6.7
108C	10.0	67.5	22.5	3.3	1.39	15.4	14.1	34.8	6.1
108D	77.0	14.4	8.45	1.8	1.50	18.4	21.6	21.4	6.5
109	9.3	66.1	24.7	3.0	1.40	16.1	15.9	37.4	6.2

5.3.3.2 Conduit Flume Analysis

Figure 5.10 shows plots of erosion rate vs. applied shear stress for three of the samples placed in the conduit flume as examples. The erosion rates were determined using the measured concentrations during each run. Bedload motion of large individual flocs was not observed in

these tests as most of the particles were predominately transported in suspension suggesting that the concentration of the suspended material follows a uniform distribution (Raudkivi, 1998).

A linear regression line was fit through the data to determine the critical erosion stress, $\tau_{c,f}$, which is where the regression line crosses the y-axis. The y-intercept is essentially equivalent to an erosion rate of zero. The erodibility coefficient, M_f , was then determined as the gradient of a best fit line through the data in a plot of E_f versus $(\tau / \tau_{c,f} - 1)$.

In Figure 5.10, we see the results of samples from (a) Tipton Creek, (b) Clear Creek, and (c) the South Raccoon. The critical shear strength values were 1.48, 2.07 and 0.89 Pa, respectively. For the sample from Tipton Creek (Figure 5.10a), the texture classified as a silty clay loam with silt+clay contents between 65-70%. The soil from Clear Creek (Figure 5.10b), a silt loam, had silt+clay contents >80%. Finally, the soil from the South Raccoon (Figure 5.10c) had loamy sand soils and silt+clay contents ~25%. The critical shear stress values increase as the silt+clay contents increase. Thus, the observation with the aerial imagery results (Table 3.2) is supported here with the conduit flume data, that the stronger soils tend to be those with the most cohesive properties.

To assess how a bank soil's critical shear stress changes over

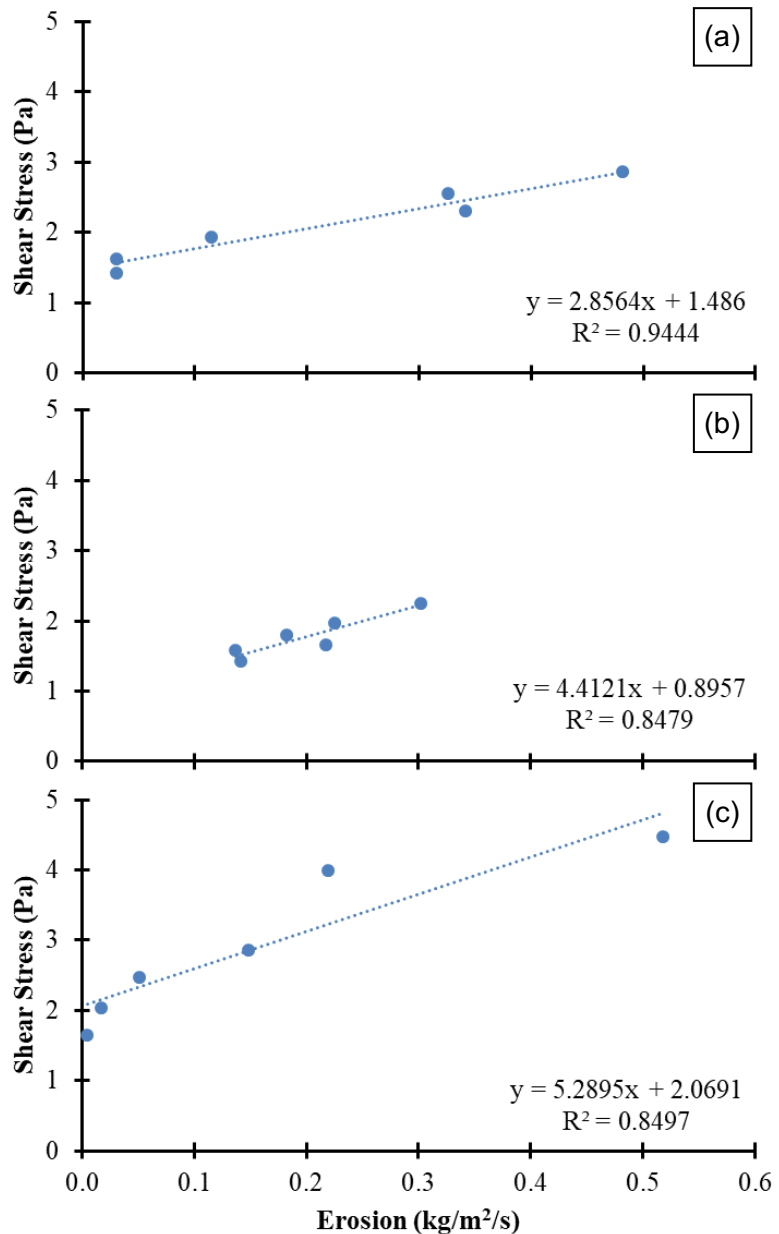


Figure 5.10. Example graphs of the erosion rate vs. the applied shear stress from the conduit flume runs for different soils. The critical erosional strength is determined where the erosion rate equals zero (i.e., where it crosses the y-axis). (a) This sample is from Tipton Creek in MLRA 103. (b) This sample is from Clear Creek in MLRA108C. (c) This sample is from the South Raccoon River in MLRA 108D.

time under weather, a sample collected in Clear Creek following a freeze-thaw cycle was measured in the conduit flume. The critical erosional strength was determined as 0.52 Pa (Figure 5.11). In comparison to the sample collected during the summer of 2015, which had a τ_c of 2 Pa (Figure 5.10b), the sample experiencing freeze-thaw had a reduced critical shear stress by a factor of 4. This type of

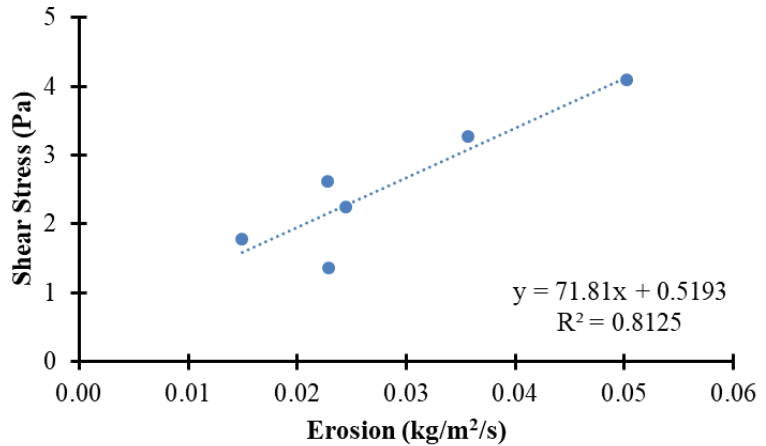


Figure 5.11. Flume run for freeze-thaw soils.

freeze-thaw analysis on banks soils has not been done before and will help to address the changes in vulnerability of banks over time. Although the conduit flume may not be the most optimal piece of equipment to measure freeze-thaw samples because it is designed for a relatively higher set of stress values. The results provide the expected decrease similar to other studies (Mostaghimi et al., 1988; Ferrick & Gatto, 2005).

5.3.4 PEEP Measurements and Mass Fluvial Erosion

5.3.4.1 Magnitude and Frequency of Mass Fluvial Erosion

The continuous time series of flow depth, h , and bank retreat length, L , recorded along a bank face at the representative site along Clear Creek are in Figure 5.12 (Papanicolaou et al., 2017). The retreat lengths measured at the crest (Figure 5.12b), upper midbank (Figure 5.12c), lower midbank (Figure 5.12d), and toe (Figure 5.12e) are seen as the staircase jumps in the solid red lines.

The hydrograph in Figure 5.12a shows there were multiple high flow events capable of inducing fluvial erosion. The translations of these flows to the applied shear stress are seen in the figures for each PEEP location. The crest location experienced more erosion events (i.e., 8 events) than the mid-bank or toe locations, and consequently the crest location had the highest retreat (i.e., 41 cm) over the series of events. The upper and lower midbank locations had 29.6 and 27.6 cm over 4-5 events. The toe location experienced only 1 event of 6.6 cm. On an event basis, the retreat lengths at each location were of a similar magnitude, between 1.6 and 13.2 cm. Temporally, the largest events occurred early in the season, when the soils had less vegetation cover.

Comparing the crest and mid-bank locations, the crest experienced more erosion even though it was inundated less often. This was most likely due to the soil being less consolidated, as the more recently deposited sediment at the crest had less time to consolidate in comparison to soil at the lower sections. Thus, the crest location was more susceptible to fluvial erosion (Sutarto et al., 2014). The toe location was inundated over the longest period of time; however, much if the time these flows were of a low magnitude and with the toe soils having the highest relative degree of consolidation, there was consequently little erosion.

High confidence was given to the PEEP measurements from the comparison with the traditional erosion pins closest to the PEEPs (Table 5.5). A close agreement was observed between the two sets of measurement (t-test; $p = 0.98$). At the crest and mid-bank locations, the PEEP measurements were higher than the corresponding pin measurements, but at the toe location the PEEP measurements were comparatively lower than the traditional measurements.

Potential reasons for this deviation are related to differences in compaction. Because of the less compacted soils at the upper locations of the bank face, there is a higher likelihood for the PEEPs to spin slightly out of the augured hole, suggesting a higher retreat length. The PEEPs have a longer exposure length and protrude more into the flow resulting in more drag forces. Finally, the turbidity from the high-sediment flow may have “stained” the PEEP diodes diluting the light intensity.

Table 5.5. Comparison of observed bank retreat lengths and rates for the PEEPs and pins. From Papanicolaou et al. (2017)

Location	Retreat Length and Rates				
	PEEP (cm)	PEEP (cm/s)	Pin (cm)	Pin (cm/s)	%difference
Crest	28	1.39×10^{-4}	21	1.02×10^{-4}	27
UpperMid	15	6.37×10^{-5}	12	5.17×10^{-5}	19
Lower Mid	8.2	2.74×10^{-5}	6.2	2.07×10^{-5}	24
Toe	0	0.00	12	2.45×10^{-5}	n/a

5.3.4.2 Erodibility

To determine the erodibility of the bank soil, the measured retreat lengths at the different locations along the bank face were integrated over the total bank height for a 1-m wide section and quantified in kg/s with the following equation (Palmer et al., 2014):

$$M = \frac{\text{mass of erosion}}{\text{time of erosion}} = H_{bank} \times W \times \left(\frac{\Delta L}{\Delta T}\right) \times \rho_{bulk} \quad (5.5)$$

where H_{bank} (m) is the bank height; W (m) is set at 1-m; ΔL (m) is the retreat length integrated over the bank height; ΔT (s) is the period of erosion (Table 5.6); and ρ_{bulk} (kg/m^3) is the bulk

density of the bank soil. For determining the period of erosion, it was assumed based on past research (Julian & Torres, 2006) that it is only immediately following the initial “punch” to the bank face from stress increase over the threshold value when the erosion occurs. The next layer of sediment would be more compacted and need a higher stress level to erode. For example, at the crest of the bank, the initial increase lasted 1800 s, or 0.5 hour, which is represented with the first rise of the line. As a result, the M_m for this event was found to be 0.332 kg/s. Because it occurred early in the season, the soil had less vegetation coverage and was more prone to the higher erosion rates.

5.4 Summary & Conclusions

A soil’s resistance to erosion under applied shear forces

and structural failure depends on both cohesive forces between particles and frictional resistance between the particles sliding over one another. The characteristics that define these resistance forces are highly variable in both space and time. The inability to consider this variability severely inhibits our prediction of the likelihood of bank erosion at bridge sites.

Herein, we examined the level of variability in the strength and erodibility parameters for surface and mass fluvial erosion, as well as mass failure across the state of Iowa at the MLRA

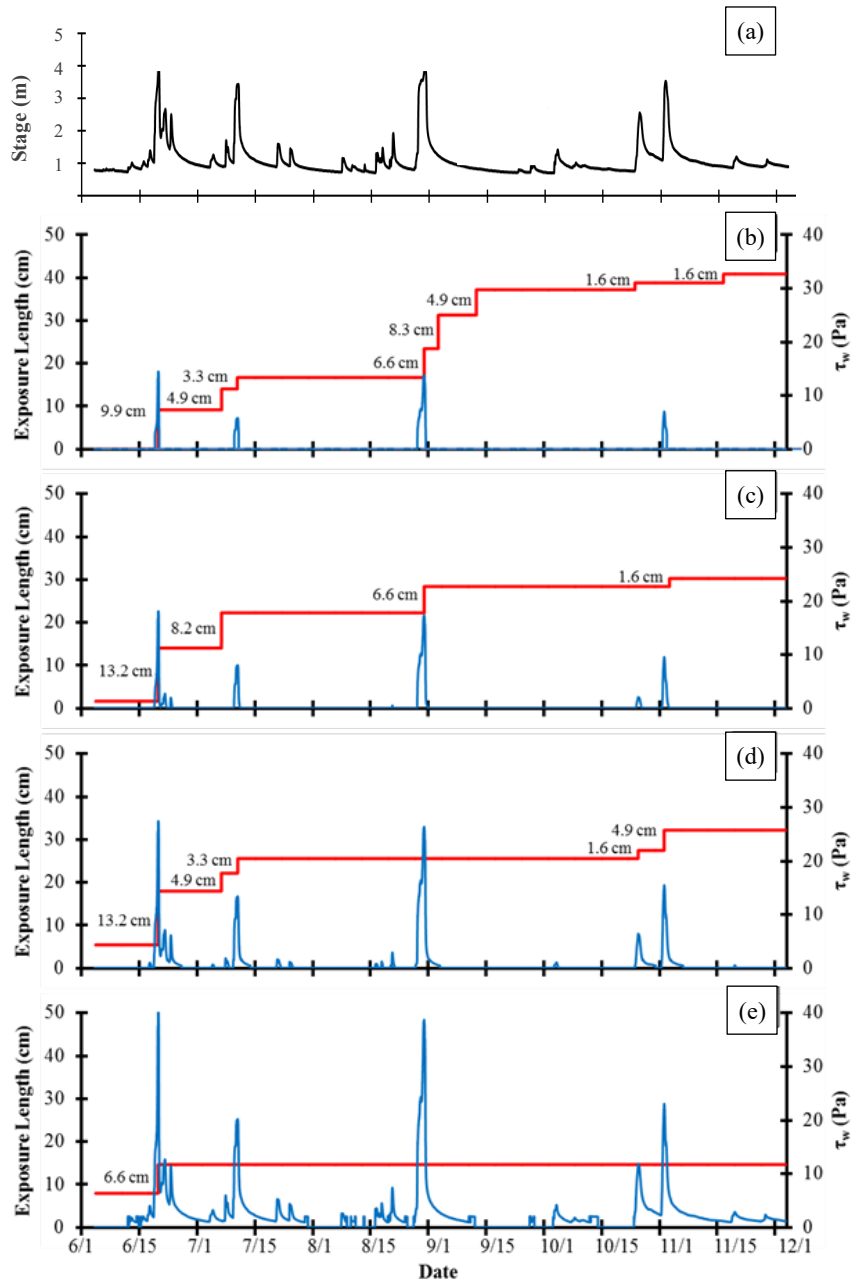


Figure 5.12. Time series of (a) water stage, applied shear stresses and the smoothed exposure lengths for the PEEPs at the (b) crest, (c) upper midbank, (d) lower midbank, and (e) toe.

level. The critical shear stress for fluvial erosion was significantly lower in MLRAs 103 and 104 than in the rest of the state. This was attributed to these soils being till-derived and having less silt+clay content than the loess-derived soils in southern and western Iowa. These results are in line with the erosion pin data discussed in Section 3.

Table 5.6. Erodibility parameters for mass fluvial erosion. From Papanicolaou et al. (2017)

Event	Integrated Erosion Length (cm)	ΔT (hr)	M_m (kg/s)
June 19 th	9.4	0.50	0.332
July 10 th	1.2	0.25	0.073
August 27 th	3.9	0.63	0.095
October 22 nd	0.14	0.50	0.005
October 29 th	0.83	0.38	0.034

The corresponding erodibility data followed suit with MLRAs 103 and 104 having the highest erodibility. However, these values were not significantly different from the other parts of the state. Erodibility values in Iowa have a wider variance than the critical shear stress values.

Regarding the parameters for mass failure, cohesion and soil strength also correlated with clay content, which does not bode well for MLRAs 103 and 104. Moreover, MLRA 103 tends to experience 1 more freeze-thaw cycle and MLRA 104 has higher annual soil moisture content than the rest of Iowa. All these factors suggest that MLRAs 103 and 104 are more susceptible to bank erosion.

5.5 Products

The first product related to this section is a peer-reviewed manuscript that was published in *Earth Surface Processes and Landforms*. The paper was entitled “Understanding mass fluvial erosion along a bank profile: using PEEP technology for quantifying retreat lengths and identifying event timing”. It was co-authored by Thanos Papanicolaou and Christopher Wilson, as well as Papanicolaou’s former students Achilles Tsakiris, Tommy Sutarto, and Fabienne Bertrand. Additionally, the co-authors included Massimo Rinaldi of the University of Florence, Subhasish Dey at the Indian Institute of Technology, and Eddy Langendoen at the USDA-ARS National Sedimentation Laboratory. It is one of the first papers to quantify mass fluvial erosion in the field using PEEPs.

A manuscript is currently being prepared that assesses stream bank erosion likelihood in the different MLRAs, while capturing seasonal and annual variability in both the bank soil strength and the applied shear stress of the flow. The critical shear strength is central in

determining the rate of fluvial bank erosion and estimating how far the streams will migrate in the near future. By knowing the extent of variability in critical erosional strength under different flow ranges over time, you can better select bank erosion countermeasures especially near critical infrastructures where soil is disturbed and more susceptible to weather seasonality.

SECTION 6: BANK EROSION MODELING AT SELECT SITES

6.1 Goal Statement

It is logistically difficult to measure the different bank erosion mechanisms over a wide range of flows because capturing a sufficient number of bank erosion events (i.e., storms) within a representative set of stream reaches would be both time-consuming and expensive. Numerical models, if properly parameterized and calibrated, can fill in the gaps in terms of the number of analyzed storms. The coupled analysis of the measured and modeled results can lead to better management decisions and support infrastructure design and rehabilitation.

To expand the usefulness of the measurements discussed in Section 5 regarding the bank soil strength and erodibility and ultimately support the development of a broad-scale, multi-mechanistic bank stability assessment approach, this section discusses the temporal (i.e., seasonal) and spatial (i.e., regional) variability of critical shear stress and erodibility values. Understanding the range of these parameters will help determine the likelihood of erosion and the degree of bank recession at a site.

6.2 Methodology

6.2.1 Methodological Overview

To expand the range of strength and erodibility values observed in the different MLRAs of Iowa, the Iowa Soil Properties And Information Database (ISPAID) provides select bulk properties of those soils found near stream channels. The properties can be used as input into a series of empirical equations derived from multiple field and laboratory studies to quantify strength and erodibility values from more easily measured parameters. These calculated values are compared with those measured in the conduit flume runs described in Section 5.3.3.2 and applied to the Bank Stability and Toe Erosion Model (BSTEM). BSTEM simulates surface/mass fluvial erosion under the ranges of flows determined using flow frequency analyses for the representative reaches mentioned in Table 5.1. Additionally, BSTEM determines if the banks became unstable due to the fluvial erosion resulting in mass failure. Factors of Safety can be determined for the different locations to quantify the likelihood of bank erosion for the representative reaches.

6.2.2 Empirical Estimates

There are a number of soil parameters that influence the resistive strength and erodibility of cohesive and semi-cohesive soils, including grain size distribution, soil bulk density, clay type and content, organic matter content, and soil pore water content and chemistry (Grissinger,

1982). Many studies have built on these relationships to develop empirical equations (Table 6.1) that quantify critical shear stress and erodibility (e.g., Smerdon & Beasley, 1961; Jepsen et al. 1997; Hanson & Simon, 2001; Wynn & Mostaghimi, 2004; Julian & Torres, 2006).

Table 6.1. Empirical relations for stress and erodibility values.

Critical Shear Strength	
Cao & Du (1986)	$\tau_{c,f} = 0.7 (\gamma_{dry})^5$
Gilley et al. (1993)	$\tau_{c,f} = 0.216clay - 183 LEP + 0.412 WC + 0.78$
Julian & Torres (2006)	$\tau_{c,f} = 0.1 + 0.1779(silt + clay) + 0.0028 (silt + clay)^2 - 2.34e^{-5}(silt + clay)^3$
Mehta (1983)	$\tau_{c,f} = 0.392 + (0.0845 \times CEC)$
Mitchener & Tofs (1996)	$\tau_{c,f} = 0.15 \left((\gamma_{dry} \times 1000) - 1000 \right)^{0.73}$
Smerdon & Beasley (1961)	$\tau_{c,f} = 0.493 \times 10^{0.0182clay}$
Smerdon & Beasley (1961)	$\tau_{c,f} = 0.163 P_i^{0.84}$
Tang (1963)	$\tau_{c,f} = \left(\frac{1}{77.5} \right) \times \left[3.2(\gamma_s - \gamma)d + \left(\frac{0.00029}{d} \right) \left(\frac{\rho_s}{\rho} \right)^{10} \right]$
Owen (1975)	$\tau_{c,f} = 6.85e^{-6} (\gamma_{dry})^{2.44}$
Thorn & Parsons (1980)	$\tau_{c,f} = 5.42e^{-6} (\gamma_{dry})^{2.28}$
Amos et al., 1997	$\tau_{c,f} = 7e^{-4} (\gamma_{dry}) - 0.47$
Erodibility	
Arulanandan (1975)	$M_f = 2230 \tau_c \times e^{(-1.3\tau_{c,f})/20}$
Bstem1	$M_f = 1.62 (\tau_{c,f})^{-0.838}$
Bstem2	$M_f = 4.62 (\tau_{c,f})^{-0.207}$
Bstem3	$M_f = 84.3 (\tau_{c,f})^{-1.17}$
Hanson & Simon (2001)	$M_f = 0.2 (\tau_{c,f})^{-0.5}$
Wynn et al., (2008)	$M_f = 3.1 (\tau_{c,f})^{-0.37}$
Wynn & Mostaghimi (2006)	$\log (M_f) = -0.68 + 0.55(FTC)^{0.5}$
Wynn & Mostaghimi (2006)	$\log (M_f) = 0.73 + 0.15(FTC)^{0.5} - \frac{0.12}{MC} - 1.46 D_{50}^{0.25}$
Wynn & Mostaghimi (2006)	$\log (M_f) = 0.53 + 0.08FTC$
γ_{dry} = bulk density; <i>clay</i> = percent clay; <i>silt</i> = percent silt; P_i = plasticity index; <i>LEP</i> = coefficient of linear extensibility; <i>wc</i> = water content; τ_c = critical shear stress; <i>CEC</i> = cation exchange capacity; <i>OM</i> = organic matter.	

Although the equations provide solid estimates, caution must be used that the soil types examined in these studies are equivalent to those being tested. Herein, we used these equations (Table 6.1), which were developed for cohesive and semi-cohesive soils, to quantify ranges of

strength and erodibility values within each MLRA for use as representative base values for the predictive modeling of erosion likelihood.

Although strength and erodibility are dynamic parameters which change with moisture, temperature, and vegetation, many of the empirical equations are based on static (or slow changing) parameters like texture, organic matter content, and bulk density (Bryan, 2000). Few equations (also in Table 6.1) have recently been developed showing how strength and erodibility values change with moisture, freeze-thaw cycles, and degree of vegetative cover (Ferrick & Gatto, 2005; Wynn et al., 2008; Pollen, 2007). Using the ranges of values for moisture and freeze-thaw cycles observed in Iowa (see Section 5.3.2.2), the temporal variability of strength and erodibility values was also determined.

6.2.3 Flow Characteristics and Frequency Analysis

The continuous streamflow data from the USGS gaging stations at the representative sites (Table 5.3) were used to perform flow frequency analyses and determine the time periods when conditions for bank erosion are favorable, as well as their durations. The flow exceedance values were used to identify the stage and discharges of different design storms for use in the BSTEM simulations. The following exceedance probabilities were used: 0.01% (100-yr flow); 0.04% (25-year flow); 0.5% (2-year flow, considered as bankfull); 1% (1-year flow); 10%; 50%; 95%.

6.2.4 Quantifying Bank Retreat Rates under Different Condition Using BSTEM

The Bank Stability and Toe Erosion Model (static version 5.4) was developed by the U.S. Department of Agriculture's Agricultural Research Service and is similarly based on the bank erosion mechanisms in the CONservational Channel Evolution and Pollutant Transport System (CONCEPTS) model. BSTEM integrates modules for both bank toe erosion (i.e., shear-driven) and bank stability (i.e., collapse).

A *bank toe erosion module* quantifies fluvial erosion along the bank toe under an applied hydraulic shear stress during a storm event. Under the toe erosion module, erosion rates are determined using an excess shear stress equation (Partheniades, 1965). The rates are integrated with respect to time to yield an average retreat:

$$E_f = M_f (\tau_w - \tau_c) D_t \quad (6.1)$$

where E is the erosion distance (m); M_f is the erodibility coefficient ($\text{m}^3/\text{N s}$); D_t is the timestep (s); τ_w is the average boundary shear stress (Pa); and τ_c is the critical shear stress (Pa). The model estimates τ_w from channel geometry, the bank coordinates, flow parameters, and channel slope using the following equation:

$$\tau_w = \gamma_w R S \quad (6.2)$$

where γ_w is the unit weight of water; R is the hydraulic radius (m) calculated from the water depth; and S is the channel slope (m/m). The τ_c and M can be entered directly or determined based on general soil texture. Please note that the subscripts denoting fluvial and mass erosion are not used as the equations can apply for both, but BSTEM only considers one at a time. In this study the strength and erodibility parameters were obtained from the flume runs and empirical equations described previously.

The erosion values are corrected considering channel curvature/meandering effects (i.e., secondary circulation; large cross-stream variations in the boundary shear stress and velocity), as well as the effective boundary shear stress, based on the Manning's n value. The effective stress considers the flow resistance resulting from viscous and pressure drag over the reach's wetted perimeter. This drag considers the ground surface with the presence of aggregates (Chow, 1959) and vegetation (Temple et al., 1987).

If enough erosion at the bank toe occurs during the event to reduce the Factor of Safety for mass failure (equation 6.3) below its threshold value, then a *bank stability module* quantifies the amount of the bank collapse. The module simulates planar failure or cantilever failure, whenever the driving force exceeds the soil strength. The bank stability module utilizes limit equilibrium-method models to calculate Factors of Safety, F_s (Thorne & Tovey, 1981; Langendoen et al., 2009).

$$F_s = \frac{\sum_{i=1}^l (c_i L_i + (\mu_a - \mu_w)_i L_i \tan \phi_i^b + [W_i \cos \beta - \mu_{ai} L_i + P_i \cos(\alpha - \beta)] \tan \phi_i^l)}{\sum_{i=1}^l (W_i \sin \beta - P_i \sin[\alpha - \beta])} \quad (6.3)$$

where c_i^l is the effective cohesion of i^{th} layer (kPa); L_i is the length of the failure plane incorporated within the i^{th} layer (m); W_i is the weight of the i^{th} layer (kN); P_i is the hydrostatic confining force due to external water level (kN/m) acting on the i^{th} layer; b is the failure plane angle (degrees from horizontal); a is the local bank angle (degrees from horizontal); and l is the number of layers. The bank is considered stable if $F_s > 1$ and banks with an F_s value less than 1 are unstable.

In opposition to mass failure, there is the strength of a soil block, which is dependent on the internal friction angle, θ , and the soil mechanical strength, c_0 . The model accounts for the strength of up to five soil layers, the effects of positive and negative porewater pressure, confining pressure due to streamflow, and soil reinforcement due to vegetation. Inputs include the bank coordinates, soil types, vegetation cover, water table depth, and porewater pressures. This version of the model assumes hydrostatic conditions below the water table and a linear interpolation of matric suction above it.

One limit equilibrium analysis uses the Mohr-Coulomb failure criterion for the saturated portion of the bank, while the Fredlund et al. (1978) criterion is used for the unsaturated portion. The other limit equilibrium analysis evaluates normal and shear forces active in the bank soil. The confining force due to the water in the channel is modeled by extending the slip surface vertically through the water and applying a horizontal hydrostatic force on the vertical portion of the slip surface. The cantilever shear failure algorithm ensures that if the bank is partially or totally submerged the weights of the layers affected by water are correctly reduced irrespective of the basal surface geometry of the cantilever.

The model was calibrated using the PEEP measurements described in Section 5.3.4. The Manning's n value used to determine the effective boundary shear stress was adjusted to match the applied shear stress determined in the field during the actual events. The simulated erosion length for the bank was compared with the integrated erosion length determined using the array of PEEPs. A Nash-Sutcliffe value of 0.67 was obtained for the calibration. The "optimal" Manning's n value was used in the simulations of the different exceedance probability events in Section 6.2.3. By calibrating with the PEEP-determined erosion rates and using the Manning's n to adjust the applied shear stress, we are in a sense compensating for the inability of BSTEM to account for fluvial and mass erosion separately.

6.3 Results

6.3.1 Analytical Estimates of Strength and Erodibility Parameters

To limit the number of soil series examined herein, the geomorphic description/ landscape position was used as a filter. The following descriptions were used: alluvial fans, depressions, drainageways, floodplains, outwash plains, terraces, river valleys. There are 284 different soil series that line the channels and drainageways in Iowa, with 31 (only 11%) covering 62% of the area. The predominant soil series in MLRAs 107A, 107B, 108C, 108D, and 109 which cover the western and southern parts of the state are the Colo, Nodaway, and Zook series. The north-central and northeast parts of the state (i.e., MLRAs 103 and 104) contain primarily the Clyde, Floyd, and Okobojo series.

The bulk properties of these stream bank soils were extracted from the ISPAID to expand the range of $\tau_{c,f}$ and M_f values observed in the collected samples. The majority of the soils had textures of silt loam (32%), silty clay loam (21%), and loam (21%). The silt loams and silty clay loams can be considered as cohesive in many cases throughout the state.

The values of the bulk soil properties were applied to the empirical equations in Table 6.1 to quantify $\tau_{c,f}$ and M_f values respective to each MLRA. For each soil series, all equations in the table were applied and the average $\tau_{c,f} / M_f$ value was considered further. The area-weighted

averages for both $\tau_{c,f}$ and M_f were quantified for each MLRA with the $\tau_{c,f}$ values being between 1.53 Pa and 2.00 Pa and the M_f values being between 0.145 and 0.162 cm³/ N s (Table 6.2).

As a form of verification, the results of the geotechnical analysis were coupled with the corresponding, measured critical shear stress and erodibility values from the conduit flume runs of this study and other previous published and unpublished bank erosion studies in Iowa (e.g., Sutarto et al., 2014). This comparison produced strong correspondences between the measured $\tau_{c,f}$ values for the different sites with clay, organic matter content, CEC, and water content (Figure 6.1) as seen through the high correlation coefficients of the linear regression best-fit lines. Moreover, the comparison yielded similar (and simple) empirical relationships as those in Table 6.1, with the $\tau_{c,f}$

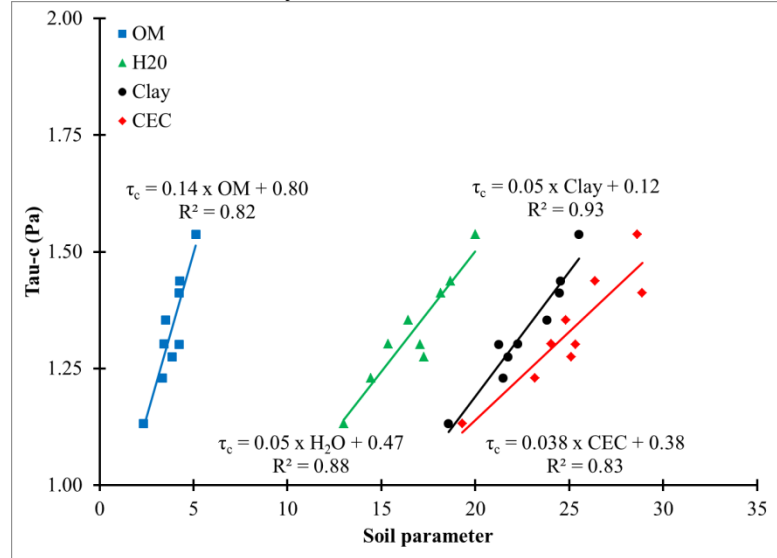


Figure 6.1. Empirical relationships between critical shear strength and inherent soil properties. OM = percent organic matter; Clay = percent clay content; H2O = available water content in percent; CEC = cation exchange capacity in meq/100 g.

values being between 1.1 Pa and 1.6 Pa. This similarity in $\tau_{c,f}$ values provided confidence in using the published relationships in Table 6.1.

6.3.2 Spatial Variability of $\tau_{c,f}$ and M_f

The critical shear stress values across the MLRAs (Table 6.2) were significantly different (ANOVA, $p < 0.001$). The soils with the highest average $\tau_{c,f}$ were found in MLRAs 107A, 107B, and 108D, while the weakest soils were found in MLRAs 103 and 104. The cumulative distribution functions (Figure 6.2) show that MLRAs 107A, 107B, 108C, and 108D appear similar in their pattern and tend to overlap.

This is most likely indicative of the relatively homogeneous loess blanket that covers the western and southern parts of the state, which has since been translocated through erosion becoming colluvium and alluvium and yielding ultimately similar soil series. MLRAs 103, and 104 show lower

Table 6.2. Strength & erodibility parameters.

MLRA	$\tau_{c,f}$ (Pa)	M_f (cm ³ / N s)
103	1.68 ± 0.17	0.157 ± 0.013
104	1.53 ± 0.11	0.162 ± 0.008
107A	1.89 ± 0.18	0.147 ± 0.012
107B	2.00 ± 0.24	0.146 ± 0.012
108C	1.76 ± 0.16	0.152 ± 0.011
108D	1.93 ± 0.21	0.145 ± 0.010
109	1.72 ± 0.19	0.156 ± 0.010

distributions of $\tau_{c,f}$ and higher distributions of M_f . In summary, these cumulative distribution functions visually reflect the separation between the $\tau_{c,f}$ and M_f values of the different MLRAs.

These observed trends correspond to the conventional thought that the loess-derived soils in western and southern Iowa, which contain higher amounts of cohesive material being silty clay and silty clay loams, are more resistant than the soil in north central and northeast Iowa where the soils are till-derived and coarser. The soils in MLRA 109 in southern Iowa have relatively low $\tau_{c,f}$ and relatively high M_f values, which most likely is attributed to the thinning loess profiles moving east and south across the state. These trends also correspond with the results of the erosion pin data in section 3.3.1 of this report. The erosion-pin-determined recession rates from northwest Iowa were highest throughout the state. In southwest Iowa, the soils had lower recession rates which was attributed to the abundance of cohesive soils.

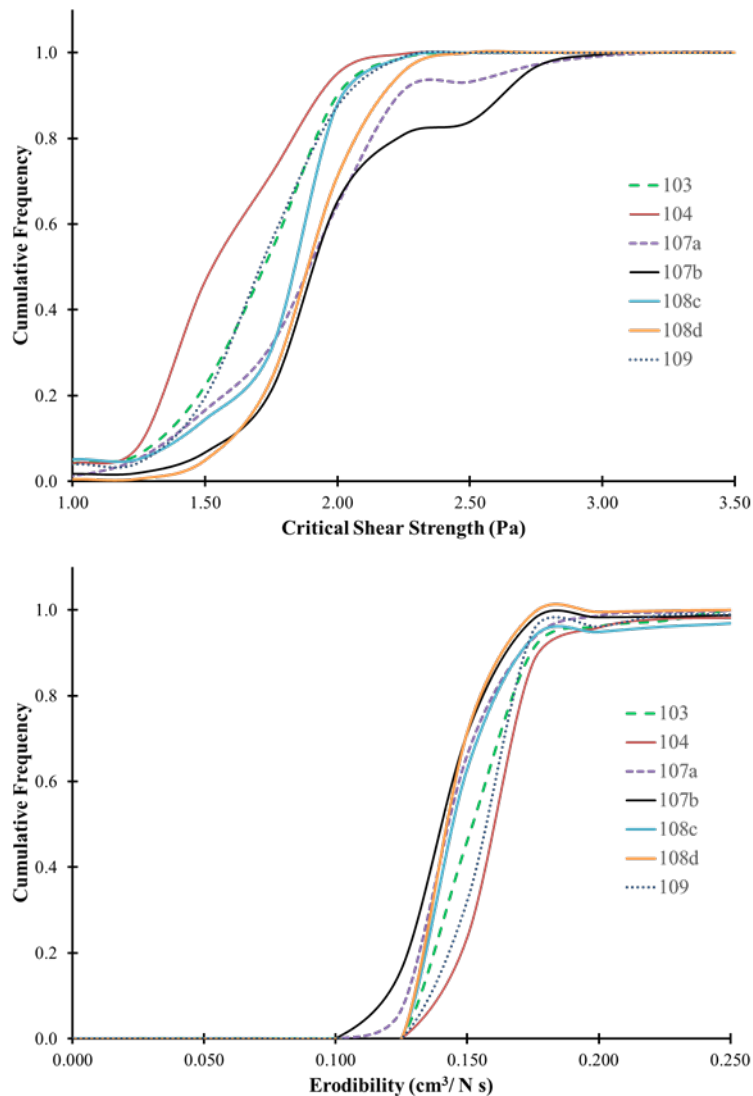


Figure 6.2. Cumulative density functions for strength and erodibility parameters.

For the most part, the erodibility values fall in line with critical shear stress values, and the erodibility values for the different regions were also significantly different (ANOVA; $p < 0.05$). The lower degree of significance is a product of the higher variability in values when using the different equations in Table 6.1. This highlights one of the major difficulties in bank erosion modeling, the determination of the erodibility values, which has been attributed to the systematic differences in the methods used to determine erodibility (Sutarto et al., 2014;

Karamigolbaghi et al., 2017; Mahalder et al., 2018). Nonetheless, MLRAs 103, 104, and 109 had the highest erodibilities, while MLRAs 107A, 107B, and 108D had the lowest values.

To put these strength and erodibility values into a context, the corresponding pairs were plotted on the same figure (Figure 6.3). The plot represents the classification scheme by Hanson and Simon (2001) developed in the cohesive soils of the U.S. Midwest, which rates soils from Very Resistant → Resistant → Moderately Resistant → Erodible → Very Erodible based on the combination of decreasing $\tau_{c,f}$ and rising M_f . The average values of the MLRAs fall to the right side of the red line, which is the breakpoint between Moderately Resistant and Erodible soils. The soils from western Iowa in the original dataset by Hanson & Simon (2001) also plotted as Moderately Resistant.

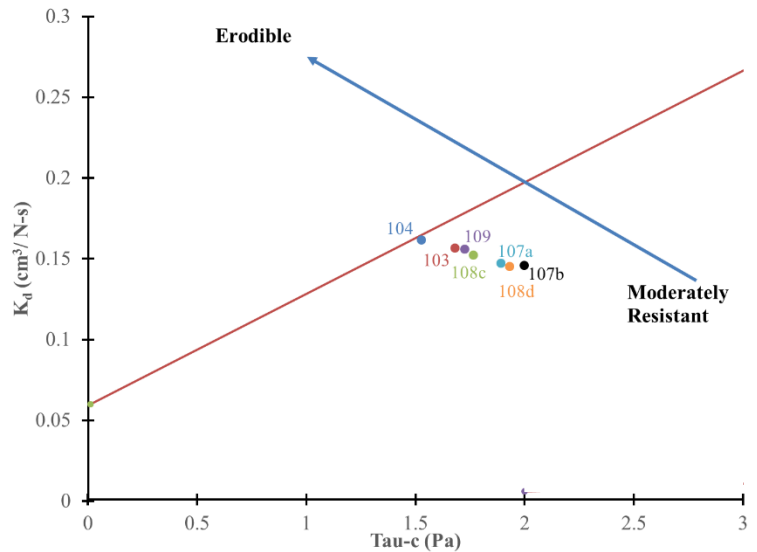


Figure 6.3. A plot of critical shear stress vs. erodibility following the classification system by Hanson & Simon (2001).

6.3.3 Temporal Variability of Strength and Erodibility Parameters

In addition to bulk properties, the strength and erodibility parameters of stream bank soils are also strongly affected by weather conditions. In Section 1, these were termed as subaerial processes and mainly relate to soil moisture and freeze-thaw cycles, which weaken the soil strength and critical shear stress. Higher levels of soil moisture decrease cohesion by causing a greater separation between clay particles and decreasing friction (Bryan, 2000). Freeze-thaw cycles disintegrate soil structure and reduce aggregation with the degree of disintegration being related to the soil water content at freezing and the rate of freezing (Mostaghimi et al., 1988).

Soil moisture in Iowa across all MLRAs tends to be highest from April through June coinciding with the rainfall peak (Table 6.3). January and February tend to have the lowest average soil moisture. MLRAs 104 and 108D have both the highest average moisture contents (> 0.3) and the lowest change in soil moisture over the year. Conversely, MLRAs 103 and 107A have the lowest average moisture contents and the biggest annual change. It is difficult to understand the effect of moisture on the strength and erodibility parameters without looking at it in conjunction with freeze-thaw (Table 6.4). Each MLRA appears to have a different trend in

terms of freeze-thaw, but across the whole state, the most freeze-thaw cycles occur in both December and March. MLRA 103 has the greatest number of cycles in the last 7 years, while MLRA 104 has the fewest number of cycles.

Table 6.3. Average monthly moisture content per MLRA.

	103	104	107A	107B	108C	108D
January	0.19 ± 0.09	0.40 ± 0.03	0.19 ± 0.09	0.22 ± 0.13	0.29 ± 0.15	0.27 ± 0.12
February	0.16 ± 0.09	0.39 ± 0.04	0.15 ± 0.08	0.22 ± 0.14	0.29 ± 0.15	0.26 ± 0.13
March	0.20 ± 0.09	0.41 ± 0.01	0.22 ± 0.10	0.24 ± 0.12	0.30 ± 0.15	0.28 ± 0.12
April	0.26 ± 0.07	0.43 ± 0.02	0.33 ± 0.06	0.27 ± 0.09	0.32 ± 0.16	0.37 ± 0.06
May	0.28 ± 0.06	0.45 ± 0.01	0.36 ± 0.04	0.29 ± 0.09	0.33 ± 0.17	0.40 ± 0.06
June	0.29 ± 0.06	0.46 ± 0.01	0.36 ± 0.05	0.27 ± 0.13	0.33 ± 0.17	0.40 ± 0.07
July	0.25 ± 0.08	0.44 ± 0.04	0.30 ± 0.07	0.26 ± 0.13	0.30 ± 0.16	0.37 ± 0.09
August	0.21 ± 0.08	0.40 ± 0.04	0.28 ± 0.06	0.24 ± 0.11	0.28 ± 0.16	0.33 ± 0.10
September	0.24 ± 0.09	0.43 ± 0.04	0.32 ± 0.05	0.25 ± 0.12	0.30 ± 0.16	0.36 ± 0.08
October	0.25 ± 0.08	0.44 ± 0.03	0.34 ± 0.03	0.27 ± 0.11	0.31 ± 0.17	0.38 ± 0.07
November	0.25 ± 0.07	0.43 ± 0.01	0.32 ± 0.05	0.26 ± 0.10	0.32 ± 0.16	0.37 ± 0.05
December	0.24 ± 0.07	0.42 ± 0.01	0.29 ± 0.07	0.26 ± 0.10	0.31 ± 0.15	0.36 ± 0.06

Table 6.4. Partition of freeze-thaw cycles.

MLRA	# of cycles since 2013	Nov	Dec	Jan	Feb	Mar	Apr
103	94	0.15	0.23	0.17	0.18	0.22	0.04
104	19	0.00	0.11	0.16	0.47	0.26	0.00
107a	52	0.13	0.29	0.10	0.10	0.35	0.04
107b	38	0.11	0.21	0.21	0.21	0.21	0.05
108c	74	0.08	0.24	0.24	0.20	0.19	0.04
108d	57	0.16	0.18	0.26	0.16	0.23	0.02
109	64	0.11	0.22	0.25	0.19	0.20	0.03

One study has looked at the combined effects of soil moisture and freeze-thaw cycles (Wynn & Mostaghimi, 2006), seen in the following equation:

$$\log(M_f) = 0.73 + 0.15(FTC)^{0.5} - \frac{0.12}{MC} - 1.46 D_{50}^{0.25} \tag{6.4}$$

Figure 6.4 shows the changes in strength and erodibility over the course of the year due to changes in soil moisture content (MC) and freeze-thaw cycles (FTC). The description that follows focuses on critical shear stress, as the description of the erodibility is just the inverse. The critical shear strength reaches minimum values during March and April when soil moisture is high and there are several freeze-thaw events. The strength climbs to a peak in August when

the effects of freeze-thaw are non-existent and soil moisture is at a moderate level. Over the winter, though, the sites exhibit different behaviors. The northwestern MLRA 107A peaks in the $\tau_{c,f}$ during the winter due primarily to low moisture content. MLRAs 104 and 108D have high moisture content over the winter and thus low values of $\tau_{c,f}$.

To put these changes in strength and erodibility values over the annual cycle into context, the Hanson & Simon (2001) classification presented in Figure 6.3 is helpful. Average annual values for each MLRA were determined and plotted in Figure 6.5. In summary, by accounting for moisture and freeze-thaw, the critical shear stress values for all MLRAs decrease (and erodibility values increase). There is a noticeable shift to the top left and the values now plot in the Erodible range (Figure 6.5). This shift is a qualitative reason for considering these temporal changes in strength and erodibility values with any modeling efforts.

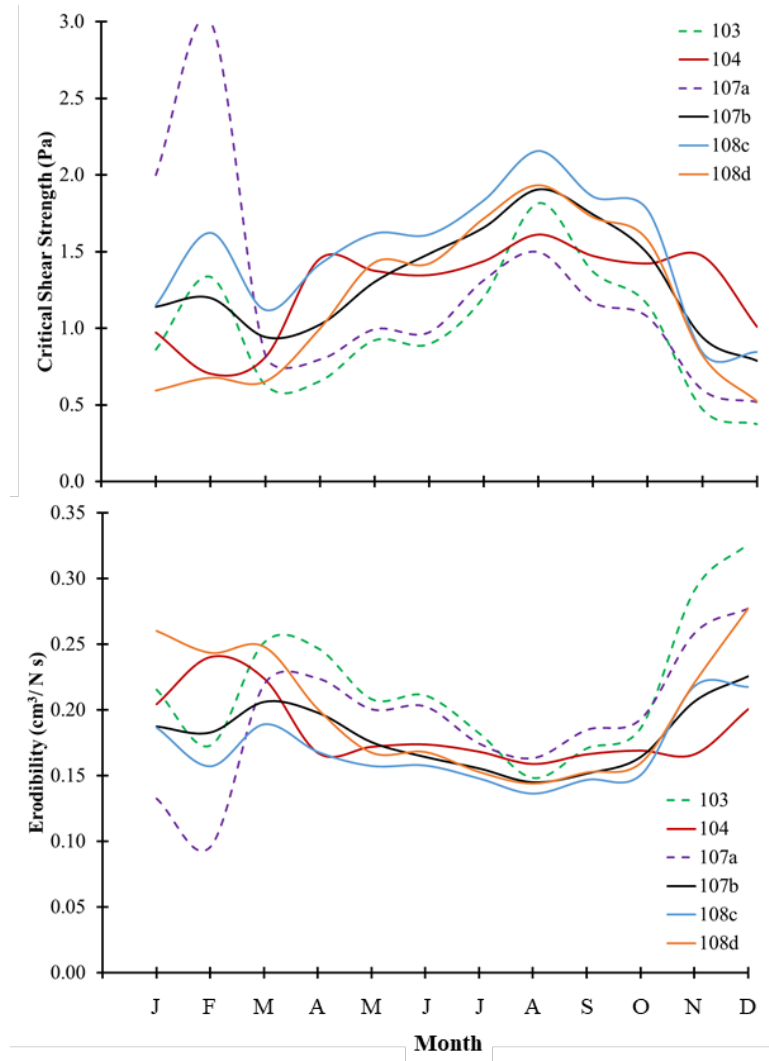


Figure 6.4. Changes in critical shear stress and erodibility over the year due to the combined effects of moisture and freeze-thaw cycles.

6.3.4 Flow Frequency Analyses

Figure 6.6 shows an example of the flow duration curves developed for the representative sites identified in Table 5.1. From these duration curves, select flows (Table 6.5) were identified for the BSTEM simulations. The flows correspond to the 100-yr and 25-year events, as well as the 2-yr (i.e., bankfull condition) and 1-year events. Additionally, because Iowa has predominantly cohesive soils along the stream banks, several lower flows were chosen to understand fluvial erosion experienced at the bank toe, which could also be a predecessor of large bank collapses. These are flows that are exceeded 10%, 50%, and 95% of the time. It is believed that these

lower flows can over time produce similar amounts of erosion as a large, catastrophic bank collapse because they occur more often. Moreover, these smaller flows are often neglected because, individually they do not cause eye-catching erosion. Yet, it is their combined effects that can be problematic.

6.3.5. Fluvial Erosion Estimates Using BSTEM

The changes in the critical shear stress and erodibility values for the channel corridor soils in Iowa are quite apparent from Figure 6.5.

The erosion classifications for these soils shift from Moderately Resistant to Erodible. Although this shift is in a sense qualitative, one does get the impression of an overall weakening of the soils when considering subaerial factors.

To provide a more quantitative effect, Table 6.6 lists the average static critical shear stress values determined using the equations in Table 6.1. For comparison, the seasonally averaged critical shear stress values for each MLRA are provided that consider the moisture changes in Table 6.3 and the number of freeze-thaw cycles in Table 6.4. In all but one instance (MLRA 108C), the combined effects of moisture and

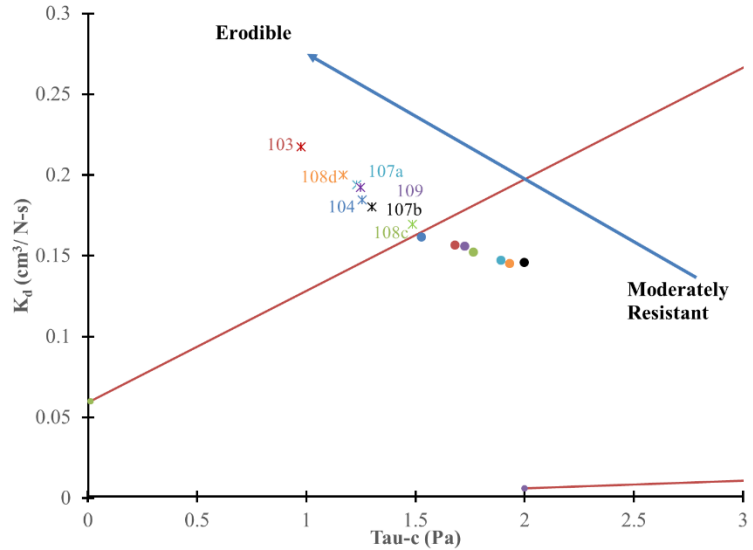


Figure 6.5. A plot of critical shear stress vs. erodibility following the classification system by Hanson & Simon (2001) when considering subaerial processes.

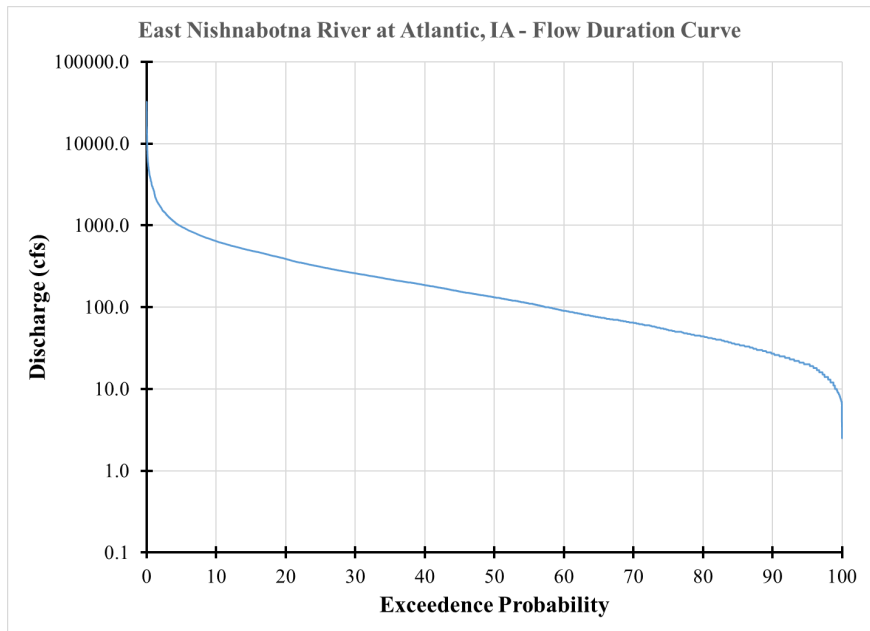


Figure 6.6. An example of the flow duration curves used to identify a range of flows for the modeling exercises. These data are from the USGS gaging station on the East Nishnabotna River near Atlantic IA.

freeze-thaw are significant in that the ranges for the static and seasonally variable critical shear stress values do not overlap.

Table 6.5. Flow exceedance values.

MLRA	River	Discharge (cfs)						
		Exceedance Probability						
		0.01	0.04	0.5	1	10	50	95
103	Tipton Cr.	4790	3300	804	370	113	19	1
104	Prairie Cr.	15800	11000	2870	1160	239	59	7
107A	Little Sioux R.	13500	9650	5355	3074	1095	216	24
107B	East Nishnabotna R.	31000	22300	6800	4870	1050	261	33
108C	Clear Cr.	4700	3200	624	77.1	14.6	2.62	0.1
108D	South Raccoon Cr.	11200	7610	1840	545	79.7	24.2	1.43

Both the static and seasonally variable critical shear stress values (and corresponding erodibility values) were used in the BSTEM simulations for a typical bankfull event at each representative site. The amounts of erosion for the two simulations of the bankfull event were compared. The amount of erosion using the seasonally variable values in all cases were higher. For the MLRAs in the southern part of the state (107B, 108C, 108D, and 109), the increase in erosion rates were on the order of a quarter to a third higher. However, for the northern MLRAs of 103, 104, and 107A, the percent increase was from 90% to 730%. For MLRAs 103 and 107A, the soils in these areas experienced the biggest decreases in soil strength during the months of December and March which see the most frequent freeze-thaw cycles (Figure 6.4). Moreover, MLRA 104 has the highest average moisture content throughout the year (Table 6.3), making it most likely for the soils to lose cohesion under high water contents.

The BSTEM simulations provide a sense of which MLRAs are most likely to experience fluvial erosion throughout the year. Table 6.7 provides the Factors of Safety for fluvial erosion quantified under the specific design flows in Table 6.5. The average applied boundary shear stress quantified by BSTEM using equation 6.2 for each design flow was compared

the seasonally variable critical shear stress. The boxes shaded in green are considered stable, with the yellow shaded boxes having marginal FS_f values. The pink shaded boxes signify

Table 6.6. The effect of seasonally variable critical shear strength on bank erosion.

MLRA	Static τ_c (Pa)	Variable τ_c (Pa)	% Increase in Erosion
103	1.68 ± 0.17	0.97 ± 0.21	730 ± 402
104	1.53 ± 0.11	1.26 ± 0.08	91 ± 31
107A	1.89 ± 0.18	1.23 ± 0.25	289 ± 298
107B	2.00 ± 0.24	1.30 ± 0.30	29 ± 16
108C	1.76 ± 0.16	1.49 ± 0.18	33 ± 24
108D	1.93 ± 0.21	1.17 ± 0.32	26 ± 16
109	1.72 ± 0.19	1.23 ± 0.30	31 ± 20

erosion would occur. MLRAs 107A and 107B have FS_f values less than one for all flows,

suggesting fluvial erosion is highly likely for all flows. This corresponds to finding in section 4 where these MLRAs had the highest density of eroding banks. This may be attributed to the high loess content in these soils.

MLRAs 103, 104, 108C have stable FS_f values for more flows suggesting they are less likely to eroded. MLRAs 103 and 104 have low channel slopes, as mentioned in section 4.4.3. Schilling and Wolter (2005) reported that basin slopes in Des Moines Lobe watersheds were typically 1.5% compared to ~7% in southwest Iowa watersheds. The channel slopes of 3rd order streams in MLRAs 103 and 104 were approximately 1/3 of the slopes in southwest Iowa. As seen with equation 6.2, slope is related to the applied shear stress, and a very high correlation (seen with the R^2 value of 0.78 in Figure 6.7) exists between the simulated erosion rate and the channel slope. Moreover, in Figure 6.7, the three data points with the highest channel slope are all located in MLRA 108C. This suggests that the applied shear stress is more influential to bank erosion rates than the critical shear stress. To examine whether adjusting the channel slope through grade control structures to limit bank erosion is better than other stabilization methods, more simulations would be needed.

Table 6.7. Factors of Safety for fluvial erosion.

MLRA	95% Duration	50% Duration	10% Duration	1% Duration	2-yr Peak Flood	25-yr Peak Flood	100-yr Peak Flood
103	1.59	1.24	0.98	0.72	0.53	0.31	0.27
104	2.21	1.15	0.80	0.49	0.32	0.17	0.15
107A	0.92	0.44	0.30	0.20	0.15	0.09	0.08
107B	0.72	0.39	0.29	0.19	0.17	0.09	0.08
108C	5.14	1.19	0.60	0.33	0.19	0.12	0.11
108D	1.06	0.43	0.27	0.18	0.13	0.12	0.11
109	1.77	0.62	0.36	0.23	0.15	0.11	0.10

6.4 Summary & Conclusions

6.4.1. Assessing Variability of Streambank Soil Strength and Erodibility Parameters in Iowa

This section discusses how the in-situ and laboratory measurements discussed in section 5 were used as a basis for assessing the spatial and temporal variability of streambank soil strength and erodibility parameters in Iowa. The measured geotechnical properties provided verification of the soil properties listed in ISPAID for developing distributions that represent the streambank soil characteristics in the different MLRAs in the state. The ISPAID values were applied to a series of published empirical equations relating more easily measure soil properties to τ_{cf} and M_f . The calculated strength and erodibility values were compared to the measured values from the conduit flume runs and PEEP measurements. The MLRA-average values were then used to

parameterize BSTEM simulations that quantified (surface/mass) fluvial erosion rates under a range of flows for the representative reaches in Table 5.1.

The critical shear stress values found in MLRAs 107A, 107B, and 108D were significantly higher than those found in MLRAs 103 and 104. The loess-derived soils in western and southern Iowa contain higher amounts of cohesive material and hence more resistant than the soils in north central and northwest Iowa which

are till-derived and coarser. Temporally, the critical shear stress reaches minimum values during March and April when soil moisture is high and there are several freeze-thaw events. The strength peaks in August when the effects of freeze-thaw are non-existent and soil moisture is at a moderate level. Over the winter, MLRA 107A had high $\tau_{c,f}$ values, while MLRAs 104 and 108D have low values due to differences in moisture content.

MLRAs 107A and 107B are highly likely to experience fluvial erosion for all flows, which support these MLRAs having the highest density of eroding banks and may be attributed to the high loess content in these soils. MLRAs 103 and 104 have low channel slopes relative to those in southwestern Iowa, which explains why these MLRAs have low bank erosion rates compared to MLRA 108C, despite them having similar seasonally variable strength and erodibility parameters. This suggests that the applied shear stress is more influential to bank erosion rates than the critical shear stress.

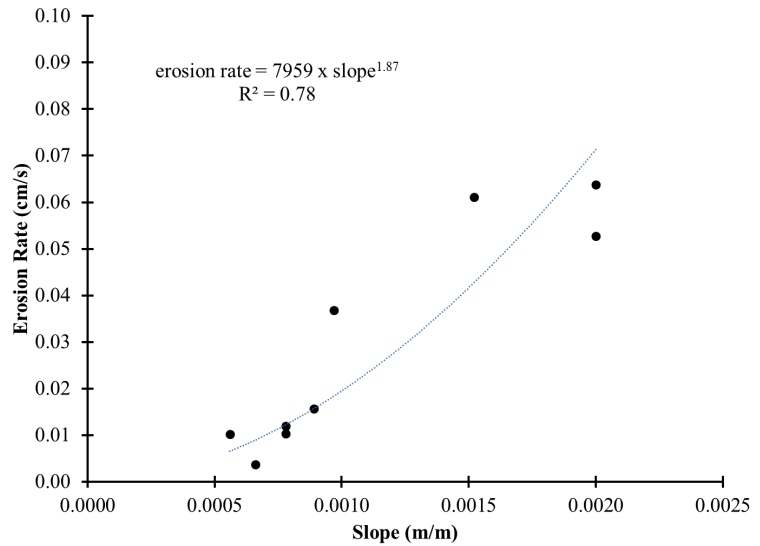


Figure 6.7. The relationship between channel slope and fluvial erosion rate determined with BSTEM.

6.4.2. *Compilation of Geomorphic, Geotechnical, and Hydraulic Assessments*

In Sections 3-6 of this report, bank erosion in Iowa was evaluated from different perspectives. Section 3 explored existing erosion pin studies coupled with aerial photography. One outcome of the section was that apparent patterns and commonalities existed within the different regions and stream orders of the state in terms of erosion rates. Section 4 built on this assessment by providing a means to identify eroding streambanks at a regional scale using high resolution LiDAR elevation data and quantify the extent of eroding lengths at watershed and landscape scales. Continuing at the regional level, Section 5 examined the geotechnical similarities to

quantify the critical shear stress and erodibility of the different streambank soils. Finally, this section examined the temporal variability of the critical shear stress and erodibility due to hydraulic changes in stream flow.

Moving forward, the outcomes of these different sections will be conglomerated for developing the broad-scale, multi-mechanistic assessment approach to identify bridge and roadway infrastructure sites under the threat of severe bank erosion and to quantify the degree of the threat. With a deeper understanding of the dominant bank erosion mechanisms within each MLRA, key parameters can be chosen to develop regression models to describe streambank migration in 3rd-6th order river segments across the state, as well as assign relative risks to roads, bridges, and right-of-ways impacted by stream migration.

The major outcome of Section 3 was that the erosion pin/aerial imagery data showed MLRAs 103, 104, 105, and 107A, which run along the northern part of the state had the highest erosion rates. These results are juxtaposed to the findings of Section 4, which suggest that MLRAs 107B, 108C, 108D, and 109 have the highest erosion lengths per area. The key contrast between the two studies is that they explore bank erosion from different mechanistic principles. The pin/aerial data are inclined to capture mass failure, which is defined in Section 1.2.4 as a high-magnitude but low-frequency process occurring discretely, both temporally and spatially. Sections 1.2.2 and 1.2.3 deal with shear driven erosion, which is a low-magnitude, high-frequency mechanism occurring potentially along several segments of the channel reach. This is better characterized by the erosion density from Section 4.

Supporting these observations and conclusions, the geotechnical data in Section 5 suggest the till-derived soils of MLRAs 103, 104, and 105, as well as the loamy soils in MLRA 107A are both coarser and lack cohesion compared to the loess-derived soils of MLRAs 107B, 108C, 108D, and 109. Thus, the soils in the northern part of the state are less inclined to erode by shear but more inclined to collapse en masse. The more cohesive soils in the southern part of the state should be more easily entrained but should remain intact as a whole.

In addition to mass failure, subaerial processes are more influential in the northern MLRAs especially 103, which experienced the highest number of freeze-thaw events in recent years and 104, which had the highest moisture content throughout the year. Both the number of freeze-thaw cycles and the moisture content of the soil affect its strength.

Understanding these key mechanisms allow for choosing more meaningful parameters when developing regression equations. For example, soils with high moisture content most likely are sensitive to hydraulic factors such as saturated hydraulic conductivity or stream flashiness. Regression equations for soils with high cohesion but experience high fluvial shear erosion may be characterized with soil related parameters. These equations are discussed more in the following chapter.

6.5 Products

The main products derived in this section include the spatially and temporally varied distributions of the critical shear stress and erodibility coefficient. The consideration of the variability translates to difference in erosion rates that could be as much as 700%. Additionally, the BSTEM simulations provides hints to the likelihood of fluvial erosion being greater in western Iowa than in central or eastern Iowa. A peer-reviewed journal paper is in preparation highlighting the spatial and temporal variability of the strength and erodibility parameters across the state.

SECTION 7: RISK ASSESSMENT OF BRIDGE AND ROAD INFRASTRUCTURE TO STREAMBANK EROSION

7.1 Goal Statement

In this section, predictive regression models were developed using relevant parameters for each MLRA, along with new GIS coverages developed during this project and existing GIS databases to describe streambank migration in 3rd-6th order river segments. The regression models were used to assign relative risks to roads, bridges, and right-of-ways and to identify those structures likely to be impacted by stream migration. The section is divided into two main components, with section 7.2 describing on the regression modeling and results, and section 7.3 presenting the final risk assessments to bridge and roadway infrastructure.

7.2 Regression Modeling of Stream Migration

7.2.1 Methodology

Segments of 3rd to 6th-order streams and rivers were randomly selected from the different MLRAs in Iowa. Geomorphic, geotechnical, and hydraulic properties identified from the previous work described in Sections 3-6 were used to develop regression equations that best predicted the measured rate of channel migration that occurred from the mid-1980s to late 2000s within these segments. In all, eleven parameters were utilized: bank height, stream sinuosity, stream slope, eroding bank lengths, percent row crop in riparian zone, soil available water capacity, soil clay content, soil bulk density, soil saturated conductivity, soil organic matter content, and depth to bedrock. A description of the parameters used, their abbreviation, and the database sources of the parameter is provided in Table 7.1.

The statistical software package Minitab was used to investigate the regression relationships among stream migration rates and the predictive parameters. Recession rates with large residuals or unusual values were individually evaluated and were removed from the analysis if human activity appeared to have affected the migration rate. Stepwise regression was used to select or retain model variables based on a significance value of $p < 0.05$.

7.2.2 Regression Modeling Results

All the predictive variables considered in the analysis appeared fairly frequently in the regression equations, ranging from 6 to 17 occurrences (Table 7.1). The most frequently occurring variables in the equations included bank height, soil clay content and eroding bank length. The final regression models for the 3rd to 6th order rivers and their coefficients of determination (R^2 and adjusted R^2) are provided in Table 7.2 through 7.5. The predicted value, called “Rate80”, is

the total rate of channel migration that occurred in the stream segment from the mid-1980s to late 2000s.

Overall, the ability to predict stream migration using the selected parameters varied considerably. The adjusted R^2 values ranged from 12.4% for 3rd order streams in MLRA 108C to 87.4% for 6th order channels in MLRA 107B. In general, the regression model performance increased with stream order, with average adjusted R^2 values increasing from 32.5%, 49.7%, 43.1% to 65.2% in stream orders 3, 4, 5 and 6, respectively. Stream channel migration was most difficult to predict in MLRA 103 (Des Moines Lobe) with adjusted R^2 values 30.8% across the different stream orders. The average adjusted R^2 value was highest for MLRA 107A (72.1%).

Table 7.1 Variables considered in regression models to describe stream migration.

Variable	Abbrev.	Description of variable	Layer Source	Number of significant occurrences in models
Bank height	BH	Average height of bank in measured stream segment	New for project	17
Stream sinuosity	Sin	Stream sinuosity in measured stream segment	New for project	10
Stream slope	Slope	Stream slope across measured stream segment	New for project	6
Eroding Bank Length	EB	Total estimated eroding bank length in measured stream segment (see Chapter 5)	New for project	15
Row crop (%) in riparian zone	RC	Percentage of land in 30 m riparian zone in corn or soybean production	www.geodata.iowa.gov	9
Available water capacity	AWC	Average available water content of alluvial soils in measured stream segment	www.geodata.iowa.gov	11
Clay content	Clay	Average clay content of alluvial soils in measured stream segment	www.geodata.iowa.gov	17
Bulk density	Db	Average bulk density of alluvial soils in measured stream segment	www.geodata.iowa.gov	7
Saturated hydraulic conductivity	Ksat	Average saturated K of alluvial soils in measured stream segment	www.geodata.iowa.gov	11
Organic matter content	OM	Average organic matter of alluvial soils in measured stream segment	www.geodata.iowa.gov	7
Depth to bedrock	BD	Average depth to bedrock in measured stream segment	www.geodata.iowa.gov	9

Table 7.2. Final regression models that describe stream mitigation in 3rd order streams and rivers.

MLRA	R ²	R ² (adj)	Final regression model
103	28.03%	23.86%	Rate80 = 13.00 - (0.00582 * BH) - (43.4 * AWC) - (0.151 * Ksat) + (1.093 * AWC * Ksat)
104	20.51%	15.42%	Rate80 = 2.60 + (0.1610 * RC) + (38.0 * AWC) + (0.363 * Clay) - (375 * AWC ²) - (0.00618 * RC * Clay)
105	40.71%	36.02%	Rate80 = 20.32 - (3.46 * Slope) - (0.0322 * RC) - (46.3 * AWC) - (0.2098 * Clay) - (0.2107 * Ksat) + (0.203 * Slope * Clay)
107A	74.66%	71.04%	Rate80 = -9.18 + (104.1 * EB) - (0.0752 * BH) - (0.0480 * RC) + (77.0 * AWC) + (0.0314 * Clay) + (0.000170 * BH ²) - (0.0536 * EB * BH) - (0.1006 * EB * RC) - (329.2 * EB * AWC) - (0.467 * EB * Clay) + (0.000333 * BH * RC)
107B	20.06%	16.99%	Rate80 = 3.23 + (0.00539 * BH) - (5.19 * Sin) + (2.54 * Sin ²)
108C	15.63%	12.42%	Rate80 = 3.019 + (0.0117 * RC) - (0.1733 * OM) - (0.000306 * RC ²)
108D	48.06%	44.19%	Rate80 = 8.87 - (0.02564 * BH) - (1.72 * Sin) - (13.93 * AWC) + (0.000025 * BH ²) + (0.01010 * BH * Sin)
109	44.31%	38.82%	Rate80 = 0.93 + (0.00653 * BH) - (0.398 * Clay) + (8.46 * Db) - (0.572 * Ksat) + (0.0386 * Ksat ²) + (0.0489 * Clay * Ksat) - (0.859 * Db * Ksat)

Table 7.3. Final regression models that describe stream mitigation in 4th order streams and rivers.

MLRA	R ²	R ² (adj)	Final regression model
103	31.28%	24.69%	Rate80 = 6.496 + (3.789 * EB) - (0.00936 * BH) - (0.0604 * Ksat) - (0.01851 * BD) + (0.000042 * BD ²) - (0.01145 * EB * BD) + (0.000392 * Ksat * BD)
104	34.23%	29.84%	Rate80 = 10.89 - (0.02673 * BH) + (0.15 * Sin) - (0.157 * RC) - (0.00311 * RC ²) + (0.218 * Sin * RC)
105	42.42%	38.10%	Rate80 = 18.11 - (9.92 * EB) - (9.1 * AWC) - (0.600 * Clay) + (0.198 * BD) + (0.537 * EB * Clay) - (1.040 * AWC * BD)
107A	69.62%	65.40%	Rate80 = -141.5 + (19.25 * EB) - (0.0546 * BH) + (8.33 * Clay) + (12.10 * Ksat) - (0.01923 * BD) - (0.1011 * Clay ²) - (0.0855 * Ksat ²) + (0.0421 * EB * BH) - (2.768 * EB * Ksat) - (0.3717 * Clay * Ksat)
107B	47.75%	43.88%	Rate80 = -51.09 + (0.957 * EB) + (0.0436 * BH) + (65.45 * Sin) - (0.00597 * BD) - (12.18 * Sin ²) - (0.04537 * BH * Sin)
108C	76.67%	75.77%	Rate80 = 10.54 - (9.11 * Sin) - (0.679 * OM) + (3.981 * Sin ²)
108D	61.97%	54.24%	Rate80 = 55.2 - (0.1651 * BH) + (11.76 * Sin) - (97.4 * Slope) + (359 * AWC) - (3.610 * Clay) - (3.38 * Sin ²) + (18.08 * Slope ²) - (2588 * AWC ²) + (0.762 * BH * AWC) + (120.5 * Slope * AWC) + (2.286 * Slope * Clay) + (13.97 * AWC * Clay)
109	69.33%	66.30%	Rate80 = -2.45 + (9.02 * EB) + (0.313 * Clay) - (9.63 * Db) + (1.143 * Ksat) + (0.00579 * BD) - (0.787 * EB * Ksat) - (0.01133 * EB * BD)

Table 7.4. Final regression models that describe stream mitigation in 5th order streams and rivers.

MLRA	R ²	R ² (adj)	Final regression model
103	63.39%	55.64%	Rate80 = 6.2 - (3.6 * EB) + (0.056 * BH) + (0.333 * RC) - (1.168 * Clay) + (3.73 * OM) - (13.31 * EB ²) - (0.0219 * RC ²) + (0.755 * OM ²) + (1.043 * EB * RC) + (0.992 * EB * Clay) - (0.01988 * BH * OM)
104	37.65%	29.41%	Rate80 = 4.32 - (14.45 * Slope) + (0.333 * Clay) - (0.83 * Db) - (0.0332 * BD) + (9.97 * Db ²) - (0.777 * Clay * Db) + (0.00324 * Clay * BD)
105	37.08%	32.59%	Rate80 = 14.76 + (0.0132 * BH) - (0.372 * Ksat) - (2.901 * OM) - (0.000011 * BH ²)
107A	70.92%	65.86%	Rate80 = 37.34 - (0.71 * EB) - (188.1 * Slope) + (58.9 * AWC) - (1.360 * Clay) + (0.143 * Ksat) + (0.717 * EB * Ksat) + (6.64 * Slope * Clay) - (5.43 * AWC * Ksat)
107B	68.20%	63.09%	Rate80 = -107.4 + (18.67 * EB) + (101.3 * Sin) + (16.2 * Db) + (23.05 * OM) - (0.0555 * BD) - (20.63 * Sin ²) - (20.18 * EB * Sin) + (0.0652 * Sin * BD) - (14.14 * Db * OM)
108C	24.86%	18.38%	Rate80 = 11.21 - (0.456 * EB) - (0.291 * Clay) - (0.0568 * BD) - (0.01707 * EB * BD) + (0.00364 * Clay * BD)
108D	29.81%	24.61%	Rate80 = 33.80 - (24.37 * OM) + (1.807 * Clay) + (4.12 * OM ²) - (0.438 * OM * Clay)
109	62.86%	54.86%	Rate80 = 8.5 + (26.78 * EB) - (0.1216 * BH) + (21.35 * Sin) - (0.665 * Clay) + (0.0258 * BD) - (0.000041 * BH ²) + (0.000126 * BD ²) - (1.333 * EB * Clay) + (0.00804 * BH * Clay) - (1.040 * Sin * Clay) - (0.00207 * Clay * BD)

Table 7.5. Final regression models that describe stream mitigation in 6th order streams and rivers.

MLRA	R ²	R ² (adj)	Final regression model
103	21.65%	18.85%	Rate80 = 28.61 - (145.2 * AWC)
104	80.28%	75.03%	Rate80 = 23.31 + (25.78 * EB) - (0.02660 * BH) + (126.7 * Slope) + (0.468 * Clay) - (14.53 * Db) - (16.59 * EB ²) - (16.02 * Slope * Clay) + (152.4 * Slope * Db)
105	71.07%	65.88%	Rate80 = -753 + (3690 * AWC) + (79.1 * Clay) - (3.838 * Ksat) - (1.057 * BD) - (12611 * AWC * AWC) - (2.653 * Clay * Clay) + (0.0825 * Clay * BD)
107A	90.36%	86.17%	Rate80 = 10.8 - (87.1 * EB) + (0.391 * RC) + (2.9 * Db) + (0.0235 * Ksat) - (0.0469 * BD) + (48.6 * EB ²) + (44.6 * EB * Db) - (0.817 * RC * Db) + (0.01356 * RC * Ksat) + (0.00813 * RC * BD)
107B	89.76%	87.42%	Rate80 = -426 + (590 * Sin) + (111.4 * Db) - (6.37 * Ksat) + (0.2011 * BH) - (126.6 * Sin ²) - (133.7 * Sin * Db) + (5.66 * Sin * Ksat) - (0.1943 * Sin * BH)
108C	86.45%	82.86%	Rate80 = -27.20 + (15.76 * EB) - (0.0506 * BH) + (37.38 * Sin) + (0.711 * Ksat) + (1.03 * OM) - (9.36 * Sin ²) - (0.01636 * Ksat ²) - (6.23 * EB * OM) + (0.01374 * BH * OM)
108D	51.71%	41.76%	Rate80 = 146.6 - (67.3 * EB) - (245 * Slope) - (602 * AWC) - (0.639 * RC) + (0.0231 * RC ²) + (293.2 * EB * AWC) + (1175 * Slope * AWC)
109	69.62%	63.54%	Rate80 = 25.5 + (0.0705 * BH) + (1.964 * RC) - (0.145 * Clay) - (26.17 * Db) - (0.000070 * BH ²) - (0.0848 * RC * Clay)

7.2.3 Application of the Regression Model at the State Level

The regression models for the stream orders within each MLRA were scaled up to all the channel lengths within the regions. Approximately 80 segments were evaluated with the regression models for 3rd and 4th order streams within the MLRAs, 60 segments for 5th order streams and 40 segments in 6th order rivers. All-together, the regression models were developed using approximately 2,111 specific stream segments across the state, and these models were then applied to the remainder of the 58,500 stream segments in the state. Overall, the mean stream migration rate developed using the assessed segments scaled to the rest of the state in a linear fashion (Figure 7.1)

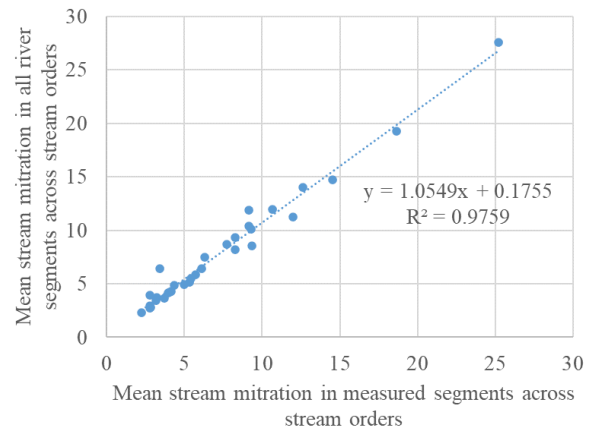


Figure 7.1. Relation of mean stream migration rates measured in stream segments to all river segments in Iowa.

7.3 Risk to Bridges and Roads from Bank Erosion due to Stream Migration

7.3.1 Methodology

Bridge locations were identified and selected for each MLRA and stream order. A buffer was created around the bridge using the bridge length as the buffer size. This buffer was then used to clip the stream segment within that buffer. Stream segment lengths were compared to bridge lengths to determine at what stream length to bridge length ratio a stream has the potential to impact the bridge in the near future. Bridges with a high ratio and a stream having a high potential for migration were flagged as bridge structures to monitor. For the roadways, stream migration polygons were buffered 20 feet and intersected with right-of-way (ROW) features to identify roads that may be impacted by lateral movement from streams that flow parallel to roadways.

Spatial joins were performed between stream segments within bridge buffers to calculate the ratio of stream length to length of bridge for all bridges by stream order and MLRA. This provided an estimate of stream segments that may be approaching a bridge at a high angle. Spatial joins were then performed between those stream segments and stream migration polygons to obtain maximum migration rates for each stream segment within the bridge buffers. This enables the selection of bridges that have a high stream segment to bridge length ratio and high migration rate.

A visual inspection of bridges with a high stream segment to bridge length ratio and high stream migration rate verified that the process was working as expected. Aerial photographs of bridges that met the specified criteria from the 1980s and 2016/2017 photography are examined below as demonstrations. The Highway 38 bridge may be impacted by the Wapsipinicon River in the near future (Figure 7.2a) whereas the East Nishnabotna River was modified to keep it from impacting the Highway 48 bridge (Figure 7.2a).

Stream migration polygons for 3rd to 6th order streams in each MLRA were buffered 20 feet and the bridge buffers previously created were subtracted from the ROW polygons. The ROW features were then clipped with the buffered stream migration polygons to create ROW features that were not at bridge crossings but may be impacted by stream migration in the near future.

A visual inspection of ROW features near the streams with high migration rates shows a number of sites that may be impacted in the near future. Photographs from the 1980/1990s and 2017 identify several of these features. The Maple River channel was modified to keep it from impacting Highway 175 in Woodbury County and the Soldier River is moving closer to Highway 183 in Monona County.

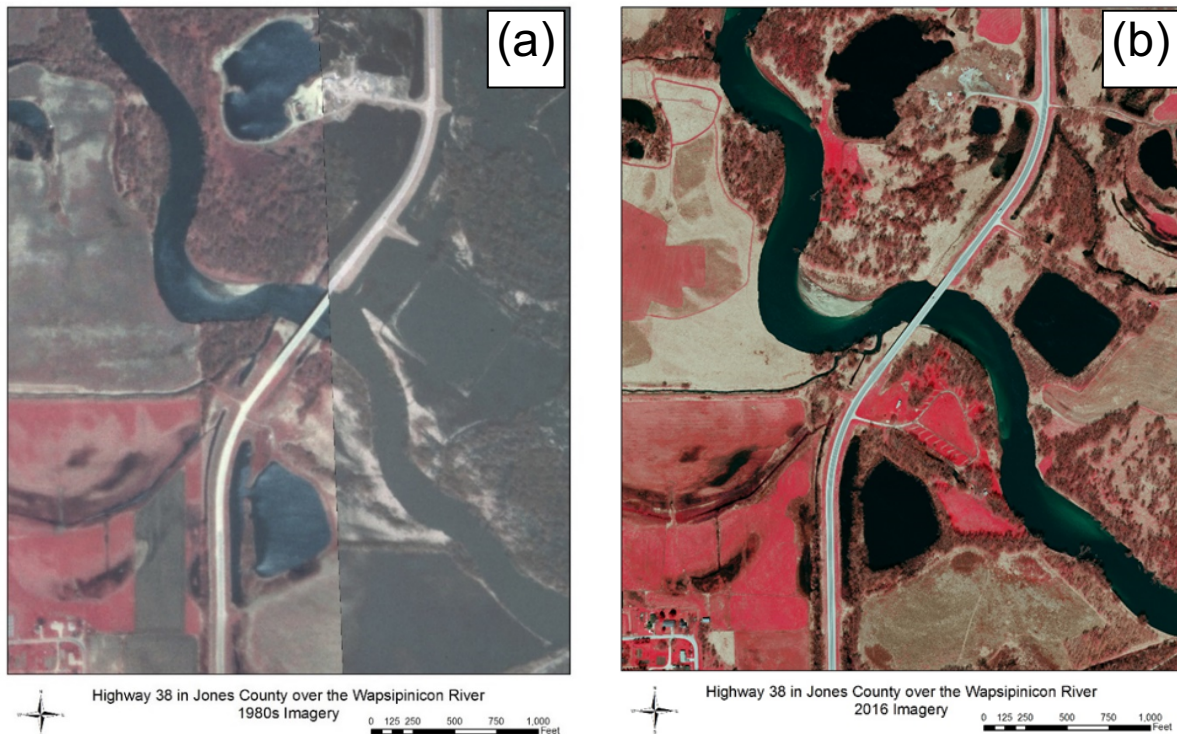


Figure 7.2. 1980 (a) and 2016 (b) photographs of Highway 38 bridge over the Wapsipinicon River showing encroaching river migration into the bridge infrastructure.

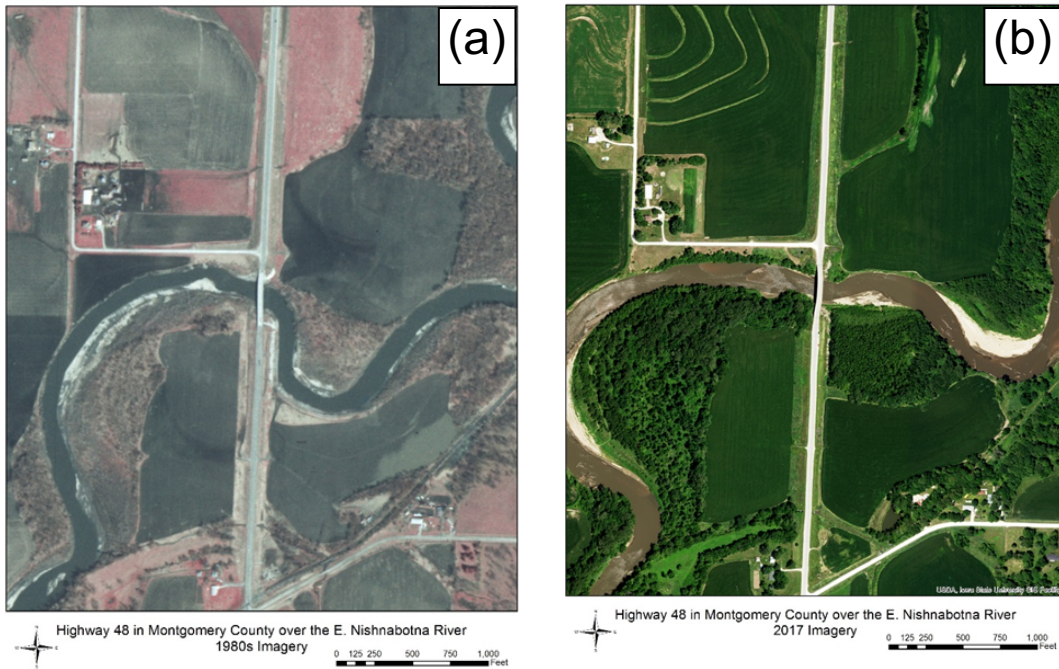


Figure 7.3. 1980 (a) and 2016 (b) photographs of Highway 48 bridge over the East Nishnabotna River showing encroaching river migration into the bridge infrastructure.

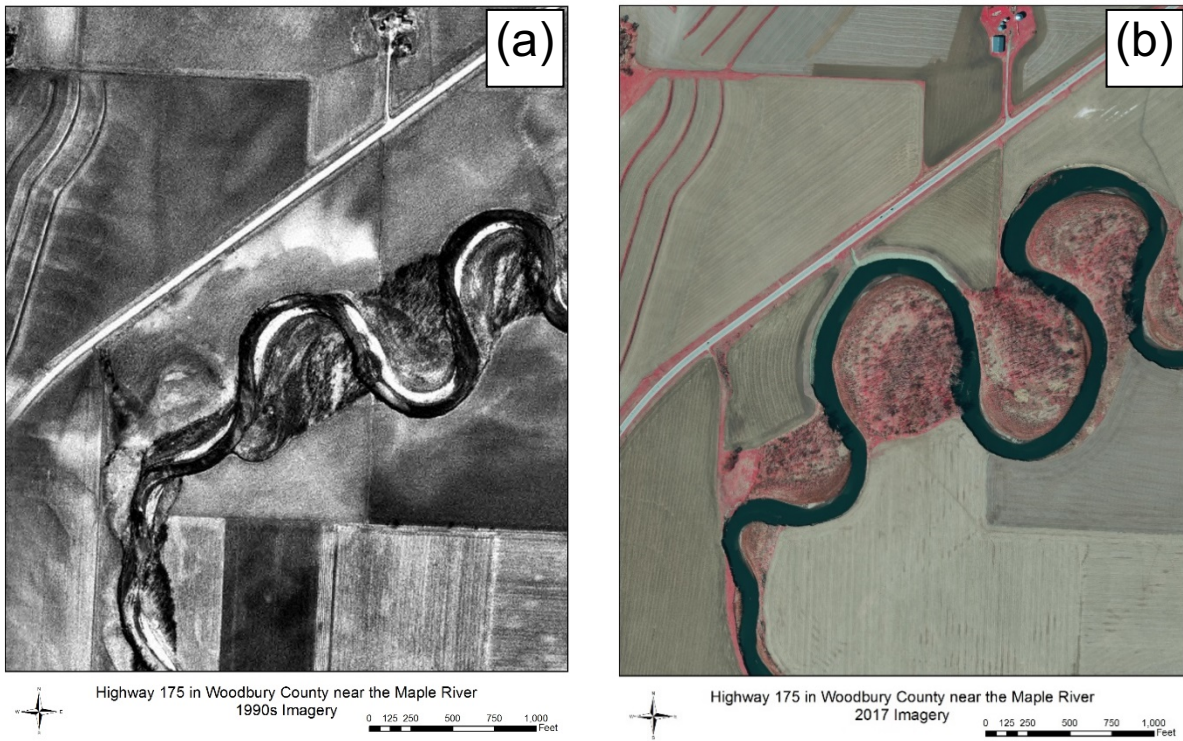


Figure 7.4. 1980 (a) and 2016 (b) photographs of Highway 175 bridge near the Maple River showing encroaching river migration into the roads.

7.3.2 Risk Assessment

Migration rates for 3rd and 4th order streams were evaluated to assign risk to bridges crossing those streams and risks were categorized as High, Moderate, Slight and Minimal. Stream migration rates of 10 m or greater were assigned a value of High; rates between 7 m and 10 m were assigned a value of Moderate; rates between 5 m and 7 m were assigned a value of Slight; and migration rates less than 5m were assigned a Minimal risk. For stream segments that approached the bridge from an angle and had been assigned a value of Slight or Minimal, the bridge crossings were visually inspected using aerial photography and the value was changed to a higher value if appropriate.

Risk values from the stream segments were assigned to the appropriate bridges in the National Bridge Inventory obtained from the Iowa Department of Transportation (IDOT). Since the data were created from the regression models, the results do not always agree with how the stream behaves. Where stream banks have been armored, streams straightened or otherwise modified recently, the results of the model may not represent how the stream behaves. Risk was assigned from stream segments that intersect the bridge, so the rate of migration was not necessarily the same for the entire segment. Therefore, the data were only an approximation of the risk for the infrastructure and should not be used without verification.

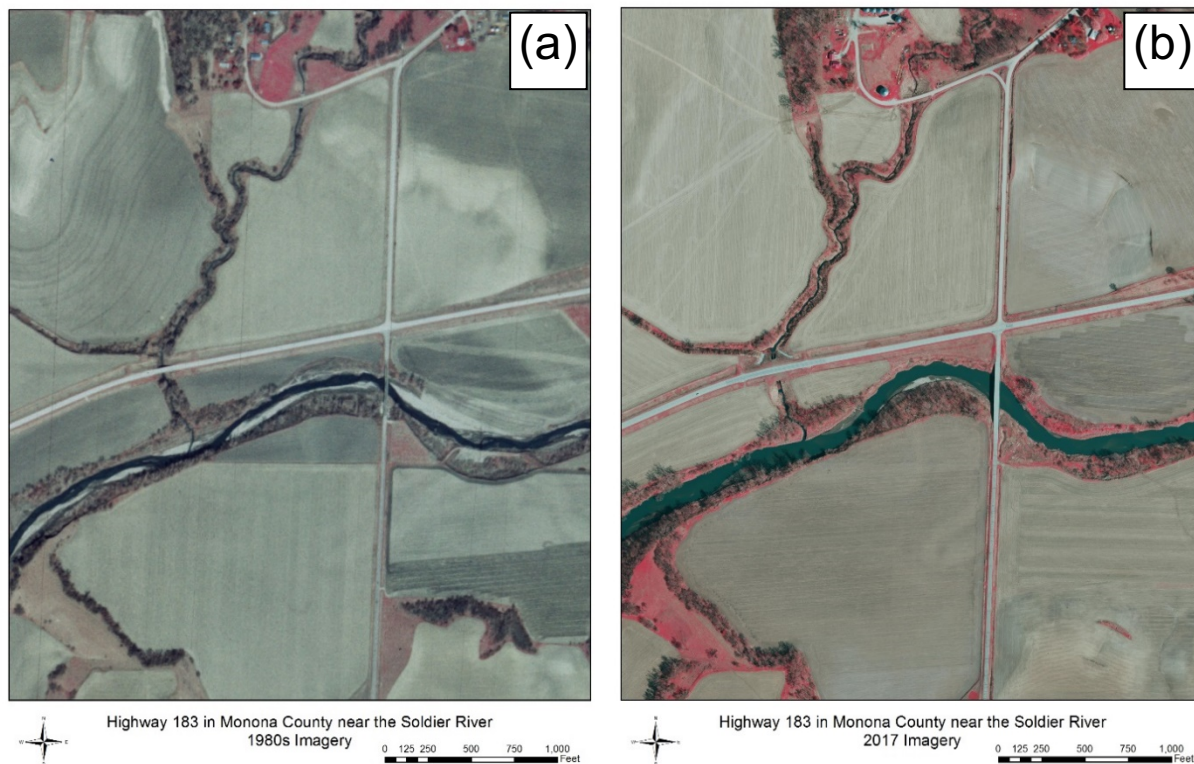


Figure 7.5. 1980 (a) and 2016 (b) photographs of Highway 183 bridge near the Soldier River showing encroaching river migration into the roads.

Migration rates for 5th and 6th order streams were also evaluated to assign risk to bridges crossing these larger streams. Rates were also categorized as High, Moderate, Slight and Minimal with stream migration rates of 10 m or greater assigned a value of High; rates between 8 m and 10 m assigned a value of Moderate; rates between 6 m and 8 m assigned a value of Slight; and values less than 6 m assigned a value of Minimal. For stream segments that approached the bridge from an angle and were assigned a value of Slight or Minimal, the bridge crossings were visually inspected using aerial photography and the value was changed to a higher value if appropriate. Risk values from the stream segments were assigned to the appropriate bridges in the National Bridge Inventory obtained from the IDOT. Like for smaller streams, it is important to note that the results do not always agree with actual on-the-ground conditions, and thus the risk classifications are only an approximation of the risk to infrastructure and not to be used without verification.

7.3.3 Risk Assessment Summary

Threats to bridges and road ROW across the state and within the MLRAs were located as spatially-explicit GIS geodatabases and these geodatabases provided to the IDOT are listed in

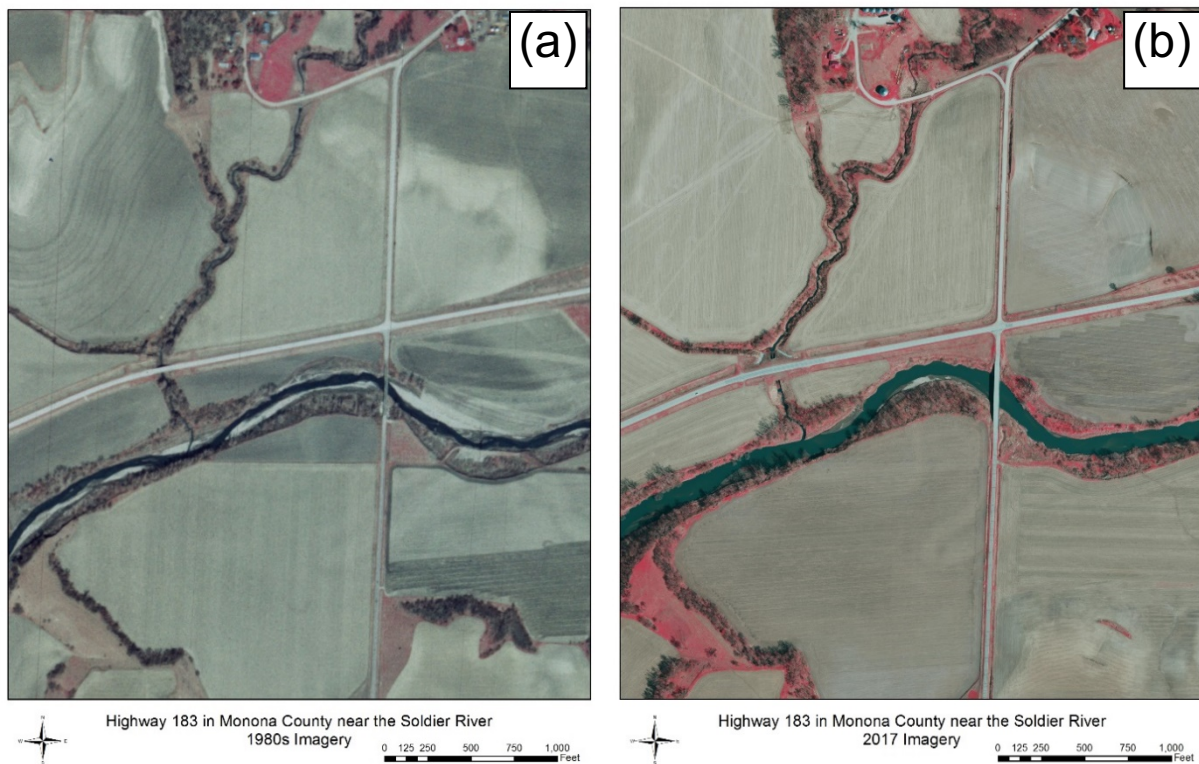


Figure 7.6. 1980 (a) and 2016 (b) photographs of Highway 183 bridge near the Soldier River showing encroaching river migration into the roads.

section 7.5 below. A summary of the results are provided below in terms of stream order (Tables 7.6 to 7.9) and total numbers by MLRA (Table 7.10) and risk (Table 7.11).

Overall, the greatest number of bridges threatened by stream migration were found in MLRA 107B and 108D, followed closely by MLRAs 103 and 107A (Table 7.10). The greatest risk to road ROWs were also assessed in MLRA 107B and 103 (Table 7.10). All-together, the project identified 1,515 bridges in Iowa that considered to be at high or moderate risk to future erosion by channel migration. In addition, 281 road ROWs were identified as high to moderate risk. As noted above, the locations of these bridges and roads are provided in spatially-referenced geodatabases given to IDOT.

Table 7.6 Summary of risk assessment evaluation for bridges and road right-of-way (ROW) by MLRA for 3rd order streams (values are numbers of structures or sites impacted).

Bridge Risk Assessment (number of structures)					ROW risk assessment (number of sites)			
MLRA	High	Moderate	Slight	Minimal	High	Moderate	Slight	Minimal
103	2	11	81	1046	1	6	6	132
104	8	56	265	760	0	12	26	125
105	10	5	42	447	1	1	2	88
107A	16	28	42	523	1	4	3	51
107B	0	0	17	920	0	0	0	197
108C	0	10	26	1173	0	0	0	133
108D	0	0	11	578	0	0	0	108
109	9	2	12	558	1	0	0	138

Table 7.7 Summary of risk assessment evaluation for bridges and road right-of-way (ROW) by MLRA for 4th order streams (values are numbers of structures or sites impacted).

Bridge Risk Assessment (number of structures)					ROW risk assessment (number of sites)			
MLRA	High	Moderate	Slight	Minimal	High	Moderate	Slight	Minimal
103	0	25	109	262	0	2	13	34
104	2	108	176	144	2	9	21	40
105	13	26	111	83	4	4	20	17
107A	42	74	96	131	2	9	7	23
107B	16	76	195	472	1	7	17	87
108C	2	9	54	578	0	0	1	86
108D	24	26	87	358	6	1	7	34
109	10	12	95	502	0	1	7	73

Table 7.8 Summary of risk assessment evaluation for bridges and road right-of-way (ROW) by MLRA for 5th order streams (values are numbers of structures or sites impacted).

Bridge Risk Assessment (number of structures)					ROW risk assessment (number of sites)			
MLRA	High	Moderate	Slight	Minimal	High	Moderate	Slight	Minimal
103	101	23	37	56	31	3	7	14
104	12	29	43	69	3	6	11	20
105	40	40	25	15	11	6	2	5
107A	28	21	16	12	8	0	5	1
107B	69	28	50	136	24	7	6	18
108C	4	11	61	155	1	1	16	29
108D	47	65	68	78	12	9	8	14
109	14	18	69	161	0	3	7	20

Table 7.9 Summary of risk assessment evaluation for bridges and road right-of-way (ROW) by MLRA for 6th order streams (values are numbers of structures or sites impacted).

Bridge Risk Assessment (number of structures)					ROW risk assessment (number of sites)			
MLRA	High	Moderate	Slight	Minimal	High	Moderate	Slight	Minimal
103	18	7	0	4	6	3	1	5
104	22	2	10	9	6	0	3	1
105	12	1	0	4	4	0	0	0
107A	16	5	1	1	8	0	0	1
107B	68	10	21	32	27	3	4	15
108C	25	16	11	37	6	3	10	9
108D	69	23	14	5	8	4	4	2
109	25	24	17	40	1	2	2	6

Table 7.10 Summary of risk assessment evaluation for bridges and road right-of-way (ROW) by MLRA for all streams and rivers (values are numbers of structures or sites impacted).

Bridge Risk Assessment (number of structures)					ROW risk assessment (number of sites)			
MLRA	High	Moderate	Slight	Minimal	High	Moderate	Slight	Minimal
103	121	66	227	1368	38	14	27	185
104	44	195	494	982	11	27	61	186
105	75	72	178	549	20	11	24	110
107A	102	128	155	667	19	13	15	76
107B	153	114	283	1560	52	17	27	317
108C	31	46	152	1943	7	4	27	257
108D	140	114	180	1019	26	14	19	158
109	58	56	193	1261	2	6	16	237

Table 7.11 Summary of risk assessment evaluation for bridges and road right-of-way (ROW) by MLRA for all streams and rivers (values are numbers of structures or sites impacted).

Bridge Risk Assessment (number of structures)					ROW risk assessment (number of sites)			
MLRA	High	Moderate	Slight	Minimal	High	Moderate	Slight	Minimal
All	724	791	1862	9349	175	106	216	1526

7.4 Conclusions

In this portion of the study, we developed predictive models to assess the risk of bridge and road infrastructure from channel migration in Iowa. Regression models developed using new GIS coverages from this project and existing GIS databases were developed from eleven parameters including: bank height, stream sinuosity, stream slope, eroding bank lengths, percent row crop in riparian zone, soil available water capacity, soil clay content, soil bulk density, soil saturated conductivity, soil organic matter content, and depth to bedrock. The most frequently occurring variables in the equations were found to be the bank height, soil clay content and eroding bank length. The coefficients of determination (adj R²) for final regression models for the 3rd to 6th order rivers ranged from 12.4% for 3rd order streams in MLRA 108C to 87.4% for 6th order channels in MLRA 107B. In general, the regression model performance were found to increase with stream order, with average adjusted R² values increasing from 32.5%, 49.7%, 43.1% to 65.2% in stream orders 3, 4, 5 and 6, respectively. Using this information, stream segments within bridge buffers and road ROWs were evaluated to assess the risk associated with predicted channel migration on existing bridge and road infrastructure. Overall, the project identified 1,515 bridges and 281 road ROWs in Iowa considered to be at high or moderate risk to future erosion by channel migration.

7.5 Products

Five geodatabases were previously provided to DOT in quarterly reports submitted to DOT engineer Dave Claman on February 28, 2019 and May 31, 2019. These geodatabases included:

- ROW_IDOT_Order_3_4_5_6.gdb
- DOT_Bridge_Order_3.gdb
- DOT_Bridge_Order_4.gdb
- DOT_Bridge_Order_5.gdb
- DOT_Bridge_Order_6.gdb

These geodatabases represent the final work products for the GIS portion of the study.

SECTION 8: OVERALL PROJECT SUMMARY

8.1 Existing Knowledge Gaps

Stream and rivers are rarely stable as they continuously adjust their boundaries following fluctuations in water and sediment discharge triggered by shifts in base-level, land-use, and climate (Ettema et al., 2010). Erosion and deposition are the primary mechanisms by which the different pedological compartments of channel boundaries adjust themselves. For streambanks consisting of cohesive and semi-cohesive soils, fluvial entrainment is a low-magnitude but high-frequency mechanism that can lead to bank collapse, channel widening, and lateral migration.

Fluvial entrainment is often not localized, occurring over the whole length of the stream channel and pretty much during the whole hydrograph of a storm event. It, along with the mass wasting and channel migration that stem from it, will eventually affect infrastructure safety, possibly leading to catastrophic failure, if not addressed. In Iowa, abutment scour and bank collapse have received a lot of attention (e.g., Odgaard and Lee, 1984; Wipf et al., 2003; Ettema et al., 2006; Papanicolaou and Elhakeem, 2006; Ettema et al., 2010), while fluvial entrainment, channel widening, and lateral migration have received much less attention (Papanicolaou et al., 2006).

The gradual shift of the bankline over time can undermine bridge abutments and adjacent roadways (Briaud et al., 2007) but the threat is hard to predict due to the lack of quantitative methods (Lagasse et al., 2004), as well as field-oriented and remotely sensed data to characterize sufficiently the spatial and temporal variability of the processes triggering and producing bank erosion (Johnson, 2006a). Current assessment methodologies of streambank recession at reach-to-watershed scales do not consider both geomorphic and geotechnical properties, as well as the multiple, interrelated mechanisms of bank erosion over a wide range of stream orders, climate conditions, and discharges.

This study helps address a critical need for developing a data-driven protocol that identifies and quantifies the severity of bank erosion near bridge sites and roadways at a suitable spatial scale and over time so that the Iowa Department of Transportation, as well as other state, county, and municipal agencies can prioritize sites for rehabilitation. We provide herein an innovative, remote-sensing, geomorphic, approach that uses aerial LiDAR surveys to map currently eroding banks in 3rd - 6th order streams intersected with bridge structures in Iowa. This is combined with geotechnical and hydraulic data that consider both the spatial and temporal variability of the bank soil strength under changing climate, moisture and land-use conditions to provide projected Factors of Safety, as well as the likelihood and severity of bank erosion across Iowa at selected sites.

8.2 Project Benefits and Key Findings

The geomorphic, geotechnical, and hydraulic factors affecting fluvial entrainment, channel widening, and lateral migration are highly variable across several spatial and temporal scales, which lead to a wide range of bank erosion rates (e.g., Johnson, 2006a; Palmer et al., 2014). Herein, we characterized the range of bank erosion rates in Iowa by examining existing studies. Annual recession rates ranged from -1.2 cm/yr (deposition) in central Iowa to 34.2 cm/yr in southern Iowa. The average recession rate in 3rd order streams was 12.4 ± 10.3 cm/yr. The mean recession rates for the higher stream orders increased systematically to 18.1, 31.9 and 53.8 cm/yr for stream orders 4 through 6, respectively. Maximum recession rates represented by the highest change in channel migration within a reach were approximately 3.5 to 4.5 times greater than the mean rate.

These past studies, though, were limited in scope, mostly focusing at the reach scale. Even combined, the spatial extent of monitored streambank erosion was a fraction of the total stream length in the state. Thus, we developed a new approach to identify severely eroding streambanks at a broader scale. The approach uses the slopes between adjacent cells in a high-resolution LiDAR coverage map to characterize the relationship between streambank angles and streambank heights. Following calibration/ validation, the method was then applied to the 3rd - 6th order streams across the state. Despite certain limitations, the approach provided a first-order approximation of eroding streambank lengths in Iowa's rivers and stream.

Approximately 35,200 km of the banks along 3rd to 6th order rivers in Iowa are severely eroding, which is 41% of the streambanks in the state. Bank erosion is considered a “natural geomorphic process”; however, a natural meandering river would have only about 20% of its streambanks severely eroding (Florsheim et al., 2008). In Iowa, the percentage of eroding bank lengths was double that of a “natural” stream, suggesting that streambank erosion has been enhanced by some external forcings.

Due to this accelerated rate of bank erosion in the state and the persistent threat to bridge sites and roadways, there is a clear need to develop a methodology that identifies and quantifies the severe bank erosion at a suitable spatial scale for the Iowa Department of Transportation and other state, county, and municipal agencies to help plan maintenance and rehabilitation strategies.

With the degree of variability in soil properties, topography, weather, and land uses throughout the state, it would seem inappropriate to develop a single predictive relationship for all of Iowa's stream miles. We observed some regional generalities, though, that could keep the number of needed relationships to a minimum. For example, longer stretches of streambank erosion per watershed area are occurring in southwest and southern Iowa (i.e., MLRAs 107B,

108D and 109) suggesting fluvial erosion is more of a concern than other portions of the state (namely MLRAs 103 and 104).

Building on these initial regional patterns, we took a more detailed look at representative reaches within the various MLRAs of the state to understand the spatial and temporal variability of bank soil strength and erodibility parameters for the different bank erosion mechanisms. Through a mixture of geotechnical analyses, flume experiments, and field monitoring, coupled with empirical and process-based modeling, we saw that the critical shear stress and erodibility values across the major MLRAs in the state were significantly different. The cumulative distribution functions of critical shear stress and erodibility (Figure 6.2) show that MLRAs 107A, 107B, 108C, and 108D have similar patterns most likely due to the loess soils covering western and southern Iowa. These soils have higher average $\tau_{c,f}$ than the till-derived, coarser soils in MLRAs 103 and 104 in north central and northeast Iowa. The aerial-imagery-determined recession rates from northeast Iowa were highest throughout the state. In southwest Iowa, the soils had less retreat which was attributed to the abundance of cohesive soils.

Along with this spatial variability in soil strength and erodibility parameters, there is temporal variability related to soil moisture and freeze-thaw cycles which weaken the soil's strength. The critical shear strength reaches minimum values during March and April when soil moisture is high and there are several freeze-thaw events. The strength climbs to a peak in August when the effects of freeze-thaw are non-existent and soil moisture is at a moderate level. Over the winter, though, the sites exhibit different behaviors. MLRAs 103 and 107A have high $\tau_{c,f}$ during the winter due primarily to low moisture content. MLRAs 104 and 108D have high moisture content over the winter and thus lower values of $\tau_{c,f}$.

The translation of the spatial and temporal variability in strength and erodibility parameters on the likelihood of fluvial erosion can be seen through the Factors of Safety. MLRAs 107A and 107B have FS_f values less than one for at least 95% of their observed flows suggesting that fluvial erosion is highly likely. This corresponds to the finding in section 4 where these MLRAs had the highest density of eroding banks (446 to 522 m/km²). Fluvial surface and mass erosion tend to occur along the entire length of channel and the loess soils in western Iowa soils are vulnerable to fluvial surface/ mass erosion (Bradford & Piest, 1977; Thomas et al., 2004). MLRAs 103 and 104 have “stable” FS_f values for at least 50% of their flows suggesting they are less likely to experience fluvial erosion. Moreover, MLRAs 103 and 104 have low channel slopes, typically 1.5% compared to ~7% in southwest Iowa watersheds. Slope is related to the applied shear stress, so low-gradient streams are less likely to experience flows exceeding the critical shear stress.

Having substantiated the regional patterns of bank erosion we developed predictive models to assess the risk of bridge and road infrastructure from channel migration in Iowa.

Regression models using existing GIS databases and new GIS coverages developed during this project were established using eleven parameters including bank height, stream sinuosity, stream slope, available water capacity, clay content, and bulk density, among other parameters. Stream length to bridge length ratios were used to identify the potential impact for bridges in the near future. Bridges with a high ratio and a stream having a high potential for migration were flagged. For the roadways, stream migration polygons were buffered 20 feet and intersected with right-of-way features to identify roads that may be impacted by lateral movement from streams.

Overall, the greatest number of bridges threatened by stream migration were found in MLRA 107B and 108D, followed closely by MLRAs 103 and 107A (Table 7.10). The greatest risk to road ROWs were also assessed in MLRA 107B and 103 (Table 7.10). All-together, the project identified 1,515 bridges in Iowa that considered to be at high or moderate risk to future erosion by channel migration. In addition, 281 road ROWs were identified as high to moderate risk.

8.3 Product Summary and Future Work

Aside from the four published peer-reviewed manuscripts (and 1 manuscript in preparation), the key product from this study are as follows:

- An estimation of bank erosion in Iowa.
- A LiDAR-based algorithm to identify eroding streambanks at a regional scale.
- An assessment of the degree of spatial and temporal heterogeneity of bank soil strength and erodibility parameters at bridge sites.
- Factors of Safety for the range of flows at selected bridge crossings identifying the likelihood of erosion over time.
- Regression models at the regional scale using common geomorphic and geotechnical parameters to quantify bank retreat.
- Geodatabases and coverage maps of severely eroding stream banks that intersects with bridge and roadway infrastructure.

Building on these regional regression models, as well as the spatial and temporal variability of strength and erodibility parameters, the study is poised to develop a decision support tool that can not only suggest bank stabilization or grade control structures but also predict the likelihood of success and the overall benefits at the watershed scale. With climate becoming more variable and the growth of urban centers, the safety of the bridge and roadway infrastructure will continue to be a prominent necessity for Iowa.

SECTION 9: REFERENCES

- Aberle, J., V. Nikora, S. McLean, C. Doscher, I. McEwan, M. Green, D. Goring, and J. Walsh. 2003. Straight benthic flow-through flume for in situ measurement of cohesive sediment dynamics. *Journal of Hydraulic Engineering*. 129(1):63-67.
- Al-Madhhachi, A.T., G.A. Fox, G.J. Hanson, A.K. Tyagi, and R. Bulut. 2014. Mechanistic detachment rate model to predict soil erodibility due to fluvial and seepage forces. *Journal of Hydraulic Engineering*. 140(5):04014010.
- Al-Madhhachi, A.T., G.J. Hanson, G.A. Fox, A.K. Tyagi, and R. Bulut. 2013. Measuring soil erodibility using a laboratory “mini” JET. *Transactions of the ASABE*. 56(3):901-910.
- Amos, C.L., A. Bergamasco, G. Umgiesser, S. Cappucci, D. Cloutier, L. DeNat, M. Flindt, M. Bonardi, and S. Cristant. 2004. The stability of tidal flats in Venice Lagoon: The results of in-situ measurements using two benthic, annular flumes. *Journal of Marine Systems*. 51:211-241.
- Arulanandan, K. 1975. Fundamental aspects of erosion of cohesive soils. *Journal of the Hydraulics Division*. 101(NHY5):635-639.
- Ayers, P.D. 1987. Moisture and density effects on soil shear strength parameters for coarse grained soils. *Transactions of the American Society of Agricultural Engineers*. 30(5):1282-1287.
- Baker, D., P. Richards, T. Loftus and J. Kramer. 2004. A new flashiness index: Characteristics and applications to Midwestern rivers and streams. *Journal of the American Water Resources Association*. 40(2):503-522.
- Bardet, J.P., M. Jesmani, and N. Jabbari. 2011. Effect of compaction on shear strength of wax-coated sandy soils. *Journal of Geotechnical Engineering*. 16:451-461.
- Barkdoll, B.D., R. Ettema, and B.W. Melville. 2007. *Countermeasures to Protect Bridge Abutments from Scour*. National Cooperative Highway Research Program Report 587. Washington DC.
- Beck, W. 2018. *Sediment and phosphorus dynamics within the channel and floodplain of Walnut Creek, Iowa*. Ph.D. Dissertation. Iowa State University. Ames, IA.
- Beck, W., T. Isenhardt, P. Moore, K. Schilling, R. Schultz, and M. Tomer. 2018. Streambank alluvial unit contributions to suspended sediment and total phosphorus loads, Walnut Creek, Iowa, USA. *Water*. 10:111.
- Beeson, C., and P. Doyle. 1995. Comparison of bank erosion at vegetated and non-vegetated channel bends. *Journal of the American Water Resources Association*. 31:983-990.
- Behm, R., G. Hadish, R. Lohnes, R. Gu, D. Wright, E. Shornhorst, and M. Adkins. 1998. *Stream Stabilization in Western Iowa: Structure Evaluation and Design Manual*. Iowa Department of Transportation Report HR-385. Ames, IA.
- Belmont, P., K.B. Gran, S.P. Schottler, P.R. Wilcock, S.S. Day, C. Jennings, J.W. Lauer, E. Viparelli, J.K. Willenbring, and D.R. Engstrom. 2011. Large shift in source of fine sediment in the Upper Mississippi River. *Environmental Science & Technology*. 45:8804-8810.
- Bertrand, F. 2010. *Fluvial Erosion Measurements of Streambank Using Photo-Electronic Erosion Pins (PEEP)*. M.S. Thesis. University of Iowa. Iowa City, IA.

- Bradford, J., and R. Piest. 1977. Gully wall stability in loess-derived alluvium. *Soil Science Society of America Journal*. 41:115-122.
- Bressan, F., C.G. Wilson, and A.N. Papanicolaou. 2014. Improved streambank countermeasures: The Des Moines River (USA) case study. *The International Journal of River Basin Management*. 12(1):69-86.
- Briaud, J.L., H.-C. Chen, K.-A. Chang, Y.-A. Chung, N. Park, W. Wang, and P.-H. Yeh. 2007. *Establish Guidance for Soils Properties-Based Prediction of Meander Migration Rate*. Texas Department of Transportation Report 0-4378-1. Austin, TX.
- Bryan, R.B. 2000. Soil erodibility and processes of water erosion on hillslope. *Geomorphology*. 32:385-415.
- Cao, S.Y., and G.H. Du. 1986. Experimental study on the erosion and deposition of cohesive soil. *Journal of Sediment Research*. 4:73-82.
- Chapuis, R.P. 1986. Quantitative measurement of the scour resistance of natural solid clays. *Canadian Geotechnical Journal*. 23(2):132-141.
- Chatfield, C. 1984. *The Analysis of Time Series: An Introduction*. Chapman & Hall: London, UK.
- Chow, V.T. 1959. *Open Channel Hydraulics*. McGraw-Hill, New York.
- Chu-Agor, M.L., G.A. Fox, and G.V. Wilson. 2009. Empirical sediment transport function predicting seepage erosion undercutting for cohesive bank failure prediction. *Journal of Hydrology*. 377:155-164.
- Couper, P. 2003. Effects of silt-clay content on the susceptibility of river banks to subaerial erosion. *Geomorphology*. 56:95-108.
- Couper, P., and I.P. Maddock. 2001. Subaerial river bank erosion processes and their interaction with other bank erosion mechanisms on the River Arrow, Warwickshire, UK. *Earth Surface Processes & Landforms*. 26:631-646.
- Couper, P., T. Stott, and I.P. Maddock. 2002. Insights into river bank erosion processes derived from analysis of negative erosion-pin recordings: Observations from three recent UK studies. *Earth Surface Processes & Landforms*. 27:59-79.
- Daly, E.R., G.A. Fox, A.T. Al-Madhhachi, and D.E. Storm. 2015. Variability of fluvial erodibility parameters for streambanks on a watershed scale. *Geomorphology*. 231:281-291.
- Darby, S.E., H.Q. Trieu, P.A. Carling, J. Sarkkula, J. Koponen, M. Kummu, I. Conlan, and J. Leyland. 2010. A physically based model to predict hydraulic erosion of fine-grained riverbanks: The role of form roughness in limiting erosion. *Journal of Geophysical Research: Earth Surface*. 115:F04003.
- Debnath, K., V. Nikora, and A. Elliott. 2007. Stream bank erosion: In-situ flume tests. *Journal of Irrigation and Drainage Engineering*. 133. 10.1061/(ASCE)0733-9437(2007)133:3(256).
- Doheny, E.J. 1996. *A Modified Index for Assessment of Potential Scour at Bridges over Waterways*. USGS Open-File Report 96-554. Reston VA.
- Eke, E., G. Parker, and Y. Shimizu. 2014. Numerical modeling of erosional and depositional bank processes in migrating river bends with self-formed width: Morphodynamics of bar push and bank pull. *Journal of Geophysical Research - Earth Surface*. 119:1455-1483.

- Elhakeem, M., A.N. Papanicolaou, and C.G. Wilson. 2017. Implementing streambank erosion control measures in meandering streams: Design procedure enhanced with numerical modeling. *International Journal of River Basin Management*. 15(3):317-327.
- Ettema, R., T. Nakato, and M. Muste. 2006. *An Illustrated Guide for Monitoring and Protecting Bridge Waterways against Scour*. Iowa Department of Transportation Report TR-515. Ames, IA.
- Ettema, R., T. Nakato, and M. Muste. 2006. *Estimation of Scour Depth at Bridge Abutments*. National Cooperative Highway Research Program Report 24-20. Washington, DC.
- Ferrick, M.G., and L.W. Gatto. 2005. Quantifying the effect of a freeze-thaw cycle on soil erosion: Laboratory experiments. *Earth Surface Processes & Landforms*. 30:1305-1326.
- Florsheim, J.L., J.F. Mount, and A. Chin. 2008. Bank erosion as a desirable attribute of rivers. *BioScience*. 58:519-529.
- Fongers, B. 2008. *Thornapple River Watershed Flashiness Report*. Michigan Department of Environmental Quality Report 2007-0137. Lansing, MI.
- Fox, G.A., R.A. Purvis, and C.J. Penn. 2016. Streambanks: A net source of sediment and phosphorus to streams and rivers. *Journal of Environmental Management*. 181:602-614.
- Fox, G.A., and G. Wilson. 2010. The role of subsurface flow in hillslope and stream bank erosion: A review. *Soil Science Society of America Journal*. 74:717-733.
- Fox, G.A., G.V. Wilson, A. Simon, E.J. Langendoen, O. Akay, and J.W. Fuchs. 2007. Measuring streambank erosion due to ground water seepage: Correlation to bank pore water pressure, precipitation and stream stage. *Earth Surface Processes & Landforms*. 32:1558-1573.
- Fredlund, D.G., N.R. Morgenstern, and R.A. Widger. 1978. The shear strength of unsaturated soils. *Canadian Geotechnical Journal*. 15: 313-321.
- Fredlund, D.G., and H. Rahardjo. 1993. *Soil Mechanics for Unsaturated Soils*. John Wiley and Sons, Inc., New York. 517 p.
- Gaskin, S.J., J. Pieterse, A. Al-Shafie, and S. Lepage. 2003. Erosion of undisturbed clay samples from the banks of the St. Lawrence River. *Canadian Journal of Civil Engineering*. 30:585-595.
- Gharabaghi, B., C. Inkratas, B.G. Krishnappan, and R.P. Rudra. 2007. Flow characteristics in a rotating circular flume. *The Open Civil Engineering Journal*. 1:30-36.
- Gilley, J.E., W.J. Elliot, J.M. Laflen, and J.R. Simanton. 1993. Critical shear stress and critical flow rates for initiation of rilling. *Journal of Hydrology*. 142:251-271.
- Gilvear, D.J., C. Davids, and A.N. Tyler. 2004. The use of remotely sensed data on channel hydromorphology: River Tummel, Scotland. *River Research and Applications*. 20:1-17.
- Grabowski, R.C. 2010. *The Erodibility of Fine Sediment Deposits in Lowland Chalk Streams*. Ph.D. Dissertation. University of London. London, UK.
- Grabowski, R.C. 2014. Measuring the shear strength of cohesive sediment in the field. *Geomorphological Techniques*. 1(3.1):1-7.
- Grabowski, R.C., Droppo, I.G., and Wharton, G. 2011. Erodibility of cohesive sediment: The importance of sediment properties. *Earth-Science Reviews*. 105:101-120.

- Griffith, G.E., J.M. Omernik, T.F. Wilton, and S.M. Pierson. 1994. Ecoregions and subregions of Iowa: a framework for water quality assessment and management. *Journal of the Iowa Academy of Science*. 101:5-13.
- Grissinger, E.H. 1982. Bank erosion of cohesive materials. In: Hey, R.D., J.C. Bathurst, and C.R. Thorne (Eds). *Gravel-Bed Rivers*. John Wiley and Sons, Ltd. New York, NY. pp. 273-287.
- Hadish, G.A., R.A. Lohnes, and C.P. Baumel. 1994. *Stream Stabilization in Western Iowa*. Iowa Department of Transportation Report HR-352. Ames, IA.
- Hamlett, J., J. Baker, and H. Johnson. 1983. Channel morphology changes and sediment yield for a small agricultural watershed in Iowa. *Transactions of the ASAE*. 26:1390-1396.
- Hanson, G.J., and K.R. Cook. 2004. Apparatus, test procedures, and analytical methods to measure soil erodibility in situ. *Applied Engineering in Agriculture*. 20(4):455-462.
- Hanson, G.J., and A. Simon. 2001. Erodibility of cohesive streambeds in the loess area of the midwestern USA. *Hydrological Processes*. 15:23-28.
- Hooke, J.M. 1979. An analysis of the processes of river bank erosion. *Journal of Hydrology*. 42:39-62.
- Hooke, J.M. 1980. Magnitude and distribution of rates of river bank erosion. *Earth Surface Processes & Landforms*. 5:143-157.
- Horn, D.P., and S.P.H. Lane. 2006. Measurement of high-frequency bed level changes in the swash zone using Photo-Electronic Erosion Pins (PEEPs). *Proceedings of the 30th International Conference on Coastal Engineering*: San Diego, CA. pp. 2591-2603.
- Huang, J., R.C. Hilldale, and B.P. Greimann. 2006. Cohesive sediment transport. In: Yang, C.T. (Ed.). *Erosion and Sedimentation Manual*. U.S. Department of Interior, Bureau of Reclamation, Technical Service Center. Denver, CO. pp. 4.1-4.54.
- Iowa Department of Transportation. 2011. *2011 Road Use Tax Fund (RUTF) Study: A report to the Iowa Legislature, per 2011 Iowa Code Section 307.31*. Iowa Department of Transportation. Ames, IA.
- Jepsen, R., J. Roberts, and W. Lick. 1997. Effects of bulk density on sediment erosion rates. *Water Air Soil Pollution*. 99:21-31.
- Johnson, P.A. 2005. Preliminary assessment and rating of stream channel stability near bridges. *Journal of Hydraulic Engineering*. 131(10):845-852.
- Johnson, P.A. 2006a. *Assessing Stream Channel Stability at Bridges in Physiographic Regions*. Federal Highway Administration Publication No. FHWA-HRT-05-072. Arlington, VA.
- Johnson, P.A. 2006b. Physiographic characteristics of bridge-stream intersections. *River Research and Applications*. 22(6):617-630.
- Jones, C.S., and K.E. Schilling. 2011. From agricultural intensification to conservation: Sediment transport in the Raccoon River, Iowa, 1916-2009. *Journal of Environmental Quality*. 40:1911-1923.
- Julian, J.P., and R. Torres. 2006. Hydraulic erosion of cohesive riverbanks. *Geomorphology*. 76:193-206.
- Kamphuis, J.W., P.N. Gaskin, and E. Hoogendoorn. 1990. Erosion test on four intact Ontario clays. *Canadian Geotechnical Journal*. 27:692-696.

- Kandiah, A. 1974. *Fundamental Aspects of Surface Fluvial Erosion of Cohesive Soils*. Ph.D. Dissertation, University of California. Davis, CA.
- Karamigolbaghi, M., S.M. Ghaneizad, J.F. Atkinson, S.J. Bennett, R.R. Wells. 2017. Critical assessment of jet erosion test methodologies for cohesive soil and sediment. *Geomorphology*. 295:529-536.
- Keil, A. 2006. *Rapid Assessment of Stream Conditions Along Length (RASCAL) Protocol*. Iowa Department of Natural Resources, Des Moines, IA.
http://jaicwc.org/current_web_site/watersheds/muddy_creek/rascal/docs-rascal-mc/RASCAL_Procedure_DRAFT.pdf (Accessed 05/19/2020).
- Kessler, A.C., S.C. Gupta, H.A.S. Dolliver, and D.P. Thoma. 2012. Lidar quantification of bank erosion in Blue Earth County, Minnesota. *Journal of Environmental Quality*. 41:197-207.
- Krintzsky, E.L., and W.J. Turnbull. 1967. Loess deposits of Mississippi. *Geological Society of America Special Papers*. 94:1-62.
- Knighton, A.D. 1999. Downstream variation in stream power. *Geomorphology*. 29:293-306.
- Knox, J.C. 1977. Human impacts on Wisconsin stream channels. *Annals of the Association of American Geographers*. 67:323-342.
- Kothyari, U.C., and R.K. Jain. 2008. Influence of cohesive on the incipient motion condition of sediment mixtures. *Water Resources Research*. 44(4):W04410.
- Lagasse, P.F., M.S. Byars, L.W. Zevenbergen, and P.E. Clopper. 2001. *Bridge Scour and Stream Instability Countermeasures*. Federal Highway Administration Publication No. FHWA-NHI-01-003. Hydraulic Engineering Circular Number 23. Arlington, VA.
- Lagasse, P.F., L.W. Zevenbergen, W.J. Spitz, and C.R. Thorne. 2004. *Methodology for Predicting Channel Migration*. National Cooperative Highway Research Program Web-Only Document 67 (Project 24-16). National Academy of Sciences. Washington, DC.
- Landemaine, V., A. Gay, O. Cerdan, S. Salvador-Blanes, and S. Rodrigues. 2015. Morphological evolution of a rural headwater stream after channelization. *Geomorphology*. 230:125-137.
- Langendoen, E.J. 2000. *CONCEPTS – Conservational Channel Evolution and Pollutant Transport System*. USDA ARS National Sedimentation Laboratory Research Report No. 16. Oxford, MS.
- Langendoen, E.J. 2010. Assessing post-dam removal sediment dynamics using the CONCEPTS computer model. *2nd Joint Federal Interagency Conference*. June 27-July 1, 2010. Las Vegas, NV.
- Langendoen, E.J., and C.V. Alonso. 2008. Modeling the evolution of incised streams: I. Model formulation and validation of flow and streambed evolution components. *Journal of Hydraulic Engineering*. 134(6):749-762.
- Langendoen, E.J., R.R. Wells, R.E. Thomas, A. Simon, and R.L. Bingner. 2009. Modeling the evolution of incised streams. III: Model application. *Journal of Hydraulic Engineering*. 135(6):476-486.
- Leonard, J., and G. Richard. 2004. Estimation of runoff critical shear stress for soil erosion from soil shear strength. *Catena*. 57:233-249.
- Leopold, L.B., and M.G. Wolman. 1957. *River Channel Patterns: Braided, Meandering, and Straight*. U.S. Government Printing Office.

- Lawler, D.M., 1991. A new technique for the automatic monitoring of erosion and deposition rates. *Water Resources Research*. 27(8):2125-2128.
- Lawler, D.M., 1992a. Process dominance in bank erosion systems. In: Carling, P.A. and G.E. Petts (Eds.). *Lowland Floodplain Rivers: Geomorphological Perspectives*. Wiley, pp. 117–143.
- Lawler, D.M., 1992b. Design and installation of a novel automatic erosion monitoring system. *Earth Surface Processes & Landforms*. 17:455-463.
- Lawler, D.M. 2008. Advances in the continuous monitoring of erosion and deposition dynamics: Developments and applications of the new PEEP-3T system. *Geomorphology*. 93:17-39.
- Lawler, D.M., C.R. Thorne, and J.M. Hooke. 1997. Bank erosion and instability. In: Thorne, C.R., R.D. Hey, and M.D. Newson (Eds.). *Applied Fluvial Geomorphology for River Engineering and Management*. John Wiley & Sons. New York, NY. pp. 137-172.
- Leate, N.S. 2013. *The Influence of Hydrologic and Riparian Factors on Stream Channel Stability in a Central Iowa Stream*. M.S. Thesis, Iowa State University. Ames, IA.
- Lyle, W.M., and E.T. Smerdon. 1965. Relation of compaction and other soil properties to erosion resistance of soils. *Transactions of the American Society of Agricultural Engineers*. 8:419-422.
- Mahalder, B., J.S. Schwartz, A.M. Palomino, and J. Zirkle. 2018. Relationships between physical-geochemical soil properties and erodibility of streambanks among different physiographic provinces of Tennessee, USA. *Earth Surface Processes & Landforms*. 43:401-416.
- McDermott, J.P., and D.J. Sherman. 2009. Using photo-electronic erosion pins for measuring bed elevation changes in the swash zone. *Journal of Coastal Research*. 25(3):788-792.
- McNeil, J., C. Taylor, and W. Lick. 1996. Measurement of erosion of undisturbed bottom sediments with depth. *Journal of Hydraulic Engineering*. 112(6):316-324.
- Mehta, A.J. 1983. Characterization tests for cohesive sediments. *Proceedings of the Conference on Frontiers in Hydraulic Engineering, ASCE*. Cambridge, MA. pp. 79–94.
- Mehta, A.J., and T.M. Parchure. 2000. Surface erosion of fine-grained sediment revisited. *Proceedings in Marine Science*. 2:55-74.
- Micheli, E.R., and J.W. Kirchner. 2002. Effects of wet meadow riparian vegetation on streambank erosion: I. Remote sensing measurements of streambank migration and erodibility. *Earth Surface Processes & Landforms*. 27:627-639.
- Midgley, T.L., G.A. Fox, and D.M. Heeren. 2012. Evaluation of the bank stability and toe erosion model (BSTEM) for predicting lateral retreat on composite streambanks. *Geomorphology*. 145-146:107-114.
- Millar, R.G., and M.C. Quick. 1998. Stable width and depth of gravel-bed rivers with cohesive banks. *Journal of Hydraulic Engineering*. 124(10):1005-1013.
- Miller, R.B., G.A. Fox, C.J. Penn, S. Wilson, A. Parnell, R.A. Purvis, and K. Criswell. 2014. Estimating sediment and phosphorus loads from streambanks with and without riparian protection. *Agriculture, Ecosystems, & Environment*. 189:70-81.
- Mitchell, S.B., J.S. Couperthwaite, J.R. West, D.M. Lawler. 2003. Measuring sediment exchange rates on an intertidal bank at Blacktoft, Humber Estuary, UK. *The Science of the Total Environment*. 314-316: 535-549.

- Mitchener, H., and H. Torfs. 1996. Erosion of mud/sand mixtures. *Coastal Engineering*. 29:1-25.
- Mogollon, E., A. Frimpong, A.B. Hoegh, and P.L. Angermeier. 2016. Recent changes in stream flashiness and flooding, and effects of flood management in North Carolina and Virginia. *Journal of the American Water Resources Association*. 52(3):561-577.
- Mostafa, T.S., J. Imran, M.H. Chaudhry, and I.B. Kahn. 2008. Erosion resistance of cohesive soils. *Journal of Hydraulic Research*. 46(6):777-787.
- Mostaghimi, S., R.A. Young, A.R. Wilts, and A.L. Kenimer. 1988. Effects of frost action on soil aggregate stability. *Transactions of the American Society of Agricultural Engineers*. 31(2):435-439.
- Motta, D., J.D. Abad, E.J. Langendoen, and M.H. García. 2012. The effects of floodplain soil heterogeneity on meander planform shape. *Water Resources Research*. 48:W09518.
- Moustakidis, I., K. Schilling, and L. Weber. 2019. Soil total phosphorus deposition and variability patterns across the floodplains of an Iowa river. *Catena*. 174:84-94.
- Myers, D.T., R.R. Rediske, and J.N. McNair. 2019. Measuring streambank erosion: A comparison of erosion pins, total station, and terrestrial laser scanner. *Water*. 11:1846, doi:10.3390/w11091846.
- Netwon, B., C. Pringle, and R. Bjorkland. 1998. *Stream Visual Assessment Protocol*. USDA NRCS National Water and Climate Center. Technical Note 99-1. Portland, OR.
- Odgaard, A.J. 1987. Streambank erosion along two rivers in Iowa. *Water Resources Research*. 23:1225-1236.
- Odgaard, A.J., and H.Y.E. Lee. 1984. *Submerged Vanes for Flow Control and Bank Protection in Streams*. Iowa Department of Transportation Report HR-255. Ames, IA.
- Owen, M.W. 1975. *Erosion of Avon-mouth Mud*. Hydraulics Research Station Report No. INT 150. Wallingford, England.
- Palmer, J.A., K.E. Schilling, T.M. Isenhardt, R.C. Schultz, and M.D. Tomer. 2014. Streambank erosion rates and loads within a single watershed: Bridging the gap between temporal and spatial scales. *Geomorphology*. 209:66-78.
- Papanicolaou, A.N., S. Dey, M. Rinaldi, and A. Mazumdar. 2006. *Research Issues for Riverine Bank Stability Analysis in the 21st Century*. Obermann Center Report. University of Iowa, Iowa City, IA.
- Papanicolaou, A., and M. Elhakeem. 2006. *Design Procedures and Field Monitoring of Submerged Barbs for Streambank Protection*. Iowa Department of Transportation Report TR-534.
- Papanicolaou, A.N., M. Elhakeem, and R. Hildale. 2007. Secondary current effects on cohesive river bank erosion. *Water Resources Research*. 43:W12418, doi: 10.1029/2006WR005763
- Papanicolaou, A.N., T. Kyriakopoulos, A.R. Maxwell, M.S. Ghaneeizad, and M.A. Wyssmann. 2020. Sediment aging effects on fluvial erosion for a newly formed kaolin sediment: Isolating the role of self-weight consolidation. *Journal of Hydraulic Engineering*. In review.
- Papanicolaou, A.N., C.G. Wilson, A.G. Tsakiris, T.E. Sutarto, F. Bertrand, M. Rinaldi, S. Dey, and E. Langendoen. 2017. Understanding mass fluvial erosion along a bank profile:

- Using PEEP technology for quantifying retreat lengths and identifying event timing. *Earth Surface Processes & Landforms*. 42(11):1717-1732.
- Parchure, T.M., and A.J. Mehta. 1985. Erosion of soft cohesive sediment deposits. *Journal of Hydraulic Engineering*. 111(10):1309-1326.
- Partheniades, E. 1965. Erosion and deposition of cohesive soils. *Journal of Hydraulics Division*. 91(HY1):105-138.
- Partheniades, E. 2009. *Cohesive Sediment in Open Channels*. Butterworth-Heinemann Publishers. 384 pp.
- Peizhen, Z., P. Molnar, and W.R. Downs. 2001. Increased sedimentation rates and grain sizes 2-4 Myr ago due to the influence of climate change on erosion rates. *Nature*. 410:891-897.
- Pizzuto, J.E. 1984. Equilibrium bank geometry and the width of shallow sandbed streams. *Earth Surface Processes & Landforms*. 9:199-207.
- Pizzuto, J.E. 2009. An empirical model of event scale cohesive bank profile evolution. *Earth Surface Processes & Landforms*. 34(9):1234-1244.
- Pizzuto, J., M. O'Neal, and S. Stotts. 2010. On the retreat of forested, cohesive riverbanks. *Geomorphology*. 116:341-352.
- Plenner, S., W.E. Eichinger, and E.A. Bettis. 2016. Simple terrestrial laser scanner for measuring streambank retreat. *Journal of Hydraulic Engineering*. 142 (11):6, doi: 10.1061/(asce)hy.1943-7900.0001184.
- Pollen, N. 2007. Temporal and spatial variability in root reinforcement of streambanks: Accounting for soil shear strength and moisture. *Catena*. 69:197-205.
- Pollen, N., and A. Simon. 2005. Estimating the mechanical effects of riparian vegetation on streambank stability using a fiber bundle model. *Water Resources Research*. 41(7):W07025.
- Preacher, R., R. Leach, R. Schultz, C. Willett, and T. Isenhardt. 2018. Factors controlling streambank erosion and phosphorus loss in claypan watersheds. *Journal of Soil & Water Conservation*. 73:189-199.
- Prior, J.C. 1991. *Landforms of Iowa*. University of Iowa Press, Iowa City.
- Prosser, I.P., A.O. Hughes, and I.D. Rutherford. 2000. Bank erosion of an incised upland channel by subaerial processes: Tasmania, Australia. *Earth Surface Processes & Landforms*. 25:1085-1101.
- Purvis, R.A., and G.A. Fox. 2016. Streambank sediment loading rates at the watershed scale and the benefit of riparian protection. *Earth Surface Processes & Landforms*. 41:1327-1336.
- Raudkivi, A.J. 1998. *Loose Boundary Hydraulics*. A.A. Balkema, Rotterdam, the Netherlands, 271-311.
- Reed, C.W., A.W. Niedoroda, and D.J. Swift. 1999. Modeling sediment entrainment and transport processes limited by bed armoring. *Marine Geology*. 154(1):143-154.
- Rhoads, B.L. 2020. *River Dynamics: Geomorphology to Support Management*. Cambridge University Press. Cambridge UK.
- Righetti, M., and C. Lucarelli. 2007. May the Shields theory be extended to cohesive and adhesive benthic sediments?. *Journal of Geophysical Research*. 112(C5):C05039, doi:10.1029/2006JC003669.

- Rinaldi, M., N. Casagli, S. Dapporto, and A. Gargini. 2004. Monitoring and modelling of pore water pressure changes and riverbank stability during flow events. *Earth Surface Processes & Landforms*. 29:237-254.
- Rinaldi, M., and S.E. Darby. 2008. Modelling river-bank-erosion processes and mass failure mechanisms: Progress towards fully coupled simulations. In: Habersack, H., H. Piegay, and M. Rinaldi (Eds.). *Gravel-Bed Rivers VI: From Process Understanding to River Restoration*. Elsevier. Amsterdam, Netherlands.
- Rinaldi, M., and L. Nardi. 2013. Modeling interactions between riverbank hydrology and mass failures. *Journal of Hydraulic Engineering*. 18(10):1321-1240.
- Roberts, J., and R. Jepsen. 2001. *Development or Optional Use of Circular Core Tubes with the High Shear Stress Flume*. SANDIA report SAND2001-0424. Sandia National Laboratories. Albuquerque, NM.
- Roberts, J.D., R.A. Jepsen, and S.C. James. 2003. Measurements of Sediment Erosion and Transport with the Adjustable Shear Stress Erosion and Transport (ASSET) Flume. *Journal of Hydraulic Engineering*. 129(11):862-871.
- Rosgen, D.L. 1994. A classification of natural rivers. *Catena*. 22(3):169-199.
- Rosgen, D.L. 2001. A practical method of computing stream bank erosion rate. *Proceedings of the Seventh Federal interagency Sedimentation Conference*. March 25-29, 2001. Reno, Nevada.: II-9-II-17.
- Schilling, K.E., T.M. Isenhardt, J.A. Palmer, C.F. Wolter, and J. Spooner. 2011. Impacts of land-cover change on suspended sediment transport in two agricultural watersheds. *Journal of the American Water Resources Association*. 47(4):672-686.
- Schilling, K.E., P.J. Jacobson, and C.F. Wolter. 2018. Using riparian zone scaling to optimize buffer placement and effectiveness. *Landscape Ecology*. 33:141-156.
- Schilling, K.E., and C.F. Wolter. 2000. Application of GPS and GIS to map channel features in Walnut Creek, Iowa. *Journal of the American Water Resources Association*. 36:1423-1434.
- Schilling, K.E., and C.F. Wolter. 2005. Estimation of streamflow, baseflow and nitrate loads in Iowa using multiple linear regression models. *Journal of the American Water Resources Association*. 41:1333-1346.
- Schmidt, M. 2017. Too many roads, not enough money? *The Gazette*. May 5, 2017. <https://www.thegazette.com/iowaideas/stories/transportation/too-many-roads-not-enough-money-20170305>.
- Simon, A. 1989. The discharge of sediment in channelized alluvial streams. *Journal of the American Water Resources Association*. 25:1177-1188.
- Simon, A., and A.J. Collison. 2002. Quantifying the mechanical and hydrologic effects of riparian vegetation on streambank stability. *Earth Surface Processes & Landforms*. 27:527-546.
- Simon, A., and C.R. Hupp. 1986. Channel evolution in modified Tennessee channels. *Proceedings of the 4th Federal Interagency Sedimentation Conference*. 2:5.71-5.82.
- Simon, A., and L. Klimetz. 2008. Relative magnitudes and sources of sediment in benchmark watersheds of the Conservation Effects Assessment Project. *Journal of Soil & Water Conservation*. 63(6):504-522.

- Simon, A., and M. Rinaldi. 2000. Channel instability in the loess area of the Midwestern United States. *Journal of the American Water Resources Association*. 36(1):113-150.
- Smerdon, E.T., and R.P. Beasley. 1961. Critical tractive forces in cohesive soils. *Agricultural Engineering*. 42(1):26-29.
- Springston, G. 2007. *Report on Streambank Stability Assessment Techniques*. Vermont Geological Survey Technical Report VGTR2007-1. Burlington, VT.
- Stoesser, T., N. Ruether, N.R.B. Olsen. 2010. Calculation of primary and secondary flow and boundary shear stresses in a meandering channel. *Advances in Water Resources*. 33:158-170.
- Sutarto, T., A.N. Papanicolaou, C.G. Wilson, and E. Langendoen. 2014. Stability analysis of semicohesive streambanks with CONCEPTS: Coupling field and laboratory investigations to quantify the onset of fluvial erosion and mass failure. *Journal of Hydraulic Engineering*. 140(9):04014041.
- Tang, C.B. 1963. Law of sediment threshold. *Journal of Hydraulic Engineering*. 2:1-12.
- Temple, D.M., K.M. Robinson, R.M. Ahring, and A.G. Davis. 1987. Stability design of grass-lined open channels. *USDA-ARS Agriculture Handbook Number 667*. DC.
- Thoma, D.P., S.C. Gupta, M.E. Bauer, and C. Kirchoff. 2005. Airborne laser scanning for riverbank erosion assessment. *Remote Sensing of Environment*. 95:493-501.
- Thomas, J.T., N.R. Iverson, M.R. Burkart, and L.A. Kramer. 2004. Long-term growth of a valley bottom gully, western Iowa. *Earth Surface Processes and Landforms*. 29:995-1009.
- Thorn, M.F.C., and J.G. Parsons. 1980. Erosion of cohesive sediments in estuaries: An Engineering Guide. *Proceedings of the 3rd International Symposium on Dredging Technology*. Bedford: BHRA. pp. 349-358.
- Thorne, C.R. 1982. Processes and mechanisms for river bank erosion. In: Hey, R.D., J.C. Bathurst, and C.R. Thorne (Eds.). *Gravel-Bed Rivers: Fluvial Processes, Engineering, and Management*. John Wiley & Sons, New York, NY. pp. 227-259.
- Thorne, C.R., and N.K. Tovey. 1981. Stability of composite river banks. *Earth Surface Processes & Landforms*. 6:469-484.
- Tomer, M., and J. Van Horn. 2018. Stream bank and sediment movement associated with 2008 flooding, South Fork Iowa River. *Journal of Soil & Water Conservation*. 73:97-106.
- Torfs H. 1995. *Erosion of Mud/Sand Mixtures*. Ph.D. Thesis, Katholieke Universiteit. Leuven, BE.
- Torri, D., M. Dfalanga, and G. Chisci. 1987. Threshold conditions for incipient rilling. *Catena Supplement*. 8:97-105.
- Trhlikova, J. 2013. *Mechanical Behavior of Cemented Fine-Grained Soils: Simulation of Undisturbed Samples*. Ph.D. Dissertation, Charles University. Prague, CZ.
- Trimble, S.W. 1997. Contribution of stream channel erosion to sediment yield from an urbanizing watershed. *Science*. 278:1442-1444.
- Tufekcioglu, M., T.M. Isenhardt, R.C. Schultz, D.A. Bear, J. Kovar, and J.R. Russell. 2012. Stream bank erosion as a source of sediment and phosphorus in grazed pastures of the Rathbun Lake Watershed in southern Iowa, United States. *Journal of Soil & Water Conservation*. 67:545-555.

- U.S. Department of Transportation. 2012. *Stream Stability at Highway Structures, 4th edition*. USDOT Federal Highway Administration Publication No. FHWA-HIF-12-004. Washington DC.
- van Kessel, T., and C. Blom. 1998. Rheology of cohesive sediments: Comparison between a natural and an artificial mud. *Journal of Hydraulic Research*. 36(4):591-612.
- van Klaveren, R.W., and D.K. McCool. 1998. Erodibility and critical shear of a previously frozen soil. *Transactions of the American Society of Agricultural Engineers*. 41(5):1315-1321.
- van Ledden, M., W.G.M. van Kesteren, and J.C. Winterwerp. 2004. A conceptual framework for the erosion behavior of sand-mud mixtures. *Continental Shelf Research*. 24(1): 1-11.
- Vardeman, S.B., and J.M. Jobe. 1999. *Statistical Quality Assurance Methods for Engineers*. John Wiley & Sons, New York, NY. pp. 561.
- Vermeyen, T. 1995. *Erosion and Depositional Characteristics of Cohesive Sediments Found in Elephant Butte Reservoir, New Mexico*. U.S. Bureau of Reclamation, Water Resources Services, Technical Service Center Technical Report R-95-15. Denver, CO.
- Villarini, G., K.E. Schilling, and C.S. Jones. 2016. Assessing the relation of USDA conservation expenditures to suspended sediment reductions in an Iowa watershed. *Journal of Environmental Management*. 180:375-383.
- Widodo, S., A.M. Ibrahim, and S. Hong. 2012. Analysis of different equations of undrained shear strength estimations using Atterberg Limits on Pontianak Soft Clay. *Challenges of Modern Technology*. 3:46-50.
- Wilkin, D.C., and S.J. Hebel. 1982. Erosion, redeposition, and delivery of sediment to Midwestern streams. *Water Resources Research*. 18(4):1278-1282.
- Willett, C.D., R. Lerch, R.C. Schultz, S.A. Berges, R. Peacher, and T.M. Isenhardt. 2012. Streambank erosion in two watersheds of the Central Claypan Region of Missouri, United States. *Journal of Soil & Water Conservation*. 67:249-263.
- Williams, F. 2019. *Combining Field and Automated Methods to Estimate Bank Erosion: A Regional Estimation of Sediment and Phosphorus Loads*. M.S. Thesis. Iowa State University. Ames, IA.
- Wilson, B.N. 1993a. Development of a fundamentally based detachment model. *Transactions of the American Society of Agricultural Engineers*. 36(4):1105-1114.
- Wilson, B.N. 1993b. Evaluation of a fundamentally based detachment model. *Transactions of the American Society of Agricultural Engineers*. 36(4):1115-1122.
- Wilson, C.G., R.A. Kuhnle, D.D. Bosch, J.L. Steiner, P.J. Starks, M.D. Tomer, and G.V. Wilson. 2008. Quantifying relative contributions from sediment sources in Conservation Effects Assessment Project watersheds. *Journal of Soil & Water Conservation*. 63(6):523-532
- Wilson, C.G., R.A. Kuhnle, S.M. Dabney, R.N. Lerch, C.H. Huang, K.W. King, and S.J. Livingston. 2014. Fine sediment sources in Conservation Effects Assessment Project watersheds. *Journal of Soil & Water Conservation*. 69(5):402-413.
- Wilson, C.G., A.N. Papanicolaou, and K.D. Denn. 2012. Quantifying and partitioning fine sediment loads in an intensively agricultural headwater system. *Journal of Soils & Sediments*. 12(6):966-981.

- Wilson, G.V., R.K. Periketi, G.A. Fox, S.M. Dabney, F.D. Shields, and R. F. Cullum 2007. Seepage erosion properties contributing to streambank failure. *Earth Surface Processes & Landforms*. 32(3):447-459.
- Winterwerp, J.C., W.G.M. van Kesteren. 2004. *Introduction to the Physics of Cohesive Sediment in the Marine Environment*. Elsevier. New York, NY. pp. 343-379.
- Winterwerp, J.C., W.G.M. van Kesteren, B. van Prooijen, and W. Jacobs. 2012. A conceptual framework for shear flow-induced erosion of soft cohesive sediment beds. *Journal of Geophysical Research* 117:C10020. doi:10.1029/2012JC008072.
- Wipf, T., F.S. Fanous, F.W. Klaiber, and A.S. Eapen. 2003. *Evaluation of Appropriate Maintenance, Repair and Rehabilitation Methods for Iowa Bridges*. Iowa Department of Transportation Report TR-429. Ames, IA.
- Wynn, T., and S. Mostaghimi, 2004. The effects of vegetation on streambank erosion. *Proceedings of the 2004 ASAE/CSAE Annual International Meeting*. Paper 042226. August 1-4, 2004. Ottawa, ON.
- Wynn, T., and S. Mostaghimi, 2006. The effects of vegetation and soil types on streambank erosion, southwestern Virginia, USA. *Journal of the American Water Resources Association*. 42(1):69-82.
- Wynn, T.M., M.B. Henderson, and D.H. Vaughan. 2008. Changes in streambank erodibility and critical shear stress due to subaerial processes along a headwater stream, southwestern Virginia, USA. *Geomorphology*. 97: 260-273.
- Yang, H., D.J. White, and V.R. Schaefer. 2005. *Innovative Solutions for Slope Stability Reinforcement and Characterization: Vol.II*. Report No. TR-489. Iowa Highway Research Board, Ames, IA.
- Zaimes, G.N., and R.C. Schultz. 2015. Riparian land-use impacts on bank erosion and deposition of an incised stream in north-central Iowa, USA. *Catena*. 125:61-73.
- Zaimes, G.N., R.C. Schultz, and T.M. Isenhardt. 2004. Stream bank erosion adjacent to riparian forest buffers, row-crop fields, and continuously-grazed pastures along Bear Creek in central Iowa. *Journal of Soil & Water Conservation*. 59:19-27.
- Zaimes, G.N., R.C. Schultz, and T.M. Isenhardt. 2006. Riparian land uses and precipitation influences on stream bank erosion in central Iowa. *Journal of the American Water Resources Association*. 42:83-97.
- Zaimes, G.N., M. Tufekcioglu, and R.C. Schultz. 2019. Riparian land-use impacts on stream bank and gully erosion in agricultural watersheds: What we have learned. *Water*. 11:1343. doi:10.3390/w11071343.
- Zhou, S., A.N. Papanicolaou, K. Wacha, C.G. Wilson, and T.R. Filley. 2020. Determining the interplay of land use and slope on SOC heterogeneity using Visible Near Infrared Spectroscopy. *Geoderma*. In review.